Reduction of Steel Usage in Timber Structures through Wooden Reinforcement Applications in Connections

A Numerical and Case Study Investigation

Master Thesis

Rens Noordam

TU Delft

IMd Raadgevende Ingenieurs

Reduction of Steel Usage in Timber Structures through Wooden Reinforcement Applications in Connections

A Numerical and Case Study Investigation

by

Rens Noordam

Thesis Committee:	Dr. T. Tankova
	Dr. A. Cabboi
	Dr. Ir. G.J.P. Ravenshorst
Company Supervisors:	Ing. R. Stark
	Ir. G. Hoogerwaard
Project Duration:	May, 2025 - March, 2026
Faculty:	Faculty of Civil Engineering and Geosciences, Delft
Company:	IMd Raadgevende Ingenieurs, Rotterdam

Cover: Liander Westpoort Amsterdam by Scagliolabrakkee

TU Delft

IMd Raadgevende Ingenieurs

Preface

This thesis was written as part of the Master's programme in Civil Engineering completed during May 2025 and March 2026. It focuses on the structural behaviour of dowel-reinforced glulam elements subjected to compression perpendicular to the grain, investigated through numerical modelling and parametric analysis. The topic reflects my interest in timber engineering and in improving the structural performance of sustainable construction systems through carefully designed connections and reinforcement strategies.

I would like to sincerely thank my thesis committee members, Dr. Trayana Tankova, Dr. Alessandro Cabboi, and Dr. Ir. Geert Ravenshorst, for their guidance, constructive feedback, and critical insights throughout this research. Their expertise significantly strengthened the scientific quality of this work.

I am especially grateful to my daily supervisor at IMd, Ir. Geert Hoogerwaard, for his continuous support and practical perspective. His input helped bridge the gap between academic research and engineering practice, which greatly enriched this thesis.

Finally, I would like to thank my family and friends for their encouragement and support during my studies. Their motivation has been invaluable throughout this final phase of my academic journey.

I look back on this research period as both challenging and rewarding, having further developed my technical skills and deepened my interest in timber structures.

Rens Noordam
Delft, March 2026

Abstract

Timber structures increasingly rely on steel components to ensure sufficient load-bearing capacity in joints subjected to compression perpendicular to the grain. While effective, this practice conflicts with ambitions to reduce material complexity and improve circularity in timber construction. Wooden dowels, particularly when densified, offer a fully timber-based alternative, but their structural behaviour and design applicability are not yet sufficiently understood or codified.

This thesis investigates the mechanical behaviour of timber elements reinforced with wooden dowels under compression perpendicular to the grain, with a focus on column–beam–column connections. A finite element modelling framework is developed to capture stress redistribution, local crushing, contact behaviour, and interaction effects between timber and reinforcement. The numerical model is validated against reference behaviour and used in a parametric study to assess the influence of dowel geometry, layout, and interaction on system-level response. In parallel, an analytical model is derived to estimate reinforcement contributions based on simplified load-transfer assumptions and is evaluated against numerical results.

The results show that wooden dowel reinforcement can enhance stiffness and load-bearing capacity, but the effective contribution of individual dowels at system level is significantly lower than their isolated capacity. Load transfer is governed by non-uniform stress mobilisation along the dowel length, with partial side interaction and a relatively large contribution from dowel tip bearing. As a result, local timber crushing beneath the dowel tip governs the global response. Analytical design approaches provide conservative lower-bound estimates but are sensitive to assumptions regarding load-transfer mechanisms.

A case study application demonstrates how the developed models can be used to assess steel reduction potential in practice and highlights the need for additional numerical verification when applying timber-based reinforcement strategies. The findings contribute to a better mechanical understanding of wooden dowel reinforcement and provide a basis for future experimental validation and design-oriented development within the framework of Eurocode 5.

Contents

Preface i

Abstract ii

1 Introduction 1
- 1.1 Research context . . . 1
- 1.2 Research problem . . . 2
- 1.3 Research objectives . . . 3
- 1.4 Research scope . . . 3
- 1.5 Research questions . . . 4
- 1.6 Methodology . . . 5

2 Literature Review 7
- 2.1 Mechanical behaviour of timber . . . 8
- 2.2 Typical timber joints . . . 9
- 2.3 Connection behaviour of timber . . . 11
- 2.4 Fasteners and reinforcements in timber joints . . . 12
- 2.5 Densified wood . . . 15
- 2.6 Fire exposure . . . 17
- 2.7 Numerical modelling . . . 18
- 2.8 Relevant design standards . . . 19
- 2.9 Research gap . . . 25
- 2.10 Synthesis: answers to sub - research questions . . . 27

3 Case Study 28
- 3.1 Part I: Steel quantification in the reference building . . . 29
  - 3.1.1 Selected building . . . 29
  - 3.1.2 Structural system and material use . . . 29
  - 3.1.3 Steel calculation . . . 30
  - 3.1.4 Potential for timber-based connection alternatives . . . 31
- 3.2 Part II: Connection analysis and design alternatives . . . 32
  - 3.2.1 Connection analysis . . . 32
  - 3.2.2 Design alternatives . . . 34
- 3.3 Synthesis: answers to sub - research questions . . . 38

4 Model 40
- 4.1 Model setup . . . 41
  - 4.1.1 Base model . . . 41
  - 4.1.2 Derived models . . . 47
  - 4.1.3 Dowel Side + Tip Test (DSTT) . . . 47
  - 4.1.4 Analytical model . . . 48
- 4.2 Model validation . . . 51
  - 4.2.1 Reference model . . . 51
  - 4.2.2 Validation model . . . 52

5 Results 58
- 5.1 Base models . . . 59
  - 5.1.1 Force - displacement curves . . . 59
  - 5.1.2 Force distribution . . . 60
  - 5.1.3 Equivalent stress block and stress spreading angle . . . 64
- 5.2 Derived models . . . 65

5.2.1 Dowel Side Test . . . 65
5.2.2 Dowel Tip Test . . . 67
5.2.3 Dowel Side + Tip Test . . . 67
5.3 Dowel material tests . . . 69
5.4 Analytical model . . . 70
5.4.1 Definition of the analytical model . . . 70
5.4.2 Analytical results . . . 71
5.5 Comparison . . . 72
5.5.1 Comparison between developed model and reference model . . . 72
5.5.2 Comparison between developed model and analytical model . . . 74
5.6 Case study: part III . . . 75
5.6.1 Reinforcement layout and assumptions . . . 75
5.6.2 Results of reinforcement assessment . . . 76

6 Discussion **77**

7 Conclusions and Recommendations **80**
7.1 Conclusion . . . 80
7.2 Answers to the research questions . . . 82
7.3 Recommendations . . . 84

References **85**

A Steel Calculation Ground Floor **89**

B Steel Calculation First Floor **93**

C Example Calculation Alternative 1 **99**

D Example Calculation Alternative 2 **103**

E Example Calculation Alternative 3 **107**

F Timber Characteristic Values **111**

G Case Study part III: Hand Calculations **113**

H BM4D Abaqus Script **117**

1

Introduction

1.1. Research context

The construction sector is undergoing a significant transition driven by the need to reduce greenhouse gas emissions, material consumption, and environmental impact. Within this context, timber has gained renewed interest as a primary structural material. Timber is renewable, lightweight, and associated with a substantially lower carbon footprint compared to traditional materials such as reinforced concrete and structural steel. These characteristics make timber an attractive alternative for sustainable structural systems.

From a structural perspective, continuity in beams and columns is an efficient design strategy. Continuous systems enable moment redistribution, reduce peak internal forces, and improve global stability. They also provide an alternate load path, enabling load redistribution to adjacent spans in the event of local damage or loss of support. In timber buildings, however, achieving structural continuity remains challenging. In practice, continuity in beam–column systems is almost always realised through the use of steel components. These elements are used to ensure adequate force transfer and stiffness at connections, particularly in column–beam–column (CBC) joints where high compressive stresses perpendicular to the grain and complex force flows occur. An example can be seen in figure 1.1 below.

(a) Construction phase of the new Municipality Building of Krimpenerwaard. Adapted from Gemeente Krimpernerwaard (n.d.). https://www.krimpenerwaard.nl/nieuw-gemeentehuis

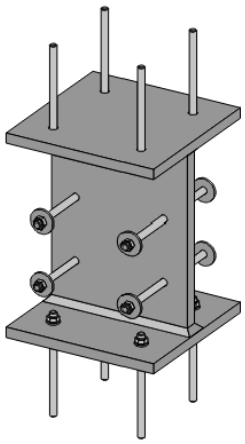

(b) Steel shoe connection detail (Detail 103). Adapted from IMd (n.d.).

Figure 1.1: Construction of the new Municipality Building of Krimpenerwaard and corresponding steel shoe connection detail.

Modern hybrid timber buildings, demonstrate this design approach clearly. While the primary load-bearing elements are made of timber, steel is introduced at critical joints to resolve continuity, load

transfer, and deformation demands. Although structurally effective, this reliance on steel compromises the ambition of fully timber-based construction and limits material circularity, disassembly potential, and physical appearance.

A key challenge in continuous timber systems is the behaviour of timber under compression perpendicular to the grain. In CBC joints, concentrated bearing stresses in the beam between adjacent columns lead to local crushing, significant deformations, and stiffness degradation. These effects govern serviceability and ultimate limit states and often dictate the use of steel reinforcement or steel-based connection solutions.

1.2. Research problem

Although fully timber-based connections exist (see figure 1.2, their application in practice remains limited. Timber-only reinforcement strategies are generally less efficient than steel-based solutions, often require complex detailing, and are insufficiently codified. As a result, designers tend to default to steel components when continuity, stiffness, or bearing capacity becomes critical, particularly in CBC connections.

(a) Exterior view of the Luftschiffhalle Mülheim. Adapted from VisitEssen (n.d.). `https://www.visitessen.de/essentourismus_convention/location_uebersicht_1/conventionLocation_1511224.en.html`

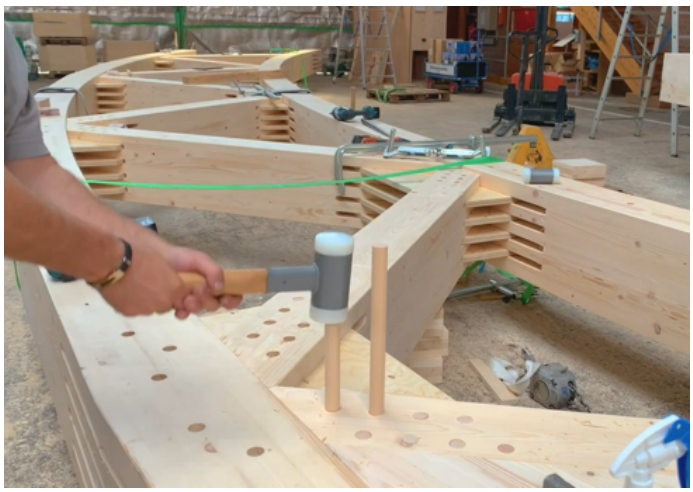

(b) Full timber connection detail of the Luftschiffhalle Mülheim. Screenshot adapted from YouTube (n.d.). `https://www.youtube.com/watch?v=Q9WGnQp__JY`

Figure 1.2: Luftschiff Mulheim.

In compression perpendicular to the grain, steel screws are commonly used as discrete reinforcement elements to locally enhance bearing capacity and stiffness. Their behaviour is relatively well understood and is implicitly covered by Eurocode 5 (EC5) through simplified design rules based on effective bearing lengths and empirical stress limits. Owing to the pronounced stiffness and strength contrast between steel and timber, screws efficiently carry load while failure is usually governed by the surrounding timber, allowing conservative lower-bound design approaches without explicit modelling of local interaction effects.

Wooden dowel reinforcement follows a fundamentally different load-transfer mechanism. In contrast to screws, which act primarily through axial forces and distributed bearing, wooden dowels also transfer load through bearing at their tip, resulting in a larger and more localised contact area. Their stiffness and strength are closer to those of the surrounding timber, particularly in compression perpendicular to the grain, even when densified dowels are used. Load transfer is therefore governed by local bearing, contact interaction, and deformation compatibility, with the contribution of individual dowels strongly dependent on their position, spacing, and mutual interaction. Stress redistribution and progressive crushing of the timber dominate the response, mechanisms not captured by current EC5 provisions, which provide no explicit design framework for wooden dowel reinforcement acting perpendicular to the grain.

The lack of reliable, codified timber-based reinforcement strategies thus represents a major obstacle to the development of continuous, steel-free timber structures. Because the governing mechanisms are highly localised and nonlinear, involving contact effects and interaction between multiple dowels, simplified analytical models are insufficient. Advanced numerical modelling is therefore required to obtain a systematic and physically meaningful understanding of dowel-reinforced timber joints.

1.3. Research objectives

The primary objective of this research is to develop and assess fully timber-based reinforcement strategies for timber joints subjected to compression perpendicular to the grain, with a specific focus on column–beam–column connections reinforced using wooden dowels. By improving the mechanical performance of these critical joints, the study aims to reduce the reliance on steel components and support the development of more circular and materially efficient timber structures.

The specific objectives of this thesis are:

- to identify and analyse timber-based reinforcement strategies for timber loaded in compression perpendicular to the grain, with wooden dowel reinforcement as the primary case;
- to investigate the governing failure mechanisms, load-transfer processes, and stress distribution in wooden dowel reinforced column–beam–column joints;
- to evaluate the structural performance and design feasibility of wooden dowel reinforcement in relation to current Eurocode 5 provisions, using alternative reinforcement systems only for comparison;
- to develop and apply a finite element modelling framework capable of capturing stress redistribution, local crushing, interaction effects, and post-peak behaviour in wooden dowel reinforced timber connections;
- to assess the potential reduction of steel components in timber construction through the application of fully timber-based reinforcement strategies.

These objectives form the basis for the research questions and methodological framework presented in the following sections and guide the conceptual, numerical, and design-oriented investigations carried out in this thesis.

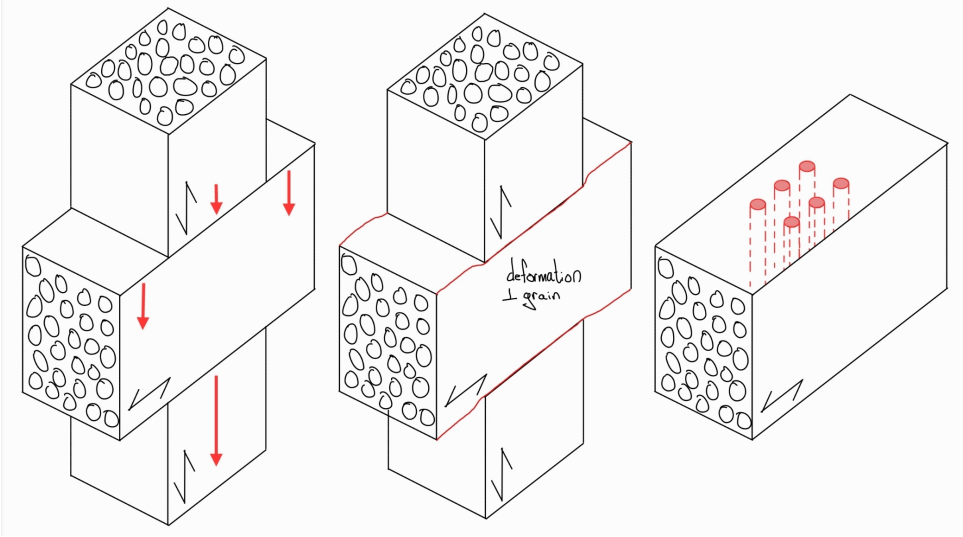

Figure 1.3: Conceptual illustrations of a CBC connection: (left) three-dimensional force flow under compression, (middle) three-dimensional deformation perpendicular to the grain, and (right) reinforced beam configuration with dowels.

1.4. Research scope

This research focuses on the mechanical behaviour and design of timber joints subjected to compression perpendicular to the grain, with particular emphasis on column–beam–column (CBC) con-

nections in multi-storey timber buildings. The study is centred on the development and assessment of fully timber-based reinforcement strategies intended to improve load-bearing capacity, deformation behaviour, and structural continuity, while reducing the reliance on steel components.

The scope of the research is limited to structural performance at the connection and member level. The primary reinforcement strategy investigated consists of timber-based dowel elements placed in the beam to enhance the compressive resistance perpendicular to the grain. The behaviour of these reinforced regions is studied under quasi-static loading conditions relevant to building structures. Both serviceability-related deformations and ultimate limit state behaviour are considered.

The analytical framework of the study is based on existing Eurocode 5 design provisions for compression perpendicular to the grain and reinforced timber members. Where applicable, updated or extended analytical models are developed to account for timber-based reinforcement strategies not explicitly covered by current design rules. These models are evaluated through numerical analysis rather than full-scale experimental testing.

A finite element modelling approach is adopted to investigate the governing mechanical mechanisms, including stress redistribution, local crushing, deformation compatibility, and post-peak behaviour. The numerical study is limited to material-level and connection-level analyses and does not include global structural modelling of entire buildings. The developed numerical and analytical models are applied to a representative hybrid timber building (IMd) to demonstrate their practical applicability and to assess their influence on connection design and steel usage.

The following aspects fall outside the scope of this research:

- long-term effects such as creep, moisture-induced deformation, and fatigue;
- dynamic and seismic loading conditions;
- fire performance beyond effective cross-section approaches used in design checks;
- detailed life-cycle assessment or environmental impact quantification;
- full-scale experimental testing of reinforced timber joints.

1.5. Research questions

Main research question:

- How can fully timber-based reinforcement strategies be applied to improve the compression-perpendicular-to-the-grain behaviour of timber joints, and to what extent can they reduce the need for steel components in such connections?

Sub-questions:

1. How have timber-based reinforcement elements been applied in previous research to enable reliable structural performance of timber joints under various loading conditions?
2. What are the dominant failure mechanisms in timber joints-reinforced with timber based elements-under various loading conditions?
3. What is the steel content (kg/m^2) in different parts of the selected hybrid timber building, and how can this be used to identify the most steel-intensive connection types for potential timber-based alternatives?
4. Which structural timber connections in buildings are most suitable for timber-based reinforcement and full timber optimization-based on EC5 design provisions-and to what extent can the use of steel components be reduced?
5. How does the placement of timber-based reinforcement elements affect the effective cross section and fire resistance of timber members?
6. To what extent does the developed numerical model have predictive value for the actual mechanical behaviour of timber under compression perpendicular to the grain?
7. How do dowel-reinforced members compare to Eurocode 5 design provisions for reinforced timber members?

8. What is the influence of the dowel material type on the compressive resistance and load–displacement response of timber reinforced perpendicular to the grain?

1.6. Methodology

The sub-questions are answered at different stages of the research, in accordance with the methodological structure of this thesis. This phased approach ensures that conceptual, numerical, and design-oriented aspects are addressed in a logical and coherent manner, progressing from qualitative understanding to quantitative evaluation and application.

- **Sub-questions 1 and 2** are addressed at the end of the **Literature Review**. These questions focus on the current state-of-the-art of timber-based reinforcement systems and the governing failure mechanisms in timber joints subjected to compression perpendicular to the grain. Their answers are derived from:
  - a systematic review of peer-reviewed publications and conference papers,
  - analysis of relevant Eurocode 5 provisions and technical guidelines,
  - comparison of experimentally observed failure modes reported in the literature.
- **Sub-question 3** is answered in the **first part of the Case Study chapter**. The steel content (kg/m^2) of the selected hybrid timber building is quantified in order to identify connections with the highest potential for steel reduction. This is achieved by:
  - extracting connection details and steel profiles from project documentation,
  - calculating the steel mass per structural component,
  - ranking connection types based on their steel intensity.
- **Sub-questions 4 and 5** are addressed in the **second part of the Case Study chapter**. At this stage, timber-based alternatives to steel-reinforced connections are explored at a design level. These questions are answered through:
  - evaluating alternative timber-based reinforcement strategies using Eurocode 5 design provisions,
  - assessing the influence of reinforcement placement on the effective cross section of timber members,
  - analysing the impact of reinforcement strategies on fire resistance using effective cross-section methods.

  pow
- The **third part of the Case Study chapter** applies the developed and updated analytical design model to a representative real-world building project (IMd). This part does not address a specific sub-question, but serves to:
  - demonstrate the practical applicability of the proposed timber-based reinforcement strategy,
  - evaluate its influence on connection design and steel usage at the building scale,
  - illustrate the implications of the developed model for engineering practice.
- **Sub-questions 6, 7, and 8** are answered in the **Results and Discussion chapters**. These questions require a detailed investigation of the mechanical behaviour of reinforced timber under compression perpendicular to the grain, which cannot be captured reliably using simplified analytical models alone. They are therefore addressed using a numerical parametric study based on the finite element method. This stage comprises:
  - development and validation of a finite element model capable of capturing stress redistribution, local crushing, and deformation compatibility between timber and reinforcement elements,
  - numerical testing of various reinforcement configurations, including dowel material type, number of dowels, and spacing,

- analytical comparison of numerical results with Eurocode 5 provisions for reinforced timber, including the sections on compression reinforcement and bonded-in rods,
- evaluation of load–displacement behaviour, failure initiation, and compressive resistance,
- synthesis of numerical and analytical results to assess the predictive value of the model and the applicability of existing design rules.

2

Literature Review

This literature review provides the scientific and regulatory background required to assess timber joints reinforced for compression perpendicular to the grain, with a focus on column–beam–column connections. The reviewed topics are selected to support the development of analytical and numerical models and to establish the context for the case study presented in later chapters.

The review covers the mechanical behaviour of timber and its governing failure mechanisms, followed by a general discussion of timber connections and fasteners. Particular attention is given to timber reinforcement strategies, including the use of densified wood fasteners, and to the differences in load-transfer mechanisms between steel- and timber-based reinforcement solutions. Relevant experimental and numerical studies on reinforced timber joints are examined to identify governing parameters and modelling approaches.

In addition, numerical modelling techniques for timber are reviewed to support the finite element framework developed in this thesis. Applicable design standards, including Eurocode 5, are discussed to clarify the current design practice and its limitations with respect to timber-based reinforcement. Fire exposure is briefly addressed to define the applicability and boundaries of the investigated reinforcement strategies.

Together, these topics define the state of knowledge relevant to reinforced timber joints, identify gaps in existing design and modelling approaches, and provide the basis for the analytical, numerical, and case-study investigations presented in this thesis.

2.1. Mechanical behaviour of timber

Mechanical properties

Wood is a highly anisotropic material, meaning its mechanical properties depend strongly on the direction of loading. More precisely, wood is orthotropic, with different properties along three main axes: longitudinal (along the grain), radial (perpendicular to the growth rings), and tangential (tangent to the growth rings) as shown in figure 2.1 [29]. Because of this structure, its behaviour under mechanical loads varies significantly [29].

In compression parallel to the grain, wood is relatively strong and stiff, with failure typically occurring through fiber buckling [29]. However, when loaded perpendicular to the grain, the strength is much lower. Wood in this direction does not show a clear ultimate failure; instead, the stress at the proportional limit is used to describe its capacity, often marked by localized crushing between growth rings [29].

Shear behaviour in wood, especially parallel to the grain, is important for resisting internal slippage along fibre planes [29]. Although wood's shear strength is lower than its compressive strength along the grain, it plays a critical role in the performance of joints and beams. In bending, wood initially behaves elastically until it reaches its modulus of rupture, after which failure occurs, typically through a combination of tensile and compressive stresses across the beam section [29].

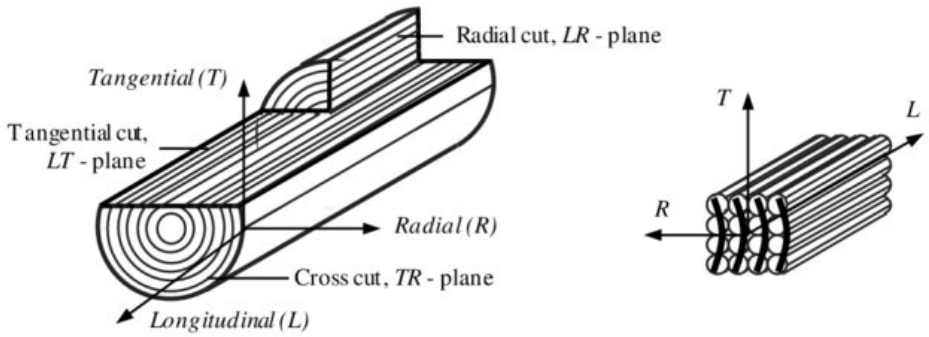

Figure 2.1: Cylindrical anisotropy of wood, and the three main directions longitudinal (L), tangential (T), and radial (R) on (global) trunk level (left) and on (local) fibre level (right). Adapted from "A non-contact method for the determination of fibre direction of European beech wood (Fagus sylvatica L.)" In: European Journal of Wood and Wood Products 76.6 (2018), pp. 925–935.

Failure modes

Wood structures are subject to several characteristic failure modes due to their material properties and environmental influences [16]. The most common issue is cracking along the grain, often caused by moisture fluctuations leading to internal stresses [16]. These cracks can significantly reduce the load-carrying capacity of timber elements and are often difficult to evaluate precisely.

In bending, failure usually occurs in the tension zone due to rupture of wood fibres, leading to brittle behaviour, while compression zones may exhibit ductile deformation through local yielding and kink bands (see drawing in the middle of figure 2.2) [16]. Compression failures happen either parallel to the grain, often causing buckling in structural members like columns, or perpendicular to the grain, where plastic deformations and local crushing typically occur at supports and points of concentrated loads (see drawing on the left of figure 2.2)[16].

Tension failures can occur both parallel and perpendicular to the grain, with the latter being particularly critical because of wood's inherently low tensile strength across fibres. These failures are especially common near notches, holes, or in curved and tapered beams [16]. Shear failures, although less frequent, are relevant for short or notched beams and are characterized by fibre slippage leading to cracks parallel to the grain (see drawing on the right of figure 2.2) [16].

Finally, biological deterioration such as fungal decay or insect attack can compromise timber strength, particularly under prolonged high moisture conditions [16]. although this is rare in dry, indoor service conditions.

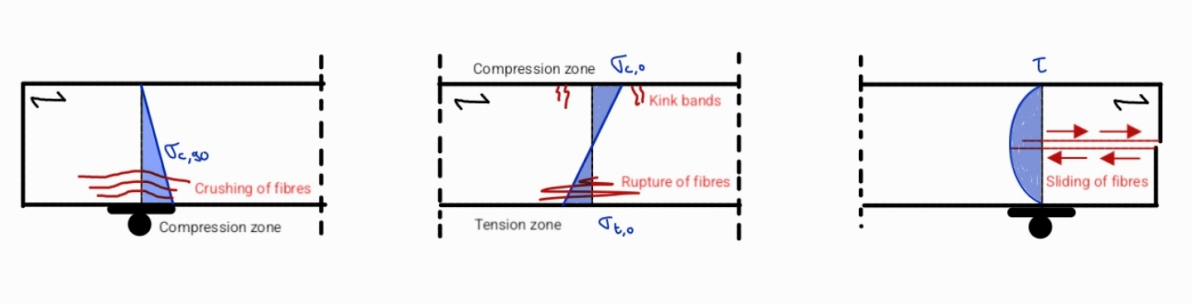

Figure 2.2: Different failure mechanisms in a simple supported timber beam.

2.2. Typical timber joints

Timber joints are critical components in structural timber systems, governing the load transfer between members and influencing the overall mechanical performance of a structure. Various joint types exist, ranging from traditional carpentry connections to modern engineered solutions reinforced with steel plates and mechanical fasteners. These modern joints are essential for ensuring sufficient strength, ductility, and stiffness in engineered timber systems [8][25].

Timber-to-timber joints

Modern timber-to-timber connections often utilize mechanical fasteners such as dowels, bolts, nails, or screws. Some common joint types include:

- **Double shear dowel joints:** Widely used in glulam or LVL members where dowels or bolts pass through timber elements, often combined with slotted-in steel plates to improve force distribution [24].
- **Inclined or self-tapping screw joints:** Particularly suited to CLT assemblies and offering high performance due to their enhanced withdrawal resistance and ductile behaviour under combined loading [44].

Timber-to-steel joints

Timber-to-steel joints are prevalent in hybrid structures, where the high strength and precision of steel components complement the sustainability and aesthetics of timber:

- **Slotted-in steel plates with dowels or bolts:** Commonly used for moment-resisting joints in glulam or LVL frames. Internal steel plates increase the joint's stiffness and allow for concealed connections (see figure 2.4) [13][4].
- **Steel brackets or angle connectors:** Allow quick assembly and high axial and shear resistance, used in post-and-beam systems and CLT connections (see figure 2.3) [26].
- **Glued-in rods:** High-capacity joints formed by bonding steel rods into pre-drilled holes using epoxy resin or adhesive. These offer excellent strength but require controlled installation [18].

Figure 2.3: Plates and connectors for timber from Rothoblaas. Adapted from Rothoblaas (n.d.). https://www.rothoblaas.com/products/fastening/brackets-and-plates

Figure 2.4: The High Line – Moynihan Connector. Reprinted from Skidmore, Owings & Merrill and Sanjuan (n.d.), via Thornton Tomasetti. https://www.thorntontomasetti.com/project/high-line-moynihan-connector

Examples in practice

Many different steel-to-timber or timber-to-timber joints can be found in practice, often designed exclusively for a certain application. Some more mainstream examples are:

- **Long-span glulam trusses:** Often use internal steel plates and dowels to achieve efficient structural profiles [48].
- **Hybrid beam-to-column joints:** Use slotted-in plates for moment transfer in multi-story frames [15].
- **CLT connections:** Employ angle brackets and self-tapping screws for reliable and repeatable performance in mid-rise buildings [9][13].

In figure 2.5 below, a complex hybrid joint is shown.

Figure 2.5: Complex hybrid steel-timber joints in Fondation Louis Vuitton. Adapted from HESS TIMBER (n.d.). https://www.hess-timber.com/en/references/detail/museum-fondation-louis-vuitton/

Understanding the design, failure modes, and stiffness characteristics of such joints is essential for both serviceability and ultimate limit state design. Eurocode 5 [13] and its upcoming 2025 update provide comprehensive design rules and models for joints with dowels, bolts, and slotted-in steel plates.

2.3. Connection behaviour of timber

Timber connections play a critical role in ensuring structural integrity, load transfer, and ductility in timber structures. However, due to the anisotropic nature of wood, these connections are often prone to specific failure mechanisms that limit the structural performance of timber assemblies, especially when loaded perpendicular to the grain.

Connection types in timber construction

Timber structures commonly use mechanical connections such as dowels, screws, bolts, and nails, often combined with steel plates. These fasteners enable various configurations, including beam-to-column, wall-floor-wall, and panel-to-panel joints [35]. They can be categorized as:

- Mechanical connections; nails, screws, bolts, dowels
- Adhesive joints; glued timber
- Hybrid systems; combining timber and steel elements

In modern engineered timber buildings, connections with steel components are common due to their predictable behaviour and high capacity. Nonetheless, the integration of steel compromises the homogeneous material properties and sustainability of fully timber-based designs.

Failure mechanisms

Timber connections may fail due to several mechanisms [10][50]:

- Embedment failure: Local crushing of wood fibres around dowel-type fasteners due to compressive stress.
- Splitting: Tension perpendicular to the grain leads to crack initiation and propagation along the grain, especially near fasteners or support zones.
- Shear failure: Occurs when shear stresses exceed the strength of the timber parallel to the grain.
- Bending failure: Beams may fail in bending due to tension on the opposite side of compression zones, especially in continuous systems.
- Fastener yield: Plastic deformation or rupture of the fastener under excessive load, often modelled using the European Yield Model (EYM).

Of these, splitting and compression perpendicular to the grain are particularly critical, since these failure modes are brittle and may occur suddenly without warning, posing safety concerns.

Influence of fastener arrangement

The number of dowel-type fasteners, their spacing, and their placement relative to the edges strongly influence the failure mechanism. For instance, a small number of fasteners tends to result in ductile embedment failure, while a larger number increases the likelihood of brittle splitting due to stress concentrations and tensile forces perpendicular to the grain [50].

The analytical work based on Linear Elastic Fracture Mechanics (LEFM) provides a framework to predict crack initiation near connections and highlights the importance of fracture energy and edge distances in design. These findings stress the need for accurate modelling of local failure modes to ensure safe and efficient connection design [50].

Relevance to structural design

In design practice, engineers must ensure that the connection's strength is not governed by the weakest failure mode. The ultimate capacity of a joint is typically determined by the lower value between the fastener capacity and the timber's splitting strength. As such, design provisions e.g. EC5 [13] include requirements for minimum edge and end distances and spacing to mitigate premature failure.

2.4. Fasteners and reinforcements in timber joints

Mechanical fasteners are essential components in timber construction, enabling the assembly of elements and the transfer of internal forces. In the following subsections, both steel and wooden fasteners, along with reinforcement strategies, are reviewed with a focus on their mechanical behaviour, applications, and limitations in timber connections.

Metal fasteners and reinforcements

In modern engineered timber structures, steel fasteners such as nails, screws, bolts, dowels, and steel plates are widely used to meet structural requirements for strength, stiffness, and durability (see figure 2.6). However, their integration introduces challenges related to sustainability, compatibility with wood, and recyclability.

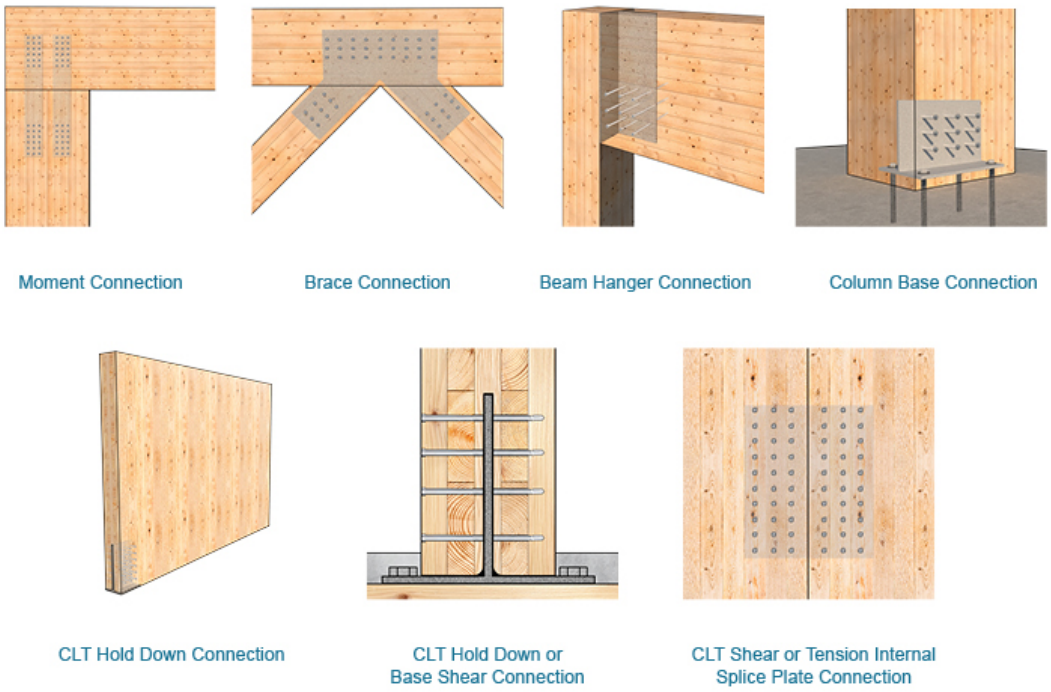

Figure 2.6: Different arrangements of nail-plated connections. Adapted from MTC Solutions (2020). `https://mtcsolutions.com/resources/tech-blogs/designing-with-internal-knife-plates/`.

Fasteners

Metal fasteners can be broadly categorized by their geometry and load transfer mechanisms:

- Nails and screws: Common in light-frame timber structures. Screws provide superior withdrawal resistance due to their threaded shank.
- Bolts and dowels: Used in larger, high-capacity joints, particularly in glulam or cross-laminated timber (CLT) construction. Dowels rely on bearing strength and are often used in multiple shear planes.
- Steel plates: Embedded or surface-mounted steel plates distribute forces and increase connection stiffness, often used in hybrid systems [35].

These components are typically designed using the *European Yield Model (EYM)*, which predicts the load-bearing capacity of dowel-type fasteners by considering fastener yielding and wood embedment failure modes [13].

Steel fasteners offer several advantages:

- High strength-to-size ratio, enabling compact connections;

- Well-documented behaviour under different loading conditions;
- Predictability and reliability in both design and construction;
- Applicability in prefabrication and modular construction [53].

These features explain their dominance in engineered timber systems, particularly where code compliance and performance guarantees are essential.

Despite their structural benefits, metal fasteners pose limitations in terms of:

- Material incompatibility: Differential thermal expansion, moisture movement, and long-term creep behaviour between wood and steel can lead to interface deterioration [23].
- Corrosion: In humid environments, fasteners may corrode, reducing their capacity and damaging surrounding wood.
- Reduced recyclability and disassembly: Metal fasteners complicate end-of-life scenarios for timber buildings, as they must be separated before reuse or recycling.
- Embodied carbon and material intensity: Steel contributes significantly to the environmental footprint of otherwise renewable timber structures [7].

These concerns are increasingly relevant as the construction sector shifts toward circular and fully bio-based design approaches. As a result, researchers and practitioners have explored alternatives such as timber-only joints or reinforcement using wooden dowels to reduce or eliminate steel in connections.

Reinforcement

Compression perpendicular to the grain (CPG) is one of the critical weaknesses in timber structures because the anisotropic nature of wood results in low compressive strength across the fibres [43]. This makes reinforced strategies especially relevant in areas like beam supports, bearing zones, and notches. The main goal of reinforcement perpendicular to the grain is to increase load-carrying capacity, prevent local crushing, and control deformations that can lead to serviceability issues [21].

Recent research has focused primarily on using fully threaded self-tapping screws as reinforcement elements. These screws improve the capacity of the timber member by engaging both the withdrawal and compression capacities of the reinforcement. The screws can prevent failure at the loaded area by redistributing stresses into the uncompressed wood zones, essentially bypassing the weaker perpendicular-to-grain zones [1]. The draft prEN 1995 Eurocode [13] introduces explicit capacity models for such reinforced members, considering both screw withdrawal and buckling limits (See chapter 2.8).

Key failure modes for screw-reinforced timber under CPG include:

- Timber crushing under the applied load;
- Withdrawal of the screws if insufficient anchorage is provided;
- Buckling of long, slender screws under compression [2].

Sensitivity studies show that the length and diameter of the screws, their arrangement, and the load plate geometry all play significant roles in the effectiveness of reinforcement [1]. Notably, the assumed load diffusion angle (typically 45°) influences the effective area used in design models, but experimental studies suggest that real stress redistribution can deviate from theoretical predictions, calling for more nuanced capacity models [11].

A critical research need is the development of probabilistic models that incorporate geometric parameters, material variability, and load configuration effects, as deterministic Eurocode models often fail to predict the observed failure modes and actual capacities [1]. This highlights a gap for future research into more adaptable, data-driven design methods.

Overall, the state of the art in reinforcement perpendicular to the grain is well developed for steel-based reinforcements but still evolving in terms of accurate predictive models, particularly under complex loading or non-standard geometries.

Wooden fasteners and reinforcements

Wooden dowels have re-emerged as a viable alternative to metal fasteners in structural timber connections, especially within the context of sustainable and fully bio-based construction. Unlike steel components, wooden dowels are compatible with the anisotropic behaviour of wood, offer better thermal performance, and are more environmentally friendly in both production and disposal. An example of the use of densified wooden dowels is shown in figure 2.7.

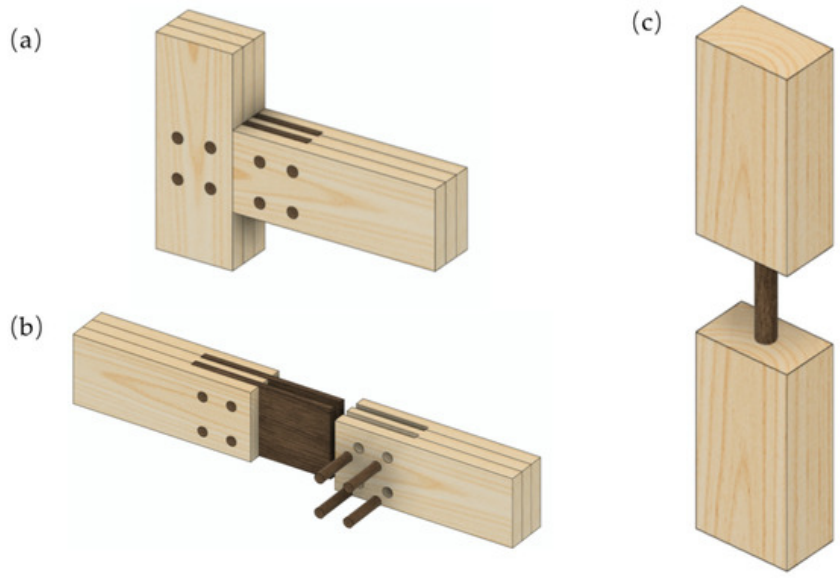

Figure 2.7: Examples of applications using the densified wood as connection materials: (a) beam-column connection, (b) beam-beam connection, and (c) glued-in-rod joint. Adapted from L. Han et al. “Adhesive- and metal-free assembly techniques for prefabricated multi-layer engineered wood products: A review on wooden connectors”. In: Forests 14.2 (2023), p. 311.

Fasteners

Several experimental studies have shown that wooden dowels, when correctly dimensioned and positioned, can achieve comparable strength to steel fasteners, particularly under shear and compression. The mechanical behaviour of wooden dowels is influenced by their diameter, length, density, and interaction with the base material. For example, densified wood dowels have been shown to achieve bending strengths exceeding 100 MPa and high stiffness, outperforming birch dowels and approaching the capacity of metal fasteners [46].

Failure modes in wood-dowel joints can include dowel bending, embedment in the timber, or shear-out. These are typically categorized using adaptations of the European Yield Model (EYM), which has been extended to include wood dowels by accounting for their lower yield moment and density-driven embedment behaviour [36]. Researchers have proposed modifications to the EYM to better reflect the unique failure characteristics of timber-to-timber joints with wooden fasteners [47].

Wooden dowels offer potential in shear-dominated connections, such as multiple shear plane joints or gusseted connections. Tests on dowels under double shear have demonstrated comparable ductility to steel pins, particularly when compressed wood is used as the dowel material [27]. This suggests suitability for replacing traditional metal fasteners in a wider variety of connection types, including beam-to-beam and beam-to-wall joints.

Furthermore, studies show that wooden dowels contribute to the global bending behaviour of dowel-reinforced members. Their placement and orientation can influence rotational stiffness and overall flexural performance, which is especially relevant in continuous beams or frame nodes [46].

Reinforcement

A key advantage of wooden dowels is their ability to enhance the transverse compression performance of timber members. Reinforcement with wooden dowels has been shown to improve the local compression strength and modulus of elasticity of wood when loaded perpendicular to the grain. Increas-

ing dowel length and diameter leads to a more favourable stress distribution and greater load-carrying capacity [60][39].

Figure 2.8: Densified wood dowel reinforced specimen preparation: a) pre-drilling, b) dowel insertion and adhesive curing, c) excess dowel removed and sanded finish. Adapted from C. O'Ceallaigh et al. "Numerical investigation of reinforcement of timber elements in compression perpendicular to the grain using densified wood dowels". In: Construction and Building Materials 288 (2021), p. 122990.

Recent studies employing finite element models (FEM) with cohesive zone modelling (CZM) have validated the potential of densified wood dowels to improve compression performance [39]. These models, developed in ABAQUS, show strong agreement with experimental data and accurately predict yielding, fibre crushing, and dowel-timber interaction damage in compression zones. The results indicate that an increase in dowel diameter and length enhances both stiffness and strength, though improvements plateau when the dowel length-to-diameter ratio exceeds 15.

Despite this progress, significant research gaps remain. Notably, most current FEM studies focus exclusively on compression perpendicular to the grain, while neglecting the modelling of bending moment and shear forces, which are essential for a comprehensive understanding of real-world structural joints. The interaction between reinforcement effectiveness and global beam behaviour (e.g., bending stiffness, crack propagation under combined loads) remains under-explored. Additionally, the group effect of multiple dowels and their simultaneous action in complex loading scenarios, such as in column-beam-column connections, requires further investigation.

These gaps highlight the need for extended parametric FEM studies that incorporate multi-axial stress states, enabling the development of generalizable design strategies for timber-only reinforcement schemes.

Despite their promise, the application of wooden dowels in structural timber design requires careful consideration of dowel-to-timber stiffness compatibility, moisture sensitivity, and manufacturing tolerances. Analytical design models need further calibration with experimental data to reliably predict dowel behaviour across different load cases and geometries. Current Eurocode provisions are still limited and may require adaptation or supplementation with project-specific testing for innovative dowel-based joints [47].

2.5. Densified wood

Densified wood (DW), also referred to as compressed wood, is an emerging high-performance, bio-based material used to enhance timber connections. Through thermo-mechanical processes involving heat, moisture, and compression, low-density wood species can be transformed into materials with significantly improved mechanical properties, including increased density, strength, and stiffness [57]. Typical densities exceed 1000 kg/m^3, enabling DW to serve as a competitive alternative to metallic fasteners or hardwood dowels in structural joints [41]. See figure 2.7 for examples of the application of DW in connections.

Applications in structural joints

Studies have demonstrated that densified wood connectors can perform effectively in a variety of applications including dowel-type joints, glued-in rods, and portal frames. Mehra et al. [33] experimentally

evaluated beam-column joints with densified wood dowels (made from Scots Pine (Pinus sylvestris)) and plates (made from Western Hemlock (Tsuga heterophylla)), reporting comparable moment capacity and rotational stiffness to traditional steel-based solutions. They also found that fully adhesive- and metal-free portal frames (made from Irish-grown Douglas fir (Pseudotsuga menziesii)) using the same densified wood dowels and plates achieved similar lateral load-carrying capacity to glued-laminated timber frames [34].

Mechanical behaviour and durability

In addition to its mechanical performance, densified wood exhibits a shape memory or ”spring-back” effect, where it tends to recover its original shape after compression. This behaviour helps maintain pressure between members and contributes to joint durability. [41]. However, the long-term behaviour under cyclic humidity or load, as well as standardization for design, remains underdeveloped.

Design optimization and failure modes

Recent experimental investigations have focused on refining geometries and connector layouts to minimize brittle failure in all-wood systems [33][34]. Optimized designs reduced the risk of premature column splitting, and tests revealed that reduced connector thickness had little effect on moment capacity, suggesting spacing and dowel arrangement as more critical factors.

Sustainability and future potential

Despite ongoing challenges related to moisture sensitivity and design codification, densified wood shows strong potential for sustainable construction. Its successful application in adhesive- and metal-free structural systems demonstrates its relevance for circular timber engineering.

Densified Wooden dowels as compression reinforcement

The use of wooden dowels, particularly densified dowels, as reinforcement for timber elements loaded perpendicular to the grain has gained attention as a sustainable alternative to metal-based solutions.

Recent experimental studies have demonstrated the performance of densified dowels in compression reinforcement. Zhang et al. [60] reinforced the support zones of glulam beams (Japanese larch (Larix kaempferi (Lamb.) Carriere)) using densified wood dowels (Schima superba (Schima superba Gardner & Champ.)) and showed increased capacity and reduced local crushing. The performance was influenced by dowel spacing, diameter, and insertion depth.

Finite element simulations by O’Ceallaigh et al. [39] showed that densified dowels redistribute stresses away from the support face and reduce local strains. The dowels (cots Pine (Pinus Sylvestris)) function as stiff inclusions within the timber matrix (Douglas Fir (Pseudotsuga menziesii)). However, failure may still occur due to dowel buckling, adhesive failure, or splitting in the surrounding wood, depending on dowel geometry and placement.

Although promising, densified wooden dowels are not yet included in structural design codes such as Eurocode 5. Design equations for their axial capacity, fire resistance, and anchorage behaviour are not available, limiting their application in engineering practice. There is a clear need for standardized testing protocols and design models to validate and implement dowel-based reinforcement in timber structures.

Withdrawal capacity

The withdrawal performance of densified wood dowels has been experimentally assessed in recent studies focusing on glued-in configurations. Densified dowels (poplar (Populus tomentosa carriere)) embedded in glued laminated timber (Mongolian Scots pine (Pinus sylvestris var. mongolica Litv.)) exhibit significantly higher pull-out capacities than non-densified dowels. Peak withdrawal forces of up to 32 kN per dowel were observed, with failure typically occurring in the timber substrate rather than the dowel itself [59][58].

Pull-out capacity increases with embedment depth, until a length of approximately 10 times the dowel diameter [58]. High-performance epoxy adhesives and proper surface preparation should be applied to fully utilize the densified dowels capacity [58][59]. Surface roughness and the densification process

contribute to improved bonding due to increased friction and mechanical interlocking along the dowel surface [59]. Mechanical interlocking occurs when adhesive penetrates surface irregularities and pores, creating a locking effect that enhances resistance against slip between dowel and surrounding timber.

Although short-term performance is promising, the long-term durability of densified wood dowels under cyclic environmental conditions (e.g., moisture changes) requires further investigation [59].

2.6. Fire exposure

Effective Cross-Section Method

The fire resistance of timber elements is commonly assessed using the Effective Cross-Section Method (ECSM), which assumes that only a reduced portion of the original cross-section retains sufficient strength and stiffness after fire exposure. The charred and thermally degraded layers are excluded from structural calculations [14].

According to Eurocode 5 (EN 1995-1-2), this method is a primary approach for designing timber beams, columns, and panels under standard fire conditions. It simplifies the residual capacity by subtracting a charring depth (d_{ch}) and an additional zero-strength layer (d_0) from the original section [6][22] (see Section 2.8).

As shown in Figure 2.9, the charred layer has no capacity, and d_0 accounts for reduced strength and stiffness in the heated but uncharred zone. Eurocode 5 prescribes $d_0 = 7,$ mm for standard fires, based on Schaffer's early tests on softwood glulam [6].

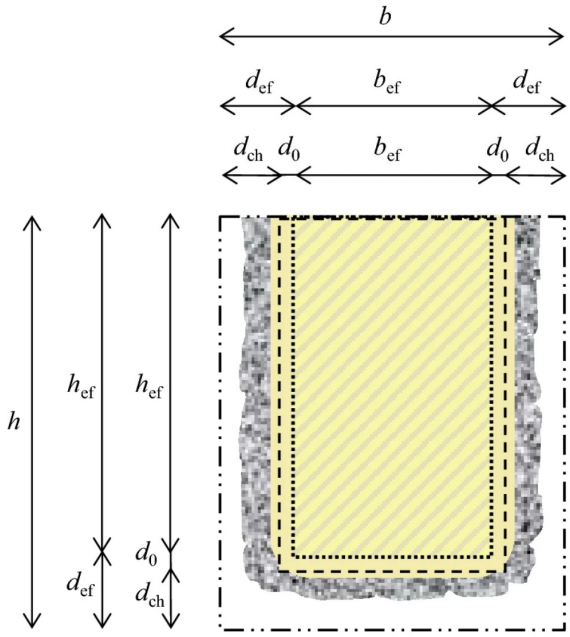

Figure 2.9: Effective cross-section with all parameters. Adapted from Sabina Huč et al. (2025) [22].

However, recent studies show that d_0 is not constant. Its thickness can vary with fire duration, loading type, the number of exposed sides, and section geometry [22][49][31]. Under natural or parametric fires, which include a cooling phase, both d_{ch} and d_0 may increase significantly. In such cases, non-linear models are often required for accurate prediction [5].

Reinforcement placement

The effectiveness of timber-based reinforcement under fire exposure depends on its location relative to the evolving char and zero-strength layers. If reinforcement is placed within the sacrificial depth, typically the outer 25–30 mm of the cross-section in standard fire scenarios, it will degrade early and offer little contribution to post-fire load-bearing capacity [22][49]. Effective reinforcement must therefore

be embedded deeper, ensuring it remains part of the residual load-bearing cross-section. Experimental tests show that reinforcements positioned near mid-depth in bending members, or in compression zones protected by surrounding wood, can help preserve structural integrity and increase time to failure [6][31].

2.7. Numerical modelling

Finite Element Modelling (FEM) has become an indispensable tool for studying the mechanical behaviour of timber joints. The anisotropic and brittle nature of wood, combined with its non-linear interaction with fasteners, makes analytical prediction challenging. Numerical simulation allows researchers to capture these complexities, enabling the assessment of load distribution, local crushing, progressive damage, and ultimate failure. Such models are particularly relevant when developing timber-only connection concepts, where the goal is to minimise reliance on steel reinforcement.

Modelling approach and orthotropic material representation

The mechanical response of timber is strongly direction-dependent. To capture this behaviour, FEM studies typically employ orthotropic constitutive models with distinct elastic moduli, shear moduli, and Poisson's ratios defined in the longitudinal (L), radial (R), and tangential (T) directions. In addition, compression perpendicular to the grain is governed not only by elastic deformation but also by non-linear processes such as plasticity, densification, and localized crushing.

Zhang et al. [60] developed a 3D FE model in ANSYS to investigate wood members reinforced with wooden dowels under transverse compression. The timber was represented as an orthotropic continuum with non-linear stress–strain behaviour to capture yielding and densification. Load transfer between dowels and surrounding timber was modelled via frictional contact formulations, allowing simulation of embedment effects. Their results confirmed that dowel reinforcement significantly enhances both load-carrying capacity and stiffness, while also redistributing stresses in the compression zone.

Cohesive zone modelling and damage mechanics

While continuum plasticity models can describe local crushing of timber, they are insufficient to capture fracture phenomena such as splitting, fibre separation, or interface debonding. To address this, Cohesive Zone Modelling (CZM) has been widely adopted. In CZM, potential crack paths are represented by zero-thickness cohesive elements governed by traction–separation laws. These laws describe the initiation of damage (typically via a maximum stress or quadratic stress criterion), followed by progressive stiffness degradation and eventual failure once fracture energy is dissipated.

O'Ceallaigh et al. [39] applied a FEM–CZM hybrid framework in ABAQUS to analyse timber members reinforced with densified wooden dowels. Timber was modelled as an orthotropic elastic solid, while dowel–timber interfaces were described by cohesive elements with bilinear traction–separation laws. This approach successfully reproduced experimentally observed behaviour, including:

- **Initial elastic stiffness**, governed by wood anisotropy.
- **Onset of fibre crushing**, localised around dowel contact zones.
- **Progressive stiffness degradation**, driven by interface separation and fibre failure.

Their study also revealed that dowel geometry (diameter, spacing, and slenderness ratio) influences performance, though the benefit plateaus beyond a dowel length-to-diameter ratio of about 15.

For dowel-reinforced joints under compression perpendicular to the grain, CZM provides a powerful means to model both local embedment and splitting behaviour, which are otherwise difficult to capture with classical plasticity formulations.

Orthotropic plasticity and the hill criterion

To simulate inelastic behaviour of timber in continuum elements, yield criteria originally developed for metals have been adapted to account for orthotropy. One of the most commonly applied formulations is the Hill criterion, which generalises the von Mises yield surface to orthotropic materials by introducing direction-dependent yield stresses.

The Hill criterion is particularly suitable for modelling compression perpendicular to the grain, since it allows differentiation between longitudinal, radial, and tangential strengths. In FE applications, this criterion can be coupled with associated or non-associated flow rules to simulate plastic deformation, capturing effects such as:

- **Local crushing** beneath dowels or bearing zones.
- **Anisotropic yielding**, with much lower resistance perpendicular than parallel to the grain.
- **Interaction effects**, where combined stresses in multiple directions govern yielding.

When combined with damage mechanics or CZM, the Hill criterion provides a robust framework for describing the full progression of behaviour in timber joints: from initial elastic response, through plastic crushing, to eventual fibre rupture or splitting.

2.8. Relevant design standards

The design of timber structures in Europe is governed by EN 1995-1-1 (Eurocode 5), which provides rules for structural members, mechanical connections, reinforcement methods, and fire design. The 2024 revision (EN 1995-1-1:2024) [13] introduces updated provisions, particularly regarding reinforcement perpendicular to the grain, composite actions, and durability.

Compression perpendicular to grain

$$\sigma_{c,90,d} \leq k_{mat} \cdot k_{c,90} \cdot f_{c,90,d} \tag{2.1}$$

where:

- k_{mat} = factor accounting for the material behaviour and degree of compressive deformation perpendicular to grain;
- $k_{c,90}$ = stress spreading factor;
- $f_{c,90,d}$ = design compressive strength perpendicular to grain;

In the 2023 draft of Eurocode 5, the strength of timber loaded perpendicular to the grain is no longer treated as a fixed material property alone, but is influenced by the level of deformation that can be tolerated in the specific structural context. This is expressed via the deformation class, which governs the value of k_{mat}.

Three deformation cases are defined:

- **Case A:** Applies when deformations result in member or system instability or causes unacceptable damage to other components.
- **Case B:** Applies when deformation has no significant effect on member or system stability.
- **Case C:** Applies when deformation has no significant effect on member stability and failure of the member does not lead to failure of the whole structure or parts of it.

The classification into Case A, B, or C depends on the allowed strain in the compressed area, which may vary between materials. For example, in solid softwood, strains up to 0.2 (i.e. 20% relative deformation) may be acceptable in Case C. Table 2.1 summarizes typical values of k_{mat} per material and deformation case.

Table 2.1: Typical values of k_{mat} based on deformation case and material type (after EC5:2023 Table 8.1)

Material	Case A	Case B	Case C
Solid wood (SWB)	1.4	2.1	2.7
Softwood LVL (edgewise)	1.0	–	–
Softwood LVL (flatwise)	1.3	1.9	2.5
Hardwood LVL (edgewise)	1.0	1.2	–
Hardwood LVL (flatwise)	1.3	1.6	–

These updated provisions allow for more performance-based design in compression zones, especially when reinforcement, stress distribution, or detailing can justify increased load-bearing capacity perpendicular to grain.

Mechanical fasteners

Steel fasteners

The design of mechanically fastened joints is based on Johansen's yield theory, which considers various failure modes involving embedment of the timber and yielding of the fastener. The characteristic load-carrying capacity of a single fastener in a shear plane (single shear) is given by:

$$F_{v,Rk} = \min\{f_{h,k} \cdot d \cdot t,\ F_{y,Rk}\} \tag{2.2}$$

where:

- $f_{h,k}$ = characteristic embedment strength of timber;
- d = diameter of the fastener;
- t = thickness of the timber side member.
- $F_{y,Rk}$ = characteristic yield moment capacity of the fastener.

The equations for the characteristic yield moment of the fasteners can be found in equation 11.15 of the new EC5 [13]. It considers all failure mechanisms of fasteners in single (and double) shear.

The characteristic embedment strength can be found in Table 11.7 of EC5. This value is based on the fastener type, plate material, diameter of the hole, and whether the hole is predrilled or not.

Wooden dowels

For wooden dowels the same equations for determining the load carrying capacity apply as for steel fasteners. However, the embedment strength and yield moment are different. The characteristic embedment strength follows:

$$f_{h,k} = 10^{-4} \cdot \rho_{dowel,k} \cdot \rho_k \frac{1,1 \cdot (1 - 0,01d)}{(3,4 - 0,045d) \cdot \sin^2 \alpha + \cos^2 \alpha} \tag{2.3}$$

Where:

- $\rho_{dowel,k}$: characteristic density of the dowel;
- ρ_k : characteristic density;
- d : diameter of the dowel;
- α : angle between the direction of the load and the grain of the wood.

The equation for the characteristic yield moment is:

$$M_{y,k} = 0,75 \cdot \frac{\pi}{32} \cdot f_{m,k} \cdot d^3 \tag{2.4}$$

Where:

- $f_{m,k}$: characteristic bending strength;
- d : diameter of the dowel.

For wooden dowels, specific rules apply for geometry and material properties. They can be found in section 11.2.3.2 (13).

Brittle failure modes of connections with dowel-type fasteners

In steel-to-timber and timber-to-timber connections where multiple fasteners are used, the failure mechanisms from figure 2.10 should be considered.

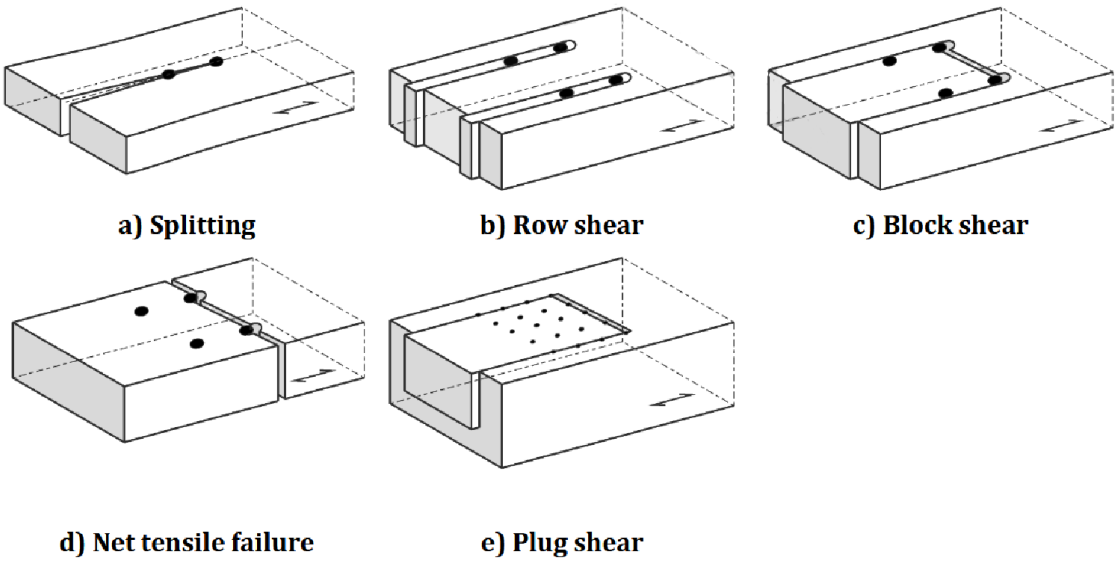

Figure 2.10: Examples of brittle failure modes. Adapted from EN 1995-1-1: Eurocode 5 (CEN, 2024) [13].

These failure mechanisms are brittle and not governed by plastic deformation but rather by the initiation and propagation of cracks, which can compromise structural safety without warning. Section 11.5 introduces requirements to ensure that such failures are avoided through detailing rules, reinforcement, or explicit verification methods.

Reinforcement should be applied where stress concentrations occur. Internal reinforcements such as fully threaded screws, bonded rods, or glued-in plates may be used, but only their axial component perpendicular to the potential crack plane may be considered in the resistance calculation. Simplified models (e.g., fracture mechanics-based approaches) or numerical simulations may be used to assess stress distributions and predict crack formation.

Bonded in rods

Eurocode 5 permits the use of bonded-in rods (typically threaded steel bars glued into timber), especially in high-performance or moment-resisting joints. These connections rely on adhesive bond strength and embedment length to transfer load. The new EC5 provides guidelines for these elements.

The axial design resistance of the bonded-in rod should be taken as:

$$F_{ax,d} = \min \begin{cases} F_{t,d} \\ F_{w,d} \end{cases} \tag{2.5}$$

Where:

- $F_{t,d}$: design tensile resistance of the rod;
- $F_{w,d}$: design withdrawal resistance of the rod.

The design tensile and withdrawal capacities of the rod are based on the diameter, (effective) withdrawal length, rod type, and other material properties.

For bonded-in rods loaded in the lateral direction, the lateral design resistance should be calculated according to formula 11.101. Embedment strength and characteristic yield moment of the rod are important factors for the lateral resistance.

Rules for minimum spacing and edge distances can be found in Figure 11.36, Figure 11.37 and Table 11.30. Minimum withdrawal length should be determined according to Table 11.29.

Compression perpendicular to grain

For members without reinforcement (EN 1995-1-1, Section 8.1.6.1), the design compressive stress perpendicular to the grain shall satisfy:

$$\sigma_{c,90,d} \leq k_{mat}\, k_{c,90}\, f_{c,90,d} \tag{2.6}$$

where the design compressive stress perpendicular to the grain is given by:

$$\sigma_{c,90,d} = \frac{F_{c,90,d}}{A} \tag{2.7}$$

The design compressive force perpendicular to the grain is defined as:

$$F_{c,90,d} = \frac{F_{c,90,k}}{\gamma_M} \tag{2.8}$$

with:

- $f_{c,90,d} = \dfrac{f_{c,90,k}}{\gamma_M}$: design compressive strength perpendicular to the grain;
- $f_{c,90,k}$: characteristic compressive strength perpendicular to the grain;
- $F_{c,90,k}$: characteristic compressive force perpendicular to the grain;
- A : loaded area subjected to compression perpendicular to the grain;
- γ_M : partial safety factor for material properties (typically $\gamma_M = 1.3$ for timber);
- k_{mat} : factor accounting for the material behaviour and degree of compressive deformation perpendicular to the grain (see Table 8.1 of EN 1995-1-1);
- $k_{c,90}$: stress spreading factor accounting for the distribution of compressive stresses within the member.

The factor k_{mat} reflects the nonlinear compressive behaviour of timber perpendicular to the grain and depends on the material type (e.g. solid timber, glued laminated timber, or CLT). The factor $k_{c,90}$ accounts for stress redistribution beyond the directly loaded area and depends on the support configuration and geometry of the bearing zone.

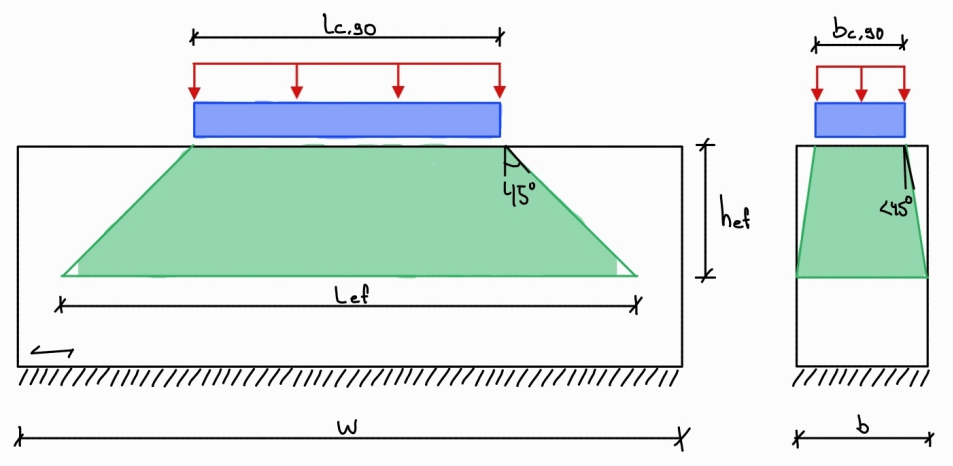

Figure 2.11: Effective stress spreading length for compression perpendicular to the grain according to Eurocode 5

According to Eurocode 5, the stress spreading factor $k_{c,90}$ accounts for the redistribution of compressive stresses perpendicular to the grain beyond the directly loaded area. It is defined as:

$$k_{c,90} = \sqrt{\frac{l_{ef}}{l_{c,90}}} \tag{2.9}$$

where the effective length l_{ef} is given by:

$$l_{ef} = \min\left\{l_{c,90} + 2 \cdot h_{ef}\,;\, w\right\} \tag{2.10}$$

with:

- $l_{c,90}$: length of the directly loaded area perpendicular to the grain;
- l_{ef} : effective length over which compressive stresses are assumed to spread;
- h_{ef} : effective depth of the member contributing to stress spreading;
- w : total width of the timber member.

The stress spreading model assumes that compressive stresses distribute into the member at an angle, leading to an increased effective bearing area. The effective length l_{ef} is limited by the total member width w to prevent overestimation of the load-carrying capacity. This formulation is applicable to unreinforced timber members and forms the basis for assessing the effectiveness of local reinforcement measures in compression zones.

The stress spreading model is also applicable in the orthogonal direction of the bearing area, using the bearing width $b_{c,90}$ and the corresponding member dimension b, and shall be evaluated similarly.

Reinforcement perpendicular to grain

Eurocode 5 allows the compression perpendicular to the grain capacity of timber members to be increased by reinforcement using fully threaded screws or rods with wood screw thread. The reinforcement enhances the load transfer in the bearing zone by combining the compressive resistance of the timber with the axial resistance of the fasteners. For reinforced contact areas, the characteristic compressive capacity perpendicular to the grain is determined as the minimum of the timber crushing capacity and the effective load distribution at the level of the reinforcement, as defined in EN 1995-1-1, Section 8.1.6.2.

When reinforcement is used (e.g., fully threaded screws), the characteristic compressive strength can be calculated as:

$$F_{c,90,Rk} = \min \begin{cases} k_{mat}\, b_{c,90}\, l_{ef,1}\, f_{c,90,k} + n \min\{F_{w,k}; F_{c,k}\} \\ b\, l_{ef,2}\, f_{c,90,k} \end{cases} \tag{2.11}$$

Where:

- k_{mat} : Load distribution factor;
- $b_{c,90}$: contact width;
- $l_{ef,1}$: effective contact length;
- $l_{ef,2}$: effective distribution length;
- $f_{c,90,k}$: timber's characteristic compressive strength;
- n : number of reinforcing elements;

The contribution of the reinforcement is governed by:

- $F_{w,k}$: the characteristic withdrawal resistance of a single fully threaded screw or rod, representing the resistance against pull-out from the timber (EN 1995-1-1, Section 11.2.2.3);

- $F_{c,k}$: the characteristic resistance of a screw or rod in axial compression, representing the load-bearing capacity of the fastener when compressed along its axis (EN 1995-1-1, Section 11.2.2.5).

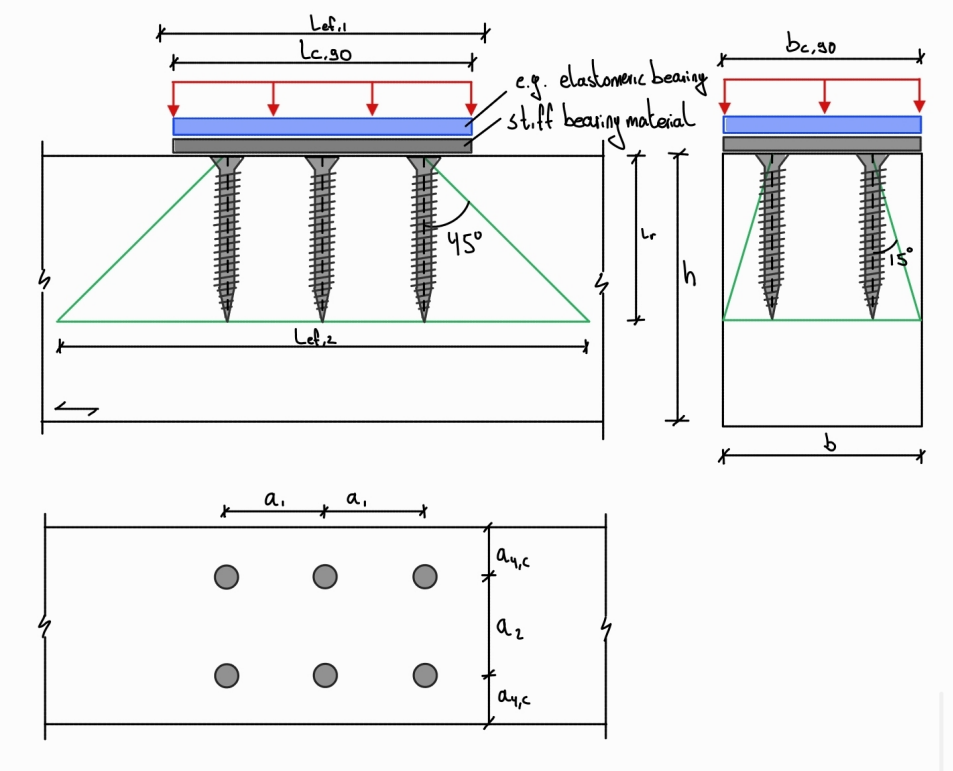

Figure 2.12: Intermediate support with reinforcement.

For intermediate supports, which are considered in this study, the effective contact length parallel to the grain $l_{ef,1}$ is defined as:

$$l_{ef,1} = l_{c,90} + 2 \cdot \min\left\{30;\ \frac{l_s}{2};\ \frac{l_{c,90}}{2}\right\} \tag{2.12}$$

In the present configuration, the load is applied directly at the support or right beside the support, such that the clear distance between the contact area and the concentrated load is zero:

$$l_s = 0 \tag{2.13}$$

As a result, the effective contact length reduces to the contact length itself.

The effective distribution length at the level of the screw or rod tips $l_{ef,2}$ for intermediate supports is given by:

$$l_{ef,2} = 2\,l_r + (n_0 - 1)\,a_1 \tag{2.14}$$

where l_r is the reinforced length from the threaded part of the screw or rod, n_0 is the number of screws or rods arranged in a row parallel to the grain, and a_1 is the spacing between them. All geometric parameters are defined in the accompanying figures.

It should be noted that the provisions described above apply exclusively to reinforcement using steel screws or rods with wood screw thread, as currently covered by Eurocode 5. Reinforcement using wooden dowels is not included in these design rules and therefore falls outside the scope of the standardised approach.

Fire design and effective cross-section

Fire resistance is covered in EN 1995-1-2 [14], using the effective cross-section method. After a time t [minutes] of fire exposure, the reduced cross-section is:

$$b_{ef} = b - k_{side} \cdot (\beta_n \cdot t + d_0) \tag{2.15}$$

$$h_{ef} = h - k_{side} \cdot (\beta_n \cdot t + d_0) \tag{2.16}$$

where:

- b, h : original width and height mm;
- β_n : one-dimensional charring rate (typically 0.65 mm/min);
- d_0 : zero-strength layer coefficient (typically 1.0),
- t : time in min;
- k_{side} : number of respective opposite sides exposed to fire.

The placement and penetration depth of reinforcements (like dowels) affect which parts of the member remain structurally effective after fire. For example, dowels located near charred surfaces may no longer contribute to load transfer. This occurs because the surrounding timber required to transfer and keep forces to the dowel is weakened or lost due to charring.

Implications for this research

While Eurocode 5 provides detailed calculations for metallic reinforcement, no formal guidelines exist for:

- Load-carrying capacity of wooden dowels under compression and withdrawal;
- Contribution of densified wood dowels to reinforcement perpendicular to the grain;
- Fire performance of timber connections reinforced with wood-based elements, including how penetration depth affects the effective width under charring.

This thesis aims to investigate whether wooden dowels can provide comparable reinforcement and to propose insights that could inform future code updates.

2.9. Research gap

Recent literature demonstrates the potential of wooden dowels as reinforcement for timber elements subjected to compression perpendicular to the grain. Experimental studies and numerical investigations indicate that wooden dowels, particularly when densified, can enhance local stiffness and delay crushing in support zones. However, existing research is largely fragmented. Studies either focus on isolated material or fastener behaviour, or on global joint performance in which steel-based reinforcement remains the dominant reference solution.

A clear gap exists in the understanding of the component-level mechanical behaviour of dowel–timber systems used as local reinforcement rather than as conventional fasteners. In particular, the interaction between compression perpendicular to the grain and additional stress components such as shear and bending is insufficiently understood. The extent to which dowel geometry, spacing, and positioning influence stress redistribution, deformation compatibility, and timber failure mechanisms has not been systematically investigated. Furthermore, while withdrawal and side interaction are often implicitly assumed, their effective mobilisation at system level remains unclear.

The influence of dowel material and surface characteristics represents an additional gap. Although densified wood fasteners have been studied in isolation, their interaction with structural timber under compression perpendicular to the grain, including the role of dowel tip geometry and local contact behaviour, is not well documented. As a result, the transferability of isolated test results to structural applications remains uncertain.

From a design perspective, current standards such as EN 1995-1-1:2024 [13] do not recognise wooden dowels as reinforcement elements for compression perpendicular to the grain. No design rules are

provided for timber-to-timber reinforcement, including spacing requirements, effective strength contributions, or verification formats. This lack of codified guidance limits the practical implementation of fully timber-based reinforcement strategies.

This research addresses these gaps by means of finite element modelling at the component scale, supported by analytical considerations. The numerical framework is used to investigate load-transfer mechanisms, stress redistribution, and partial mobilisation of dowel contributions in reinforced timber elements. A parametric study is conducted to assess the influence of dowel geometry and configuration, and the findings are applied in a structural case study to evaluate the implications at system level and in comparison with steel-based reinforcement solutions.

2.10. Synthesis: answers to sub - research questions

Research question 1: *How have timber-based reinforcement elements been applied in previous research to enable reliable structural performance of timber joints under various loading conditions?*

Different timber-based reinforcement elements have been applied in structural joints. Most research is devoted to wooden dowels as fasteners or as reinforcement perpendicular to the grain. Both compressed wood (CW) and densified wood (DW) are used with dissimilar types of wood for both processes. As fasteners they can achieve comparable strength to steel counterparts, particularly under shear and compression, if positioned right. The draft version of the new EC5 incorporated guidelines for wooden dowels as fasteners.
Reinforcement with wooden dowels has been shown to improve the local compression strength and modulus of elasticity of wood when loaded perpendicular to the grain. An increase in dowel diameter and/or length increases both stiffness and strength, although stagnating when the dowel length-to-diameter ratio exceeds 15. Implementation of 2 to 6 dowels can increase the compressive strength perpendicular to grain with 16-30% and the stiffness of the system perpendicular to grain with 13-36% .
Other research focused on DW plates in beam-column connections together with DW dowels reporting comparable moment capacity and rotational stiffness to traditional steel-based solutions.
Additionally, the withdrawal capacity of glued-in dowels has been tested from which emerged that DW dowels exhibit significantly higher pull-out capacities than non-densified wooden dowels. Surface roughness and the densification process contribute to improved bonding due to increased friction and mechanical interlocking. This provides a foundation for further research, including the investigation of glued-in rods or shear reinforcement at supports.

Research question 2: *What are the dominant failure mechanisms in timber joints, reinforced with timber-based elements, under various loading conditions?*

For timber connections the following five failure mechanisms are critical: Embedment failure, splitting, shear failure, bending failure and fastener yield. The first two failure mechanisms are brittle and should be avoided in design. The different brittle failure modes can be seen in figure 2.10. Embedment failure and fastener yield are part of the European Yield Model (EYM). Failure modes for connections with wooden fasteners and connectors are still governed by this model, but utilize their own equations. This has been incorporated into the forthcoming Eurocode.
For wooden dowels used as compression reinforcement, buckling of the dowel and adhesive failure are additional failure mechanisms besides the standard failure mechanisms of wood.
Failure modes in case of dowel pull-out typically occur in the timber substrate rather than the dowel itself, provided high-performance adhesives and proper surface preparation.

3

Case Study

This chapter presents a case study of a hybrid timber building to evaluate the potential for reducing steel content through the application of timber-based reinforcement strategies. The case study serves to translate the analytical and numerical insights developed in the preceding chapters into a structural design context and to assess their relevance at building scale.

In the first part of the chapter, the steel content of the selected building is quantified on a per-area basis. Structural components and connection details are extracted from the project documentation, and the steel mass associated with individual members and connections is calculated. Based on this assessment, connection types are ranked according to their steel intensity in order to identify those with the greatest potential for material optimisation.

In the second part of the chapter, timber-based alternatives to selected steel-reinforced connections are investigated at design level. Alternative reinforcement strategies are evaluated using Eurocode 5 design provisions, with attention to the influence of reinforcement placement on the effective cross section of timber members. In addition, the implications of the proposed reinforcement strategies for fire resistance are assessed using effective cross-section methods.

Through this two-step approach, the case study provides a structured evaluation of where steel reduction is most impactful within the structural system and how timber-based reinforcement strategies may be applied in practice under current design frameworks.

3.1. Part I: Steel quantification in the reference building

3.1.1. Selected building

The selected case study is the new municipality building of Krimpenerwaard, located in Bergambacht. With completion expected in 2026, it is widely recognized as one of the most sustainable and circular municipal buildings in the country [55]. The project consolidates five former municipal offices into a single central one, improving operational efficiency and enabling adaptive reuse of former buildings [56].

Figure 3.1: Impression of the final design of the municipality building Krimpenerwaard. Adapted from Gemeente Krimpenerwaard (2023). https://www.krimpenerwaard.nl/definitief-ontwerp-nieuw-gemeentehuis

Figure 3.2: Impression of the design of the municipality building Krimpenerwaard. Adapted from Gemeente Krimpenerwaard (2023). https://www.krimpenerwaard.nl/definitief-ontwerp-nieuw-gemeentehuis

The building was designed by Ector Hoogstad Architecten in collaboration with DOOR Architecten. The design consists of three parts connected through a central atrium, referencing the linear structure of the surrounding 'slagen' polder landscape [30]. Transparent facades and integrated interior greenery connect the building to the local environment.

The building is designed to be energy-neutral and gas-free. It features a fully PV-covered roof, visible rainwater management systems, and climate-adaptive landscaping. In addition, the project supports biodiversity through porous paving and integration with adjacent ecological networks [55, 28]. The design sticks to four circular principles: use of renewable/secondary materials, reuse of structural elements, ease of disassembly, and future adaptability [20].

The gross floor area is approximately 7200–8000 m². Construction began in early 2025 and is expected to be completed by early 2026. The total construction budget is around €35 million [56].

This building was selected for the case study because it is representative of a broader design approach used in several recent timber projects by IMd. The structural system, material use, and joint detailing closely reflect the firm's general design philosophy for timber buildings. Specifically, the use of modular glulam elements and connections is consistent with other IMd projects, making this building a relevant and transferable example for evaluating connection design, steel usage, and potential alternatives.

3.1.2. Structural system and material use

The primary load-bearing structure is composed almost entirely of timber. Glued laminated timber (glulam) is used for the columns and beams, while the floors consist of prefabricated timber channel-plate elements (LIGNATUR) [20]. These floor elements are integrated with the beams in a modular system that supports efficient on-site assembly and future disassembly. The structural grid consists of three timber volumes connected via a central atrium, forming a rigid frame structure without permanent internal walls [30].

The building utilizes continuous beams and column, which reduces bending moments at mid-spans and enables smaller cross-sections compared to simply supported systems. This continuity not only lowers material use but also improves stiffness and deformation control, resulting in better overall performance

under both vertical and horizontal loads. It also minimizes the number of complex joints, simplifying construction and enhancing demountability.

The design also incorporates several steel components. These elements are employed where timber performance is limited, for instance in high-stress connections or for additional bracing against lateral loads. Although no full steel frames are present, localized hybrid solutions increase overall structural resilience and easy disassembly. New concrete is used only where unavoidable, like foundations and stair cores, and even then in reduced quantities.

Overall, the structure is designed for minimal environmental impact through:

- Use of renewable and secondary materials
- Structural modularity and ease of disassembly
- Visible and accessible connection detailing
- Limiting permanent bonds (e.g., glued joints) to allow future reconfiguration

3.1.3. Steel calculation

Method

To quantify the total amount of steel used in the structure, a bottom-up estimation was carried out based on architectural and structural detail drawings provided in the design documents. The procedure involved identifying and analysing individual connection details, determining the steel components within each, and scaling their usage based on their frequency across the building.

Each connection detail was examined for its components, such as base plates, connection plates, bolts, screws, self-tapping dowels, and other steel parts. For each detail, the volume and type of steel used was recorded, along with whether it involved prefabricated steel components such as column 'shoes'. These shoes act as transition elements between two glulam columns, and look like welded H- or I-profiles as can be seen in figure 1.1b.

Using the ground floor and first floor plans, the number of occurrences of each detail type was counted manually. This yielded a detailed steel inventory per floor level. The first floor was assumed to be representative of the second floor in terms of structural layout and connection typologies. The third floor, however, contains project-specific features, including atypical and custom connections, and was therefore excluded from the calculation. This conservative approach ensures that the results reflect typical IMd-type timber-hybrid structures rather than project-specific exceptions.

All component quantities and steel weights were organized in a structured Excel sheet, with separate entries for each detail. This provides a traceable link between the drawings, connection logic, and estimated steel usage per structural element.

This steel usage analysis serves as a baseline for later comparison with alternative connection strategies developed in Section **??**. It also enables a material efficiency evaluation of the existing structure, particularly in terms of steel optimization in hybrid timber buildings.

Results

The steel content for each floor was estimated by multiplying the steel weight per connection detail by the number of occurrences across the structural grid. Table 3.2 summarizes the total estimated steel use for the ground floor and Table 3.3 for the first floor. These two levels are representative for most of the building; the second floor follows the same structural logic as the first floor, while the third floor contains more project-specific elements and is excluded from the general estimate.

To provide insight into the underlying calculations, Table 3.1 presents a component-level breakdown for one of the most frequently used details, Detail 103. This connection, used primarily to join two vertical timber columns via a steel shoe and multiple bolts, demonstrates how the total steel weight per detail is built up from plates and fasteners. Similar calculations were performed for all other details used in the project.

Table 3.1: Steel content detail 103

Detail 103									
Object		Name	Length [mm]	Width [mm]	Height [mm]	Diameter [mm]	Amount	Volume [mm^3]	Weight [kg]
Shoe	f1		370	370	25		1	3,422,500	26.9
	l1		440	350	30		1	4,620,000	36.3
	f2		370	370	25		1	3,422,500	26.9
	Bolt	M16	250			16	8	402,124	3.2
	Bolt	M16	360			16	4	289,529	2.3

Table 3.2: Steel content ground floor

Ground Floor										
Element	Plate	Rod	Anchor	L	Screw	Bolt	Nail	Tube	Other	Total
Steel content [kg]	3,209	344	718	373	42	39	7	102	1,075	5,908
Steel content [kg/m^2]										1.9

Table 3.3: Steel content first floor

First Floor										
Element	Shoe	Opleghandje	T	L	Plate	Bolt	HEA	Screw	Other	Total
Steel content [kg]	8,564	1,623	1,615	1,746	2,222	258	547	4	450	17,030
Steel content [kg/m^2]										5.6

Conclusion

The calculated steel content for the structural connections indicates a significant variation between the ground floor and the first floor, both in total weight and in distribution per square meter. The ground floor has an average steel usage of approximately 1.9 kg/m^2, resulting in a total of around 6,000 kg of steel. The majority of this steel is concentrated in column-base connections, which account for approximately 3,200 kg in base plates, 350 kg in steel rods (used to anchor the plates into the timber columns), and 700 kg in anchor elements for fixing the assemblies into the concrete foundation.

In contrast, the first floor exhibits a higher steel intensity of about 5.6 kg/m^2, with a total estimated steel mass of around 17,000 kg. This is largely due to the frequent use of steel shoes for column-to-column connections. These shoes, together with their associated bolts, contribute to approximately 50% of the total steel usage on this floor.

These findings illustrate that while both floors are highly dependent on steel for structural connections, the nature and location of those connections lead to different distributions of material use. The data from this analysis forms a critical baseline for evaluating the efficiency and circularity potential of alternative connection strategies.

3.1.4. Potential for timber-based connection alternatives

The analysis of the current building highlights a significant use of steel components in structural joints, especially in column-to-column and column-to-base connections. While these connections are effective in terms of strength and stiffness, they contribute substantially to the building's overall environmental footprint. The estimated total steel weight used in joints alone exceeds 40,000 kg, with most of it concentrated in shoes, plates, rods, and anchors.

This presents a clear opportunity for material optimization through the substitution of selected steel components with engineered timber alternatives. Potential replacements include timber dowels, higher strength timber plates, or hybrid wood-steel systems that reduce the reliance on full steel shoes. Such substitutions could improve material circularity, reduce CO_2, and enhance the architectural and tactile integration of timber structures. The case study building provides a realistic baseline against which the performance, feasibility, and environmental benefit of these alternatives can be evaluated in later chapters.

3.2. Part II: Connection analysis and design alternatives

3.2.1. Connection analysis

Ground floor

All structural connections at the ground level are column-base connections, where timber columns are anchored to the concrete foundation. In the majority of cases, these connections are subjected primarily to axial compression. Only a limited number of connections experience tension, typically in locations where vertical bracing elements terminate at the column base.

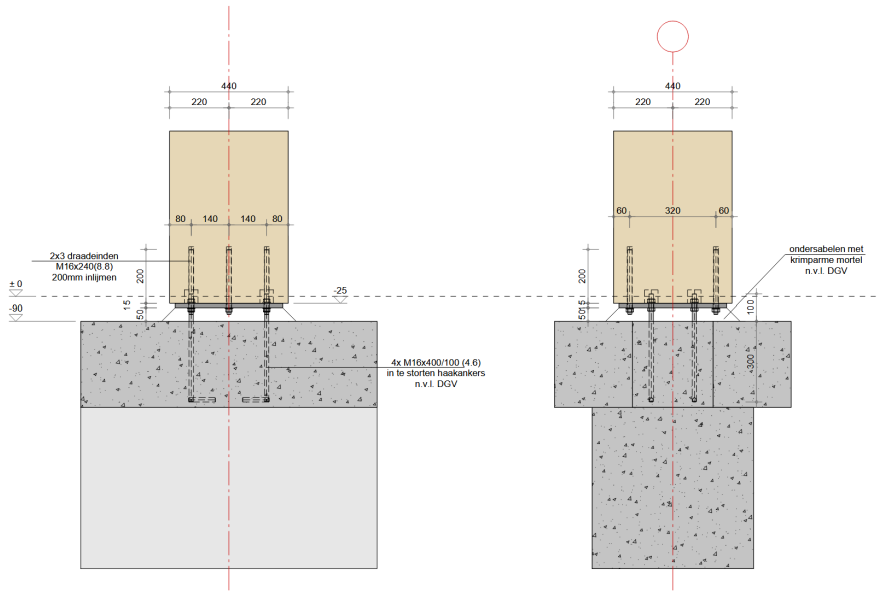

Figure 3.3: Example of a column-base connection used in the new municipality building.

The standard column-base connection consists of three key steel components: rods, plates, and anchors. Each of these elements presents different challenges and opportunities with regard to substitution by timber-based alternatives.

Rods, used to anchor the steel base plate into the timber column, show potential for replacement in purely compressive connections. In these cases, the axial force transfer can potentially be achieved using compressed timber blocks or glued-in wooden dowels, reducing the reliance on high-strength steel elements. However, for connections under tension or with lateral load transfer requirements, timber alternatives may not yet provide sufficient capacity or ductility.

Plates, forming the interface between the column and foundation, are more difficult to replace. In order to maintain load transfer efficiency, especially in the direction perpendicular to the grain, the replacement material would need to exhibit a high compressive strength perpendicular to grain ($f_{c,90,k}$). This is a known weak point of timber, and replacing plates would require either high-performance engineered wood products or novel reinforcement strategies. Additionally, the plate region is highly susceptible to interaction with moisture and concrete, which introduces durability concerns that fall outside the scope of this study.

Anchors, used to fix the column-plate assembly to the concrete slab, face similar challenges. Their exposure to moisture, interaction with concrete, and load path complexity make a direct timber replacement difficult. Addressing these issues would require in-depth research into long-term behaviour, corrosion protection, and hybrid joint systems, which also exceeds the current scope.

Finally, a small number of connections at the ground floor involve the termination of bracing systems at the column foot. These locations are more complex due to their combined axial and lateral loading, and the need for reliable force transfer paths. The resulting connection detailing is highly project-specific and poses additional challenges for standardisation or material substitution.

First floor

The first floor features a large number of steel-intensive connections. Of the 146 total connection details identified on this floor, approximately two-thirds make use of steel shoes,custom-welded sections, that resemble small I- or H-profiles. These shoes serve as column-to-column connectors and are a key structural feature in the hybrid timber design used in this and other IMd buildings.

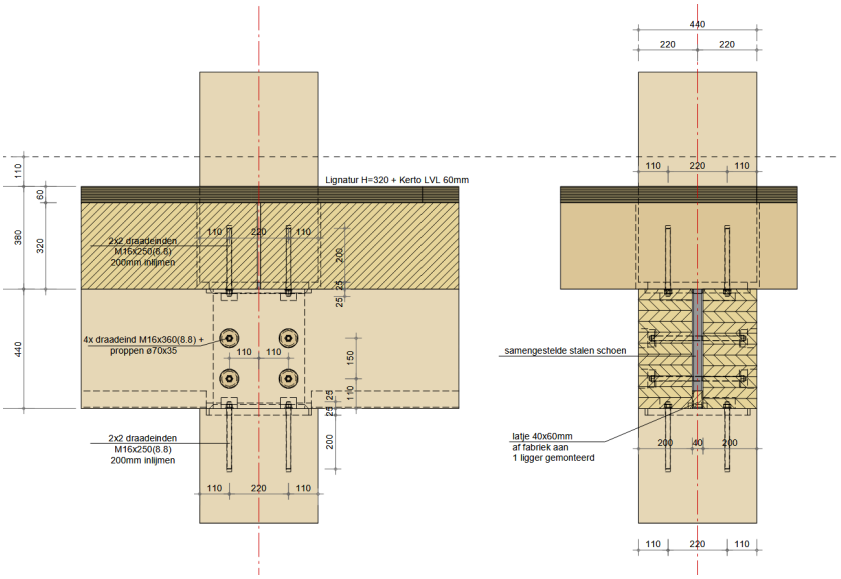

Figure 3.4: Example of a simple CBC connection with a steel shoe. This shoe can be see in figure 1.1b in more detail.

Roughly half of these shoe-based connections (about 50) are more complex assemblies that incorporate additional elements, such as T-stubs or so-called ”opleghandjes” (support brackets), to facilitate beam support or brace anchorage (see example figure 3.7). These assemblies not only require more material, but also more labor-intensive fabrication and installation. The shoes are produced in two sizes to accommodate the differing column geometries across the building: the smaller type weighs approximately 70 kg and requires 4–6 kg of steel bolts per connection, while the larger type weighs around 90 kg and uses 5–8 kg of fasteners. This brings the average weight of one connection to approximately 75–98 kg of steel.

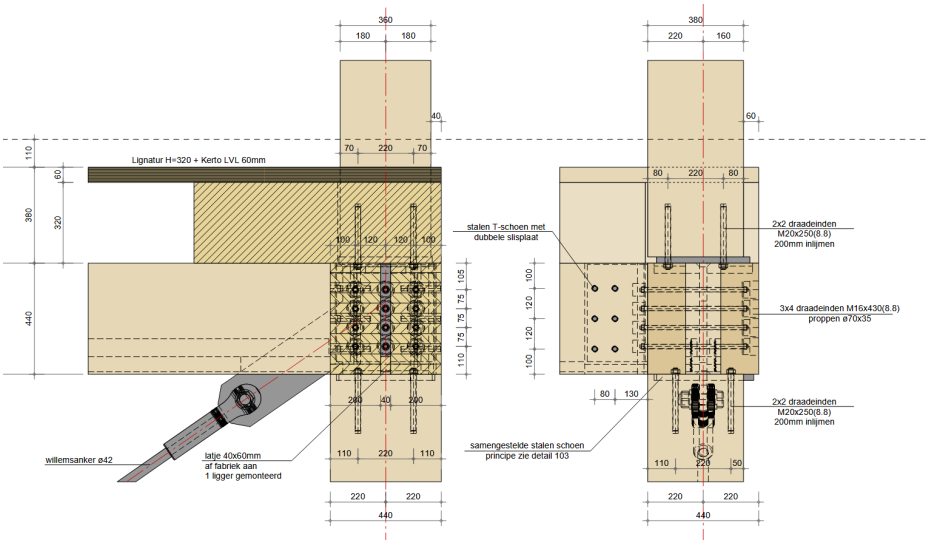

Figure 3.5: Example of a more complex CBC connection with bracing and T-stubs.

The high frequency of these connections results in a substantial material footprint: the shoes alone account for around 8,500 kg of steel on the first floor. This represents half of the total steel weight on that floor. Given their repetitive use, both within this project and in other hybrid timber buildings designed by IMd, these connections are a prime target for material optimization.

Replacing the steel shoes with engineered timber alternatives could significantly reduce embodied carbon. Moreover, because the connections are standardized and modular, the design of timber-based substitutes could follow a repeatable approach with wide applicability across projects.

This combination of high steel volume, repetitive use, and structural modularity makes the shoe-based connections a promising candidate for further study into timber alternatives.

Conclusion

The connection analysis of the ground and first floors reveals distinct patterns in steel usage and opportunities for material optimization. On the ground floor, the connections are primarily column-base joints subjected to axial compression. While certain components, such as steel rods, may be replaceable with timber-based alternatives in compression-only cases, other elements like steel base plates and anchors present challenges due to their exposure to moisture, high stress perpendicular to the grain, and interaction with concrete.

In contrast, the first floor contains a large number of standardized column-to-column connections using welded steel shoes. These elements alone account for approximately 8,500 kg of steel, about half the total steel usage on that level. Given their repetitive nature, modular geometry, and prevalence in other hybrid timber projects, these connections offer the greatest potential for replacement by timber alternatives. Substituting steel shoes with engineered timber or hybrid solutions could significantly reduce the environmental impact and improve circularity without compromising structural performance.

Together, this analysis highlights that while not all connections are suitable for timber substitution, the first floor presents a particularly promising area for the development and implementation of alternative connection strategies.

3.2.2. Design alternatives

To assess the feasibility of proposed timber-based alternatives, simplified hand calculations were carried out for each concept. These calculations are based on the updated Eurocode 5 (2025) guidelines, with a focus on compression perpendicular to the grain, dowel-type fasteners, and load transfer mechanisms in timber. This approach also helped to identify several limitations and gaps in the current design code when evaluating non-standard, fully timber-based connections, highlighting opportunities for further research and refinement.

The calculations were not performed on the Krimpenerwaard case directly, but rather on a comparable building: the woonzorgvoorziening Aveleijn in Wierden. This two-storey timber structure also makes use of steel shoe connections and shares similar structural principles. However, the geometry, force distribution, and member dimensions differ. The use of a separate case allows for a more generalized assessment of the alternative designs, without being overly dependent on project-specific variables.

Alternative 1

In this concept, the connection consists of a column–beam–column (CBC) arrangement with elements stacked vertically as can be seen in figure 3.6 on the left. The beam is reinforced at the bottom with dowels. In between the elements, interlayers are placed made of a material to be determined. This layer functions to distribute local forces and prevent stress concentrations on the top end of the lower column due to the dowel tips.

The dowels may be made from LVL S, BauBuche S, or compressed wood, depending on the required mechanical performance. To estimate the capacity of the reinforced bearing area, equation 8.11 from the updated EC5 2025 on reinforcement with screws is applied, with modifications. In particular, the final term, normally related to the tensile capacity of steel screws, is replaced with the compressive (buckling) resistance of timber dowels, as suggested in recent literature [38]. However, this method lacks a standardized procedure, leaving uncertainties about how buckling was verified. While the influence of dowel slenderness (length-to-diameter ratio) is known, other critical aspects remain undefined,

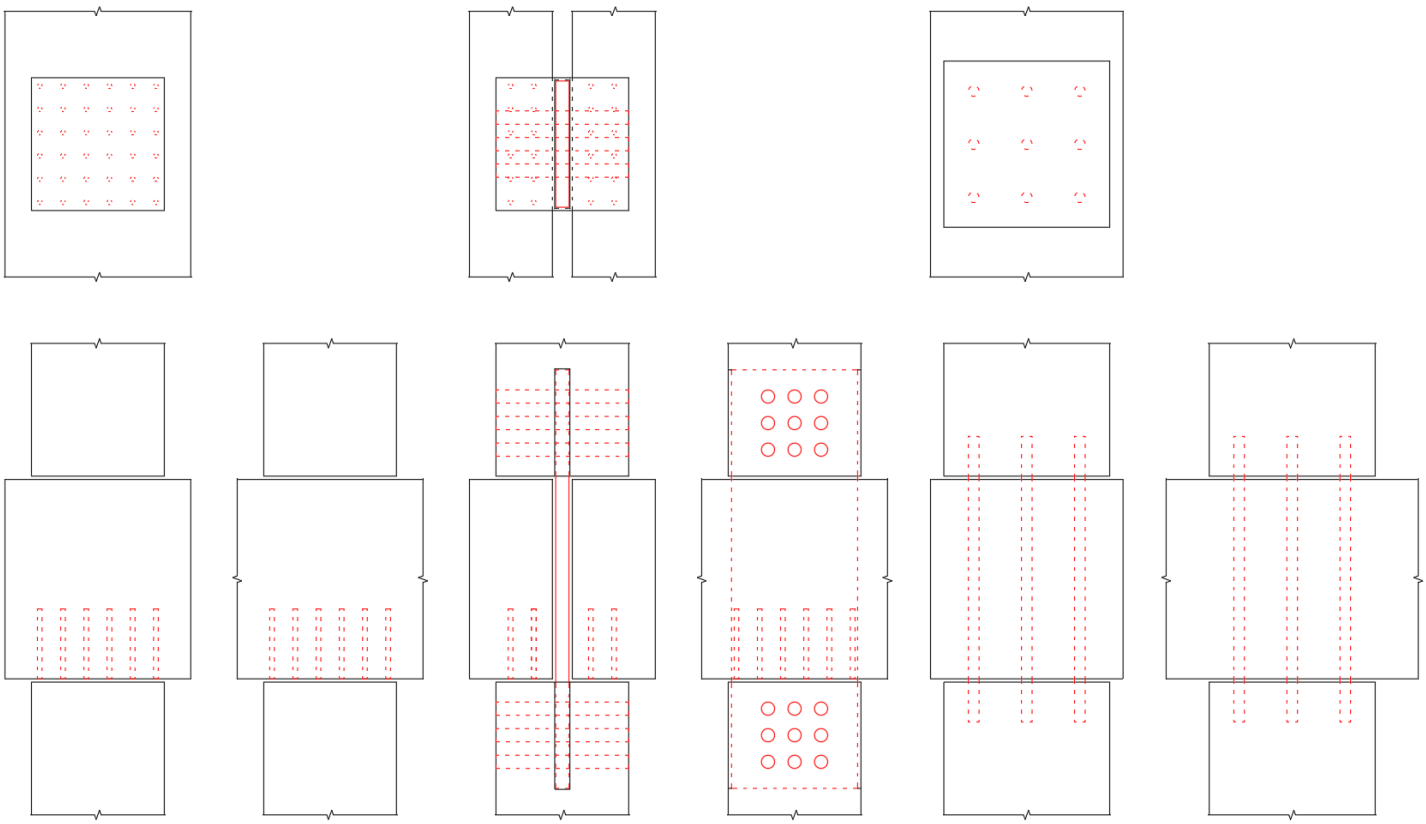

Figure 3.6: The three proposed design alternatives

such as the effect of increased dowel quantity, edge distances, dowel spacing, dowel end conditions (e.g. chamfering, rounding) and dowel finishing (e.g. smooth, knurled, threaded).

The beam is loaded perpendicular to the grain, while the reinforcing dowels are loaded parallel to the grain. This mismatch in loading directions complicates the prediction of joint behaviour, as the beam is more susceptible to deformation in compression perpendicular to the grain than the dowels. Since the connection is stacked vertically, deformation of the beam directly affects the alignment and load distribution in the columns, which may influence the overall response and stress distribution within the joint.

Since the beam is wider than the column, the reinforcement area (dowels) is confined to the width of the column and thus falls within the reduced cross-section used for fire design. However, if the relative dimensions change, particularly if the column becomes wider than the beam, some dowels might fall outside the reduced cross-section, potentially affecting fire resistance. The actual impact depends on load combinations and member proportions and must be assessed case-by-case.

Pros:

- Simple design, easy to fabricate and assemble
- Minimal deviation from conventional detailing

Cons / research gaps:

- Lack of guidance for sizing the interlayer
- Unclear deformation behaviour and load distribution
- Limited code provisions for compressed timber dowels
- Requires further investigation (via FEM or physical testing)
- (Long-term) creep deformation

Alternative 2

This design introduces an internal vertical timber plate positioned between the upper and lower columns, connected via horizontal timber dowels (figure 3.6 in the middle). As in Alternative 1, the beam is placed directly on the lower column and reinforced with dowels if necessary. The internal plate and dowels can be made from high-performance timber materials such as BauBuche S, LVL S, or compressed wood.

The concept allows for a separated force flow: vertical loads from the upper column are transferred through the vertical plate, while loads from the floor beam are transferred independently into the lower column. This potentially reduces stress concentrations and improves performance under load combinations. The connection is designed following the 2025 EC5 rules, including requirements for double shear joints (e.g. $t_{h,2} \geq 2d$), dowel diameters between 16–30 mm, and spacing rules.

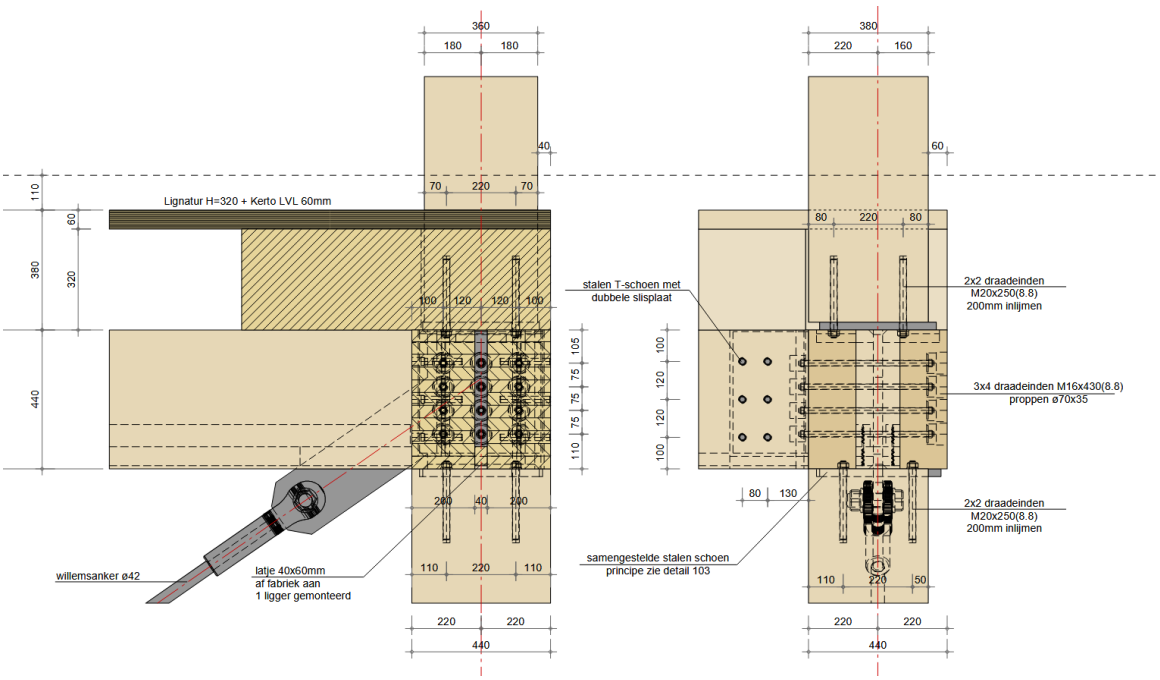

Figure 3.7: Example of a more complex CBC connection with bracing and T-stubs.

Despite being code-compliant in principle, the alternative raises several important research questions, particularly regarding:

- The validity of EC5 rules when using densified timber products like BauBuche or compressed wood,
- The local stress distribution at the lower dowel rows under high compression,
- The possibility of group effects between dowels in densely packed regions,
- The total deformation capacity of the joint under service and ultimate loads.

Possible variations include gluing the internal plate to the columns or redirecting the floor beam loads through the plate into the lower column, offering different structural and constructibility benefits.

This alternative provides a more favourable structural configuration, as the columns and internal plate are connected using dowels that are all loaded parallel to the grain. Although the beam remains subjected to compression perpendicular to the grain, its deformation is largely confined to the beam itself and does not significantly influence the columns, since the beam is supported on top and not structurally tied to the vertical load path formed by the plate and columns. This separation of load paths improves the robustness and predictability of the overall structural response.

The internal timber plate matches the width of the column, meaning its effective width is also reduced by the fire protection depth (typically 2 times the effective char depth, d_{ef}. This applies to the horizontal dowels connecting the plate to the columns as well, which lose length equal to 2 times d_{ef}, influenc-

ing parameters such as $t_{h,1}$. The dowel reinforcement in the beam behaves similarly to Alternative 1 in terms of cross-sectional reduction. The precise effect on fire resistance depends on the specific geometry and load conditions of the case.

Pros:

- Clear separation of vertical load paths
- Fully timber-based, adhesive-free solution

Cons / research gaps:

- Complex detailing and construction
- High dependency on unverified design assumptions
- Requires further investigation via FEM or physical testing

Alternative 3

In this design, long timber dowels are inserted vertically from the top column through the beam and into the bottom column (figure 3.6 on the right). The beam itself is not connected to the dowels; it only bears directly on the lower column. The dowels form a direct load path between the columns, bypassing the beam, and ensuring continuity in the vertical structural system.

Spacing and edge distance requirements from EC5 for glued-in rods are used as a basis for the layout of the dowels. To satisfy these detailing and member checks, larger column and beam cross-sections are typically required. This is because the area occupied by the dowels is subtracted from the net cross-section, effectively reducing the load-bearing area and necessitating increased member dimensions to compensate.

Critical design uncertainties include:

- How to determine the anchorage length of long dowels under compression,
- Whether buckling effects reduce performance for smaller dowel diameters,
- The influence of end- and surface finishing (e.g. pointed, flat or smooth, knurled, threaded) on insertion and capacity.

While the concept is straightforward to execute on site, it might require adhesives to prevent dowel loosening and ensure long-term performance.

Alternative 3 is comparable to Alternative 2 in terms of the global load path. As in Alternative 2, the beam is not part of the direct vertical load-carrying system, and the dowels primarily transfer axial loads through the columns, which are loaded parallel to the grain.

Similar to Alternative 1, dowels are generally placed within the reduced cross-section defined by the smaller member's dimensions, as they run continuously through the top column, beam, and bottom column. If the smallest member changes, dowels may extend outside the reduced section, affecting fire resistance. The evaluation is therefore dependent on the smallest cross-sectional dimension involved.

Pros:

- Very simple and fast to construct
- Few components and minimal machining

Cons / research gaps:

- Larger member sizes required to satisfy detailing rules
- Use of adhesives
- Limited guidance on dowel anchorage and long-term behaviour

3.3. Synthesis: answers to sub - research questions

Research question 3: *What is the steel content (kg/m^2) in different parts of the selected hybrid timber building, and how can this be used to identify the most steel-intensive connection types for potential timber-based alternatives?*

The analysis of the selected building revealed a significant variation in steel content across different floor levels. On the ground floor, the steel content was approximately 1.9 kg/m^2, with a total estimated steel weight of around 6000 kg. This steel was primarily concentrated in column-base connections, consisting of base plates, anchoring rods, and anchor systems embedded in concrete. These connections are largely subjected to compression, and in a few cases tension due to bracing elements.

On the first floor, the steel content was considerably higher, at approximately 5.6 kg/m^2, corresponding to a total of roughly 17 tons of steel. Approximately two-thirds of the connections involved standardized steel “shoes” that connect continuous beams to stacked columns. These shoes, including bolts and fasteners, weigh between 75 and 95 kg per connection and are repeated frequently throughout the structure. The high degree of repetition and relatively modular design of these connections make them key targets for timber-based alternatives. Thus, the steel distribution across floors provides insight into where replacement efforts would have the greatest material impact. Specifically, in repeated intermediate column-beam-column (CBC) connections on upper levels.

Research question 4: *Which structural timber connections in buildings are most suitable for timber-based reinforcement and full timber optimization—based on EC5 design provisions—and to what extent can the use of steel components be reduced?*

Among the connection types investigated, intermediate CBC Connections on the first floor showed the greatest potential for timber-based redesign due to their frequent occurrence and standardized layout. Three timber-based design alternatives were proposed and assessed using simplified calculations based on the (new) Eurocode 5 provisions.

- Alternative 1 introduces a timber plate between stacked members, with the beam reinforced by vertical dowels. This solution is simple and modular but includes uncertainties related to deformation and creep interaction between components.
- Alternative 2 features a vertical internal timber plate connecting columns with horizontal dowels. It separates load paths from upper and lower floors and avoids adhesives, but it is complex and introduces several design gaps related to dowel layout, local stresses, and deformation.
- Alternative 3 uses long dowels running through all members. While easy to construct, it requires larger cross-sections due to reduced effective timber area and presents uncertainties regarding anchorage length and buckling.

Each alternative demonstrates a path toward reducing or eliminating steel in CBC connections. Full timber solutions appear feasible, especially for compression-dominated load cases and connections with modular geometries. However, advanced numerical modelling or dedicated experimental validation is required to address limitations in EC5 for dowel-reinforced compression zones, as simplified analytical approaches cannot adequately capture stress distribution, local interaction effects, and load sharing within the joint. In summary, a significant portion of the steel in hybrid timber buildings. Particularly in intermediate CBC connections, where up to 50% can potentially be replaced with engineered timber alternatives, provided that current design limitations are resolved through further research.

Research question 5: *How does the placement of timber-based reinforcement elements affect the effective cross section and fire resistance of timber members?*

The placement of reinforcement elements relative to the reduced cross-section area defined for fire design is critical. If dowels or plates fall within this reduced section, they contribute to the structural capacity under fire exposure. However, when reinforcement elements extend beyond the effective char depth zone (outside the reduced cross-section), their contribution to fire resistance diminishes, potentially weakening the member’s performance.

In the studied alternatives, dowels and plates are generally designed to fall within the reduced section based on the smaller member width. However, variations in member proportions (e.g., column wider

than beam or vice versa) can lead to dowels partially outside this zone, complicating fire resistance predictions.

Ultimately, the impact on fire resistance is case-specific and depends on member geometry, load combinations, and reinforcement layout. Further research and testing may be needed to fully understand these effects and to develop practical design guidelines for timber-only reinforced connections under fire conditions.

4

Model

The mechanical behaviour of timber reinforced with wooden dowels is governed by localized stress concentrations, contact phenomena, and progressive damage mechanisms that cannot be adequately captured using analytical design models alone. Existing design approaches provide conservative estimates of resistance but offer limited insight into load redistribution, interaction effects, and the influence of reinforcement geometry. To address these limitations, a finite element modelling (FEM) approach is adopted in this study.

This chapter presents the development and validation of a component-scale numerical model intended to represent timber elements reinforced with wooden dowels under compression perpendicular to the grain. The model is designed to capture orthotropic material behaviour, contact and crushing beneath reinforcement elements, and interaction between multiple dowels. The numerical framework enables a systematic investigation of parameters that are difficult to isolate experimentally or analytically, such as dowel spacing, edge distances, and load-transfer mechanisms.

Model validation is performed by comparing numerical results with reference data from literature and simplified analytical calculations, ensuring that the model reproduces relevant stiffness, strength, and failure trends. Once validated, the model forms the basis for the parametric studies presented in subsequent chapters and provides the mechanical input required to interpret and assess the design-level implications explored in the case study.

In this way, the numerical model serves as a link between the theoretical background discussed in the literature review and the applied evaluation of timber-based reinforcement strategies at structural scale.

4.1. Model setup

4.1.1. Base model

The base model serves as the foundation for all subsequent numerical analyses in this study. Its primary purpose is to establish a validated representation of the timber compression behaviour and the interaction between the timber matrix, dowels, and loading plate. By first developing a reliable and well-understood reference configuration, the effects of reinforcement, geometric variations, and material substitutions can be assessed in a controlled and consistent manner. The base model therefore functions both as a benchmark for comparison and as a verification tool to ensure that the underlying modelling assumptions, material definitions, boundary conditions, and contact formulations produce physically realistic results.

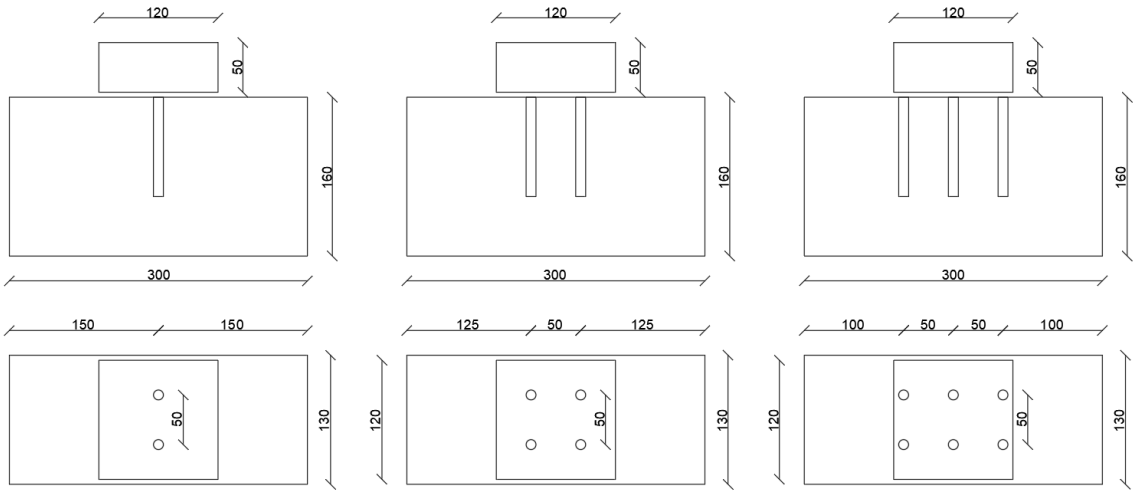

Figure 4.1: The dimensions of the base model including the loading plate.

Modelling approach

The numerical modelling approach builds upon the reference model developed by O'Ceallaigh et al. (2021), which provides a validated finite element framework for timber and densified wood under compression perpendicular to the grain. Their model forms the conceptual and methodological foundation for the present study, particularly regarding orthotropic material definitions, anisotropic plasticity using the Hill criterion, and cohesive representation of the timber–densified-wood interface.

In this thesis, the reference model from O'Ceallaigh et al. is adopted, adapted, and extended to investigate the reinforcement effect of densified wood dowels under perpendicular-to-grain compression. While the underlying modelling principles are consistent with the reference model, the present work introduces new derived models to capture the contribution of individual dowels, incorporates alternative dowel material properties, and enables a detailed assessment of stress distribution and load-transfer mechanisms within the joint.

A consistent numerical framework was maintained across all configurations—unreinforced and reinforced—to ensure comparability of results. This includes identical mesh strategies, loading procedures, contact formulations, and material implementations for timber, densified wood, and steel. The dowel-reinforced variants were derived directly from the baseline model by introducing 2, 4, or 6 densified wood dowels, inserted perpendicular to the grain.

The reference model itself, its verification, and its adaptation for the current research are presented and discussed in detail in a separate chapter. The present section provides only an overview of the general modelling strategy, while the subsequent sections describe the geometric setup, material properties, contact interactions, boundary conditions, loading scenarios, and mesh refinement adopted in this study.

Geometry & model configurations

The finite element model consists of three primary components: timber, densified wood (DW) dowels, and a steel loading plate. Each part was modelled as a three-dimensional deformable solid with an independent local coordinate system (datum CSYS) to capture material anisotropy accurately. The orthotropic directions of the timber and densified wood were defined following the longitudinal (L), radial (R), and tangential (T) axes, corresponding to the grain orientation, radial growth direction, and tangential plane of the wood, respectively.

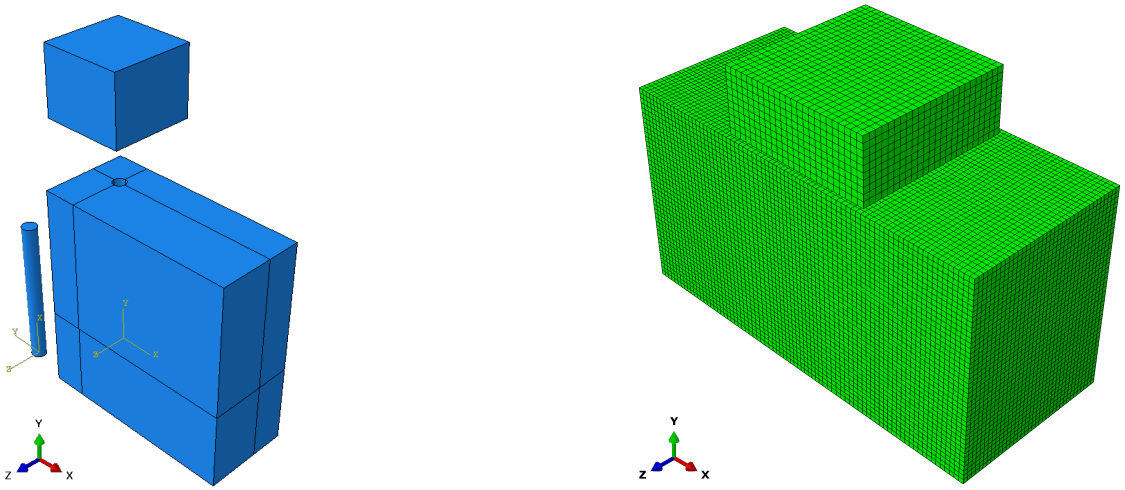

(a) Overview of all model parts in Abaqus prior to assembly.

(b) Assembly of all components forming the complete Abaqus model.

Figure 4.2: Model components and final assembly of the numerical model in Abaqus.

The timber specimen geometry has a nominal cross-section of 160 mm × 130 mm and a total height of 300 mm. The densified wood dowels were modelled with a diameter of 10 mm and a length of 100 mm, inserted perpendicular to the grain. The dowels were positioned symmetrically relative to the central axis of the specimen, with three reinforcement configurations: 2, 4, and 6 dowels.

The steel plate used to apply compressive loading was modelled as a rigid analytical surface with negligible deformation compared to the timber. Symmetry conditions were implemented in the longitudinal and transverse directions to reduce computational cost, allowing the use of a quarter-model representation while maintaining full accuracy of stress and deformation fields. Partitioning was applied to the timber body to enable local mesh refinement near dowel interfaces and stress concentration zones; the mesh strategy and convergence behaviour are further discussed in Section 4.1.1.

Material properties

3 materials were modelled in this study: Douglas Fir glulam (timber), densified Scots Pine (DW dowel), and structural steel (loading plate). The orthotropic elastic and plastic parameters for both timber and densified wood were based on the experimental and numerical work of O'Ceallaigh et al. (2021). Steel was modelled as an isotropic material with elastic–plastic behaviour.

For Timber and DW, all material definitions were implemented in ABAQUS/Explicit using the `*Elastic, Type=ENGINEERING CONSTANTS` and `*Plastic, Hardening=ISOTROPIC` keywords, and the Hill criterion was defined using `*Plastic, Potential` following guidance from the ABAQUS User Manual (v2024).

Timber (Douglas Fir Glulam): Timber was defined with orthotropic elastic behaviour using engineering constants (E_L, E_R, E_T, G_{LR}, G_{LT}, G_{RT}, and Poisson's ratios ν_{LR}, ν_{LT}, ν_{RT}) as given in Table 4.2. Plasticity was modelled using the Hill yield criterion to capture anisotropic yielding under compression perpendicular to the grain. The plastic parameters were defined as follows: yield stress and plastic strain pairs of (37.5 MPa; 0.0) and (38.5 MPa; 0.1). The Hill potential parameters were set to $(R_{11}, R_{22}, R_{33}, R_{12}, R_{13}, R_{23}) = (1.0, 0.133, 0.133, 0.231, 0.231, 0.231)$, representing the relative yielding behaviour along the orthotropic axes.

Densified wood (Scots Pine): Densified wood was modelled as an orthotropic solid following the same formulation as the timber, with increased stiffness and strength due to thermo-mechanical densification. The plastic definition used yield and strain pairs of (130.0 MPa; 0.0) and (132.5 MPa; 0.1). The Hill potential coefficients were determined according to Abaqus documentation and adjusted to match experimental data: $(R_{11}, R_{22}, R_{33}, R_{12}, R_{13}, R_{23}) = (1.0, 0.615, 0.615, 1.066, 1.066, 1.066)$. The elastic properties were scaled according to the increased density of the material (approximately 54% radial compression).

Steel (S355): The loading plate was assigned isotropic material properties typical for structural steel, defined with a Young's modulus of 210,000 MPa and Poisson's ratio of 0.3. Plastic behaviour was included with a single yield stress of 355 MPa, representative of S355 structural steel.

Contact & interaction

Two interaction properties were defined to represent the contact behaviour between the model components:

- **Steel–timber interface** (figure 4.3a): The interaction between the steel plate and timber surface was modelled using a standard "hard contact" formulation in the normal direction, with a friction coefficient of 0.5 in tangential slip. This represents the dry frictional condition between the loading plate and timber surface during compression testing.
- **Dowel–timber interface** (figure 4.3b): A cohesive zone model (CZM) was implemented to simulate the adhesive bonding between densified wood dowels and the surrounding timber. The tangential behaviour was defined using a friction coefficient of 0.5. The normal contact was specified as "hard" to prevent interpenetration. The cohesive behaviour was modelled with stiffness parameters $k_{nn} = 120$ [MPa/mm], $k_{ss} = 36$ [MPa/mm], and $k_{tt} = 36$ [MPa/mm]. Damage initiation was governed by nominal stress criteria with normal and shear strengths of 5 MPa in all directions, while damage evolution followed a linear law with complete degradation at a total relative displacement of 2.5 mm. This implementation captures the progressive debonding and slip observed experimentally at the dowel–timber interface.

To ensure proper contact initialization, a small prescribed displacement of 0.1 mm was applied to the top of the steel plate and 0.05 mm to the top of the densified wood dowel in the initial analysis step.

Boundary conditions

The bottom surface of the timber specimen was clamped. The model was reduced to one-quarter of the full specimen, and appropriate symmetry constraints were applied on the zy and yx planes (see figure 4.4a and 4.4b).

The top surface of the steel plate was constrained in all directions except for the loading (radial) direction. The vertical displacement was applied directly to the nodes on the top surface of the steel plate. No reference point or multi-point constraint was used. By prescribing a uniform displacement field to this surface, a consistent compression perpendicular to the grain was ensured across the entire contact area.

Loading scenarios

A total prescribed displacement of 10 mm was applied to the top surface of the steel plate, oriented perpendicular to the grain direction (see figure 4.4c). The displacement was introduced incrementally to capture the transition from the initial elastic regime to the post-yield crushing behaviour of the timber.

This displacement-controlled procedure allows for the extraction of key structural response parameters, including the load–displacement relationship, stiffness, and ultimate compressive strength ($f_{c,90}$). Furthermore, the use of displacement control contributes to numerical stability in Abaqus/Explicit, particularly during large deformations and progressive damage evolution at the dowel–timber interface.

Mesh strategy & convergence

A structured meshing strategy was adopted to balance numerical accuracy and computational efficiency. All solid components(timber, dowels, and steel plate) were discretised using 8-node linear brick elements with reduced integration (C3D8R). This element type was chosen due to its robustness

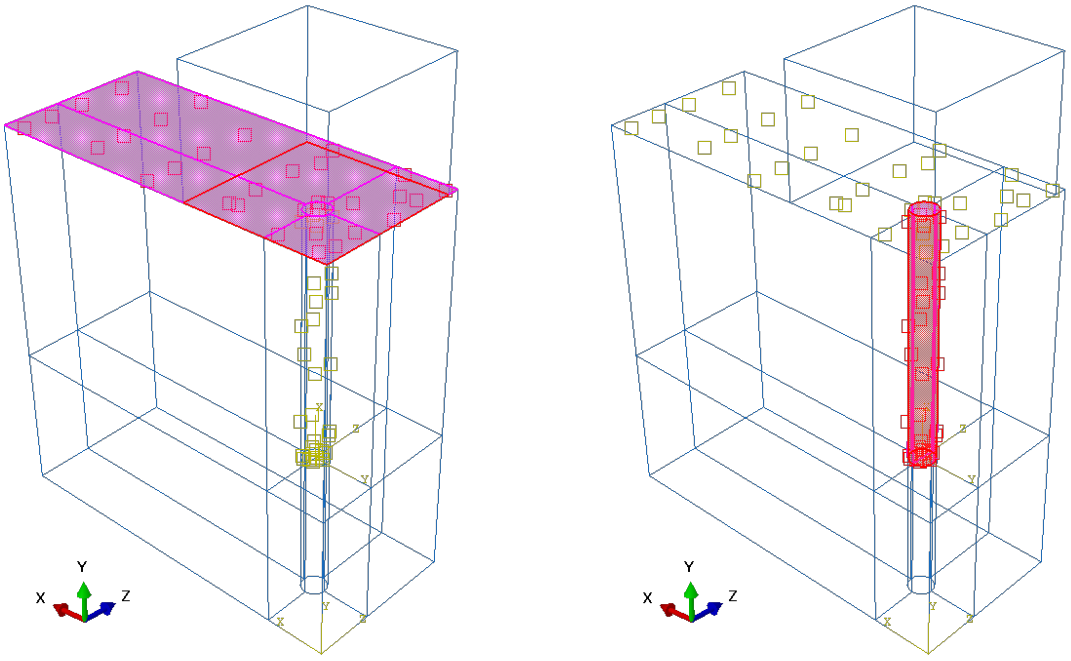

(a) Contact interaction between the loading plate and the timber surface.

(b) Contact interaction between dowel reinforcement and surrounding timber.

Figure 4.3: Contact interaction definitions used in the Abaqus model for load introduction and reinforcement–timber interaction.

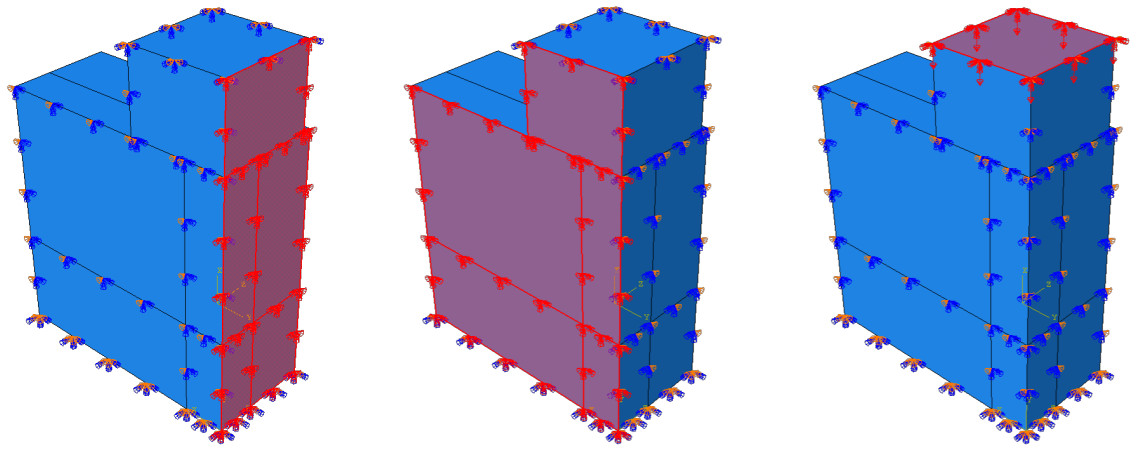

(a) Application of the X-symmetry boundary condition in the Abaqus model.

(b) Application of the Y-symmetry boundary condition in the Abaqus model.

(c) Imposed vertical displacement of the top steel plate.

Figure 4.4: Boundary conditions applied in the Abaqus model: symmetry conditions and imposed displacement used to simulate compression perpendicular to the grain.

in handling large deformations, contact interactions, and anisotropic material behaviour, while maintaining stable performance in analyses.

To accurately capture stress gradients in critical regions, a locally refined mesh was implemented around the dowel–timber interface and within the dowel body itself. The mesh in these areas was refined progressively toward the contact surface to improve the resolution of interfacial stresses and to ensure stable cohesive zone behaviour. The densified wood dowel, being the stiffest component, was assigned a finer mesh to better represent the stress distribution along its length and to avoid artificial stress concentrations at the contact edges.

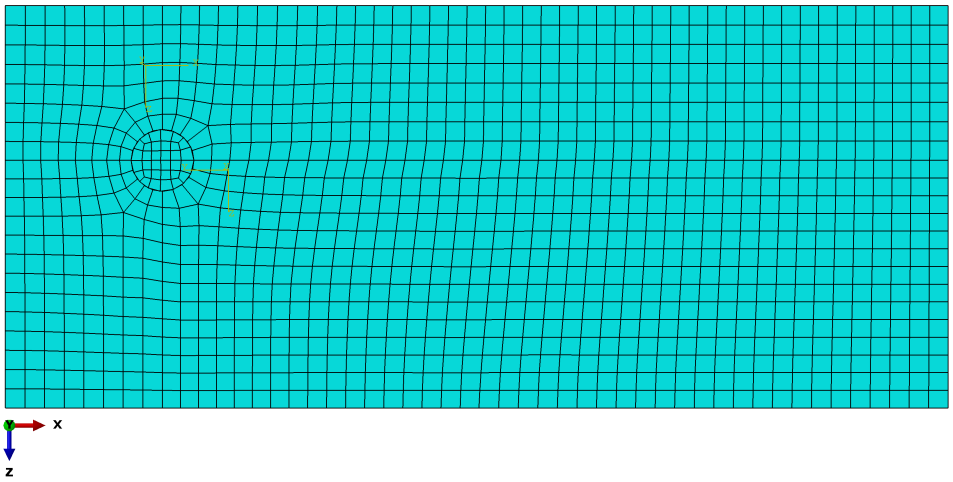

Figure 4.5: Top view of the finite element mesh used in the Abaqus model.

In contrast, the surrounding timber volume was meshed with a coarser element size away from the reinforcement zone to reduce the total element count. This graded mesh approach provided an efficient transition between the refined and coarse regions while maintaining accuracy in the high-stress zones near the dowel and loading area.

The global mesh size for the timber body was determined through sensitivity studies, starting from an average element size of 5 mm and reducing to 2 mm in the reinforced region. Further refinement below this level did not significantly change the predicted load–displacement response or the failure pattern, indicating mesh convergence. The cohesive zone interface was defined using surface-based contact with automatically generated cohesive elements, which adaptively refined based on the underlying element size of the adjacent surfaces.

The final mesh contained approximately 60,000–80,000 elements for the quarter-model configuration, depending on the reinforcement layout. This setup achieved a good balance between computational cost and result precision, ensuring stable convergence and physically realistic deformation behaviour during the non-linear loading phase.

Reference material properties for Eurocode 5 comparison

Table 4.1 summarises the timber material properties adopted in the numerical model and compares them with reference values for Eurocode 5 strength classes C24 and C30. The Abaqus input parameters are defined as mean material properties, while the Eurocode values are primarily characteristic values unless stated otherwise. For comparison purposes, mean compressive strengths for Eurocode classes were obtained by applying a conversion factor of 1.3 to the characteristic values. The table reports absolute values and relative differences for stiffness, strength, and density parameters used in the numerical analyses.

Table 4.1: Comparison of timber material properties used in Abaqus with Eurocode 5 strength classes C24 and C30

	Strength properties [MPa]			Difference [%]	
Property	Abaqus	C24	C30	C24	C30
$E_{0,k}$	–	7400	8000	56.8	45.0
$E_{0,\text{mean}}$	11600	11000	12000	5.5	-3.3
$E_{90,\text{mean}}$	350	370	400	-5.4	-12.5
$G_{0,\text{mean}}$	385	690	750	-44.2	-48.7
$f_{c,0,k}$	–	21	24	78.6	56.3
$f_{c,0,\text{mean}}$	37.5	*27.3*	*31.2*	37.4	20.2
$f_{c,90,k}$	–	2.5	2.7	100.0	85.2
$f_{c,90,\text{mean}}$	5.0	*3.3*	*3.5*	53.8	42.5
ρ_k	–	350	380	58.6	46.1
ρ_{mean}	555	420	460	32.1	20.7

Consistency of material properties with Eurocode 5

To enable a consistent comparison between the numerical simulations performed in Abaqus and the analytical formulations based on Eurocode 5, the material properties adopted in the numerical model are evaluated against the reference values for strength classes C24 and C30 as defined in EN 338. This comparison establishes the level at which stiffness and strength parameters are represented and provides a clear reference framework for later result interpretation.

The Douglas Fir glulam implemented in the numerical model exhibits stiffness characteristics comparable to strength classes C24–C30. The elastic parameters used in Abaqus correspond to mean values derived from experimental data and literature sources, whereas Eurocode 5 primarily defines characteristic values for design. Table 4.1 summarises the elastic and strength properties used in the numerical model alongside the corresponding Eurocode 5 reference values.

The longitudinal modulus $E_{0,\text{mean}} = 11.6\ \text{GPa}$ lies within the range associated with C24–C30 timber. The perpendicular modulus $E_{90,\text{mean}}$ and the shear modulus $G_{0,\text{mean}}$ are lower than the Eurocode reference values. Mean compressive strengths parallel and perpendicular to the grain were obtained by converting Eurocode characteristic values using a factor of 1.3.

The densified wood dowels are manufactured from Scots Pine compressed in the radial direction and therefore fall outside the Eurocode 5 strength class system, which is limited to solid timber and glulam. Their elastic and strength properties exceed those of the highest C- and D-classes defined in Eurocode 5 and are therefore implemented directly in the numerical model rather than assigned to a standard strength class.

Equivalent shear yield stress

In the numerical model, material nonlinearity is governed by an anisotropic Hill yield criterion, in which yielding is defined in terms of normal stresses parallel and perpendicular to the grain. Consequently, no explicit shear yield stress is defined as an independent material parameter.

To allow comparison with the analytical formulation based on Eurocode 5, an equivalent shear yield stress is derived from the normal yield stress according to

$$\tau_y = \frac{\sigma_y}{\sqrt{3}}. \tag{4.1}$$

This expression follows from the von Mises–type stress interaction underlying the Hill criterion and provides a consistent scalar measure of shear-related yielding within the numerical framework. The resulting value represents the shear stress level associated with the onset of yielding under combined stress states and is used solely for comparison purposes with the analytical model.

4.1.2. Derived models

To improve the comparison between the numerical results and the analytical model, two additional models were developed. The objective of these derived models is to isolate the lateral (side) bearing capacity and the tip bearing capacity of the dowels when loaded perpendicular to the grain. By decoupling these mechanisms, the FEM results can be directly linked to hand calculations based on elementary stress assumptions and empirical formulations.

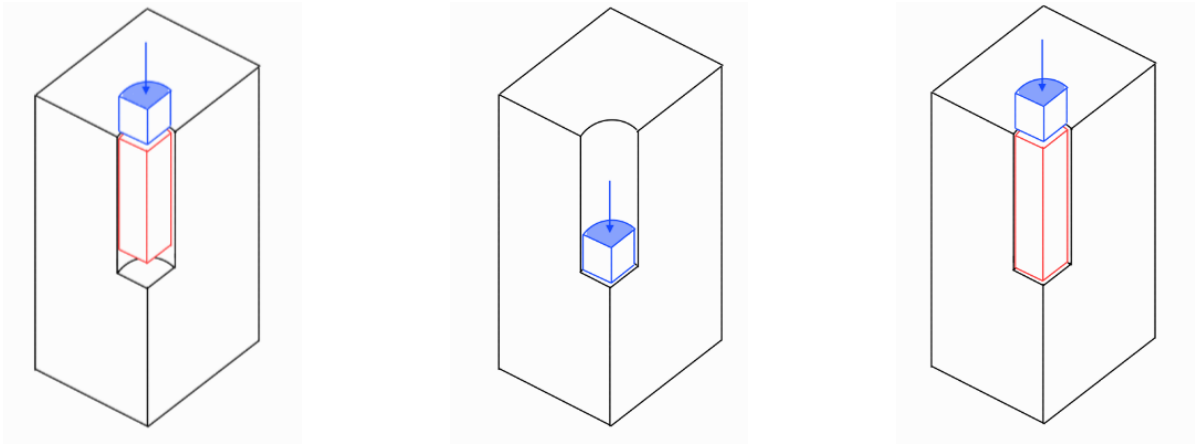

(a) Dowel Side Test (DST). **(b)** Dowel Tip Test (DTT). **(c)** Dowel Side and Tip Test (DSTT).

Figure 4.6: Sketches of the three different modified models.

Dowel Side Test (DST)

The first derived model is designed to investigate only the interaction between the dowel's lateral surface and the surrounding timber. The timber matrix and the dowel are modelled identically to the base models, except that the final 5 mm of the dowel is removed. Instead, a steel loading component with the same diameter as the dowel is placed on top of the truncated dowel.

This setup ensures that the load is transferred solely through the lateral contact surface between the dowel and the wood, eliminating any contribution from the dowel tip. A prescribed displacement is applied to the steel component, and the vertical reaction force at the bottom of the timber block is recorded. By varying the dowel diameter and embedded length, the influence of geometric parameters on the lateral bearing capacity can be quantified.

Dowel Tip Test (DTT)

The second derived model focuses on evaluating the bearing capacity at the dowel tip. In this model, only the final section of the dowel, the tip zone, is modelled as steel, together with the surrounding timber volume. This steel tip is subjected to a prescribed displacement.

This approach captures the local compressive stress field underneath the dowel tip and the resulting load transfer mechanism, independent of the lateral contact stresses. The corresponding reaction forces are used to compare the FEM results with analytical predictions of end bearing stresses in timber (e.g., $\sigma_{c,90}$, effective contact area, stress spread/conical distribution, or strut-and-tie assumptions depending on the analytical model).

4.1.3. Dowel Side + Tip Test (DSTT)

The third derived model combines the mechanisms studied in the DST and DTT models and represents the full interaction between the dowel and the surrounding timber. In this model, the complete dowel is retained, while a steel loading component with the same cross-sectional area as the dowel is placed on top. A prescribed displacement is applied to this steel component, ensuring that the load is transferred simultaneously through both the lateral dowel–timber contact and the compressive bearing at the dowel tip.

This configuration allows for the concurrent activation of embedding stresses along the dowel shaft and compressive stresses beneath the dowel tip. The vertical reaction force measured at the bottom

of the timber block therefore represents the combined contribution of both load transfer mechanisms. By comparing the results of this model with those of the individual DST and DTT models, the relative influence and possible interaction between side and tip resistance can be evaluated.

4.1.4. Analytical model

The analytical reference model is based on the reinforcement provisions given in EN 1995-1-1:2023, Clause 8.1.6.2, which defines the characteristic capacity of a contact area reinforced perpendicular to the grain. The full expressions and theoretical background were presented in Chapter 2.8, and are therefore not repeated here. Instead, this section describes how the standardised formulation is adapted to the specific case of dowel-type reinforcement studied in this thesis.

Adaptation of the analytical expressions for dowel reinforcement

The general expression for the characteristic capacity,

$$F_{c,90,Rk} = \min \begin{cases} k_{mat}\, b_{c,90}\, l_{ef,1}\, f_{c,90,k} + n \min\{F_{w,k}; F_{ax,k}\} \\ b\, l_{ef,2}\, f_{c,90,k} \end{cases} \tag{4.2}$$

The general expression for the characteristic capacity $F_{c,90,Rk}$ retains the distinction between timber crushing in the contact area and load distribution at the level of the reinforcement. However, the contribution of the reinforcement is reformulated to account for the axial resistance mechanisms governing wooden dowels, as represented by the terms $F_{w,k}$ and $F_{ax,k}$. These parameters replace the withdrawal and axial compression resistances defined in Eurocode 5 for steel screws and rods and are discussed in detail in the following sections.

$$l_{ef,1} = l_{c,90} + 2 \cdot \min\left\{30;\ \frac{l_s}{2};\ \frac{l_{c,90}}{2}\right\} = l_{c,90} \tag{4.3}$$

The effective contact length $l_{ef,1}$ is simplified for the considered configuration. As the load is applied directly at, or in the immediate vicinity of, the support, the clear distance between the contact area and the concentrated load is zero ($l_s = 0$), resulting in $l_{ef,1} = l_{c,90}$.

$$l_{ef,2} = 2\, \tan(\alpha_1)\, l_r + (n_0 - 1)\, 5d \tag{4.4}$$

The effective distribution length at the level of the reinforcement $l_{ef,2}$ is reformulated to reflect the geometric spreading of compressive forces along the dowel axis. In contrast to the EC5 definition based on screw spacing, the present expression explicitly includes the inclination angle α_1 and the dowel embedment length l_r, thereby providing a geometry-based representation of force transfer for dowel reinforcement.

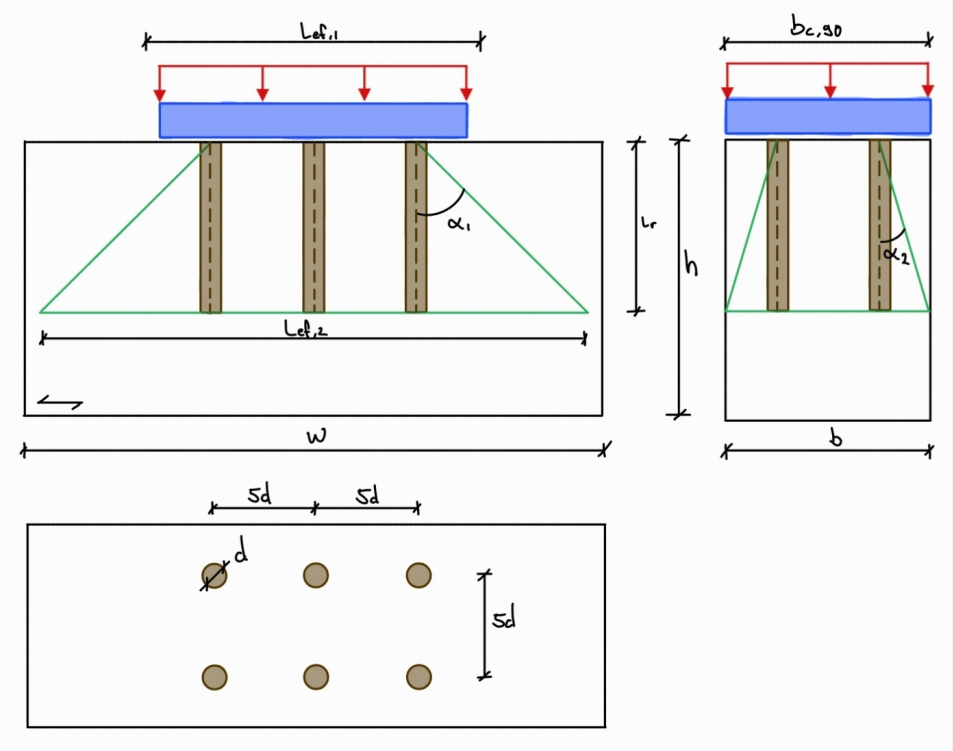

Figure 4.7: Parameters for the analytical model for timber dowels.

Axial compression resistance

For dowels, the axial compressive force capacity is governed by compression parallel to the grain of the dowel material itself. The characteristic axial compressive resistance of the dowel was therefore taken as:

$$F_{\mathrm{ax},k} = A_{\mathrm{dowel}}\, f_{c,0,dowel} \tag{4.5}$$

where $A_{\mathrm{dowel}} = \frac{\pi d^2}{4}$ is the cross-sectional area of the dowel tip.

Withdrawal-type resistance

For dowels, withdrawal-type resistance does not originate from thread engagement, but from frictional resistance mobilised by lateral bearing stresses acting along the dowel–timber interface. This was modelled as:

$$F_{\mathrm{fr},k} = \pi\, d\, l_r\, f_{v,k} \tag{4.6}$$

where d_d and l_r denote the dowel diameter and the embedded length, respectively.

The characteristic shear strength $f_{v,k}$ represents the governing shear resistance mobilised at the dowel–timber interface. Unlike threaded fasteners, this resistance does not arise from mechanical interlock but from frictional stresses induced by lateral bearing between the dowel and the surrounding timber. The value of $f_{v,k}$ is therefore taken as the minimum shear resistance of the components, considering failure in the timber substrate, in the dowel material, or in the adhesive layer.

It is noted that the direction of shear differs for the two materials involved. In the timber, the bearing stresses acting on the dowel generate shear perpendicular to the grain, whereas in the dowel the corresponding shear stresses act predominantly parallel to the dowel axis and thus parallel to the grain direction of the dowel material. The adopted definition of $f_{v,k}$ implicitly accounts for this orthotropic interaction by selecting the lowest governing shear resistance, ensuring a conservative representation of the dowel withdrawal-type behaviour.

Compressive resistance under the dowel tip

In addition to the side-bearing mechanism, a compressive resistance develops beneath the dowel tip. This contribution was evaluated as:

$$F_{\mathrm{tip},k} = k_{c,90}\, A_{dowel}\, f_{c,90,k,timber} \tag{4.7}$$

where $f_{c,90}$ is the compressive strength perpendicular to grain, and $k_{c,90}$ is the force-spreading factor according to prEN 1995-1-1:2023, Clause 8.1.6.1(3).

The total withdrawal-type resistance for use in the reinforced capacity model was taken as the sum of these two mechanisms:

$$F_{w,k} = F_{\mathrm{fr},k} + F_{\mathrm{tip},k} \tag{4.8}$$

in figure 4.8 below, this is visually explained.

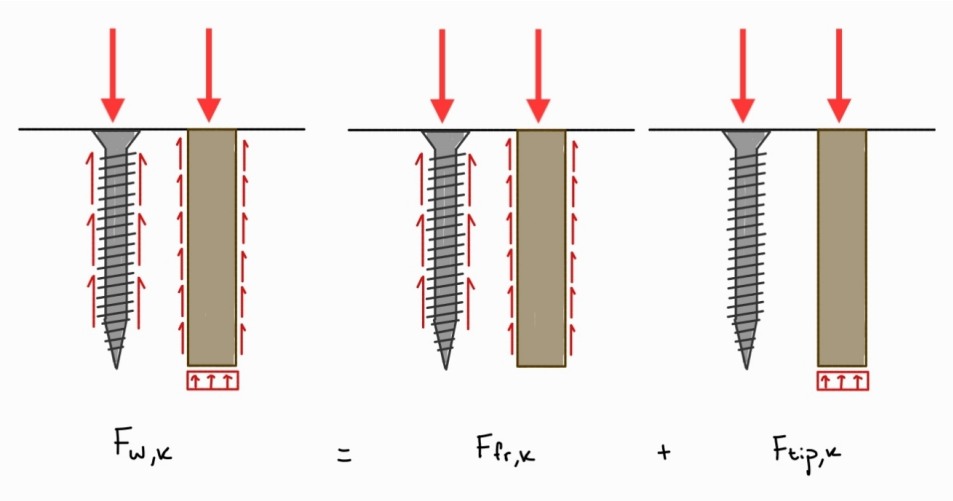

Figure 4.8: The assumed individual contributions of the frictional and tip forces for dowels and screws.

Purpose of the analytical model

The analytical model provides a reference capacity based on the effective contact area, reinforcement layout, and dowel contribution. By comparing these analytical values with the capacities obtained from the Base Models and derived models, the validity of the numerical model can be assessed and the contribution of each reinforcement mechanism can be quantified.

4.2. Model validation

4.2.1. Reference model

The reference model provides an external benchmark based on the numerical framework developed by O'Ceallaigh et al. (2021) [39]. In their work, a three-dimensional finite element model was constructed in Abaqus/Explicit to simulate the load-bearing behaviour of timber specimens reinforced with densified wood dowels, and its performance was verified against experimental data.

In the present study, this modelling framework is replicated and used as a reference to verify the modelling strategy adopted for the base model. By comparing the response of the base model to the behaviour predicted by the reference model, key modelling choices—such as orthotropic material definitions, plasticity formulation, cohesive interaction properties, and boundary conditions—can be evaluated and, where necessary, calibrated. The reference model therefore strengthens the reliability of the numerical methodology and ensures that the assumptions implemented in this work remain consistent with state-of-the-art research.

The model geometry was based on glued laminated timber (glulam; Douglas Fir) specimens subjected to compressive loading perpendicular to the grain. The timber specimens had a cross-section of 160 × 130 mm and a length of 300 mm, matching the experimental programme described by O'Ceallaigh et al. (2021)[39]. Reinforcement was introduced in the form of densified wood dowels of 10 mm diameter and 100 mm length made from Scots Pine, compressed in the radial direction with a compression ratio of approximately 54%. Three reinforcement configurations were modelled: specimens with 2 dowels, 4 dowels, and 6 dowels, alongside an unreinforced reference specimen. To reduce computational cost, symmetry conditions were applied, enabling a quarter-model representation of the full geometry while maintaining accuracy.

Both timber and densified wood dowels were treated as orthotropic materials. Elastic moduli, shear moduli, and Poisson's ratios were defined along longitudinal (L), radial (R), and tangential (T) axes (see Table 4.2). Timber was modelled as linear elastic in tension and elastic–plastic in compression, with failure governed by the Hill plasticity law. Densified wood dowels were assigned higher stiffness and yield values to reflect the increased density achieved by thermo-mechanical compression. A cohesive zone interface was introduced between dowels and timber to represent adhesive bonding and possible debonding under shear.

Table 4.2: Material properties of timber and densified wood dowels (values based on [39], Wood Handbook (USDA 2010), and density scaling relationships)

Property		**Timber**	**Densified Wood**
Elastic Modulus (MPa)	E_L	11600	28000
	E_R	350	2240
	E_T	350	1400
Poisson's Ratio	ν_{LR}	0.48	0.48
	ν_{LT}	0.30	0.30
	ν_{RT}	0.56	0.35
Shear Modulus (MPa)	G_{RL}	385	2000
	G_{LT}	338	1880
	G_{RT}	38.5	200
Yield (MPa)	Parallel	37.5	130
	Perpendicular	5	80

Contact interactions were modelled at two levels:

- Steel–timber interface: Hard contact in the normal direction with a friction coefficient of 0.5 for tangential slip.
- Dowel–timber interface: Cohesive Zone Modelling (CZM) was used, defined by nominal stress criteria and a linear damage evolution law. Maximum nominal stresses of 5 MPa were assumed in normal and shear directions, with complete degradation occurring at 2.5 mm of relative displacement. This approach enables simulation of progressive failure at the dowel–timber bond line, which was observed experimentally.

The bottom surface of the timber specimen was constrained in radial direction to simulate the support condition in the laboratory tests. The planes of symmetry in the quarter model were restrained appropriately to enforce geometric symmetry. On the top surface, a rigid steel plate was modelled to apply compressive loading, ensuring uniform stress distribution across the loaded area.

In the next step, a displacement-controlled loading protocol was applied to the top surface of the steel plate, replicating the experimental testing conditions in accordance with EN 408. The prescribed displacement was applied in the radial direction until failure, enabling capture of both the elastic stiffness and plastic crushing behaviour of the timber beneath the loading plate.

All solid components (timber, dowels, and steel plate) were meshed using 8-node linear brick elements with reduced integration (C3D8R). Mesh density was determined through sensitivity studies to balance accuracy with computational efficiency. The refined mesh was concentrated around the dowel–timber interface and loading area to resolve high stress gradients and capture damage initiation. Symmetry modelling reduced the total element count by approximately 75%, significantly improving computational performance.

The FEM predictions were validated against experimental results reported by O'Ceallaigh et al. (2021). Key validation metrics included load–displacement curves, maximum compressive strength (fc,90), and failure patterns. The model reproduced the increase in stiffness and capacity with dowel reinforcement and captured the delayed yielding observed in reinforced specimens. While the FEM did not explicitly model longitudinal cracking observed experimentally, the overall agreement confirmed the suitability of the model for further parametric studies.

4.2.2. Validation model

This subsection presents the validation of the developed base finite element model. The model response is assessed in terms of global deformation behaviour, local stress and strain fields, observed failure modes, and dowel–timber contact interaction. In addition, the sensitivity of the model to key parameters is evaluated to verify robustness and to identify the dominant mechanisms governing load transfer. The validation focuses on qualitative agreement and consistency of trends rather than absolute resistance values.

Deformation

The load was applied as a prescribed displacement at the top surface of the steel plate. This displacement was equally transferred to the top of the dowel and to the timber surface in contact with the steel plate, ensuring a uniform loading condition across this interface.

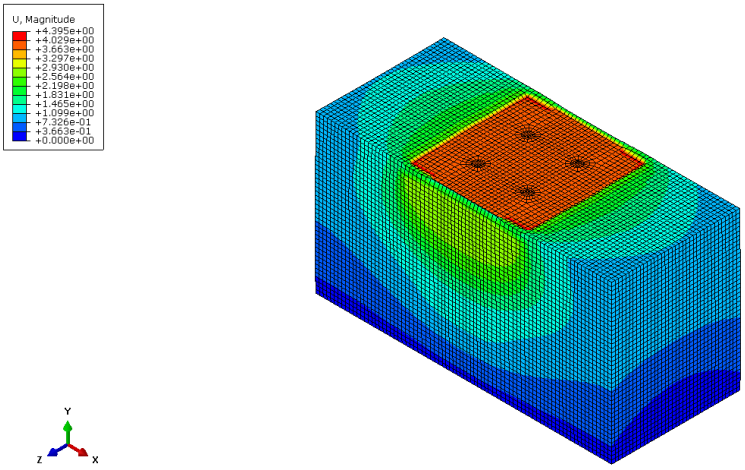

Figure 4.9: Global Deformation of the full scale model

During the analysis, some localized hourglassing was observed in the timber elements along the edges of the steel plate. This led to minor, localized unrealistic deformations but the effect remained limited

and did not significantly influence the global response. Similar behaviour was noted at the bottom of the dowel hole, where slight hourglassing occurred due to local stress concentration and element distortion.

Plastic deformation developed progressively around the dowel and at the contact interface, consistent with the expected material response under compression perpendicular to the grain. The vertical displacement field (U2) showed lower values near the bottom of the timber block and higher displacements around the dowel hole, while the displacement along the dowel length remained almost constant.

In addition, deformation in the out-of-plane direction (U3) was observed in both the timber and the dowel. The timber exhibited localized bending near the dowel hole, which induced a small rotational movement of the dowel in the YZ-plane. This bending effect explains the non-uniform stress distribution observed later in the stress analysis.

Overall, the deformation profile of the specimen closely matched that of the reference model, confirming that the global deformation behaviour is well captured by the numerical model.

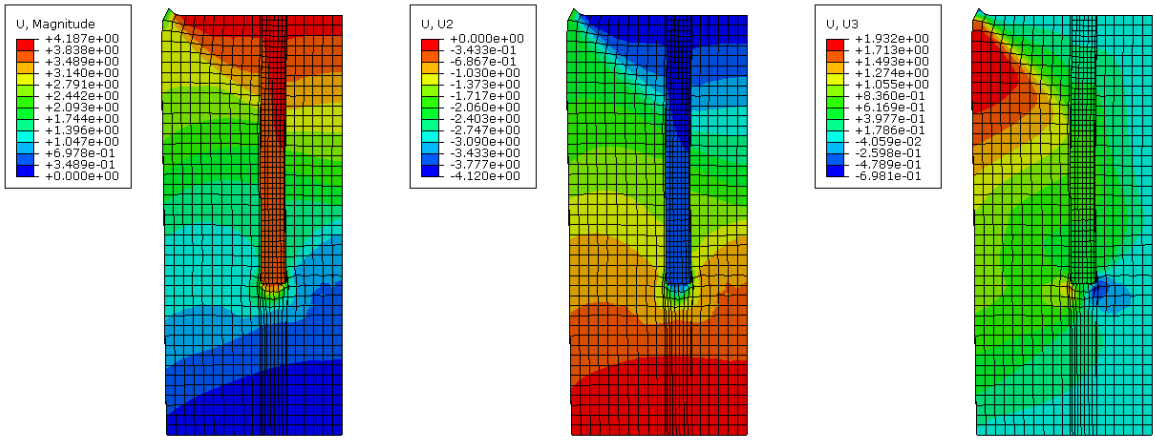

(a) U at increment 11 (u=4) **(b)** U2 at increment 11 (u=4) **(c)** U3 at increment 11 (u=4)

Figure 4.10: Comparison of deformation vectors at u=4 for BM4D.

Stress & strain fields

The stress analysis indicates that the maximum stresses in both the dowel and the timber remain below the material strength limits, confirming that the model behaves within the expected elastic–plastic range. The peak stress concentrations occur at the top of the dowel and at the bottom of the dowel hole in the timber. In these regions, plastic strain (PEEQ) develops progressively during loading, corresponding to localized crushing and yielding of the timber in compression perpendicular to the grain.

Additional zones of plastic deformation in the timber element were observed along the edges of the steel plate, where stress concentrations arise due to the constraint imposed by the rigid contact boundary.

The stress distribution in the dowel is non-uniform in the YZ-plane, which can be attributed to bending of the dowel in this direction. This bending results from the out-of-plane deformation (U3) of the timber surrounding the dowel, leading to asymmetric stress development along the dowel cross-section.

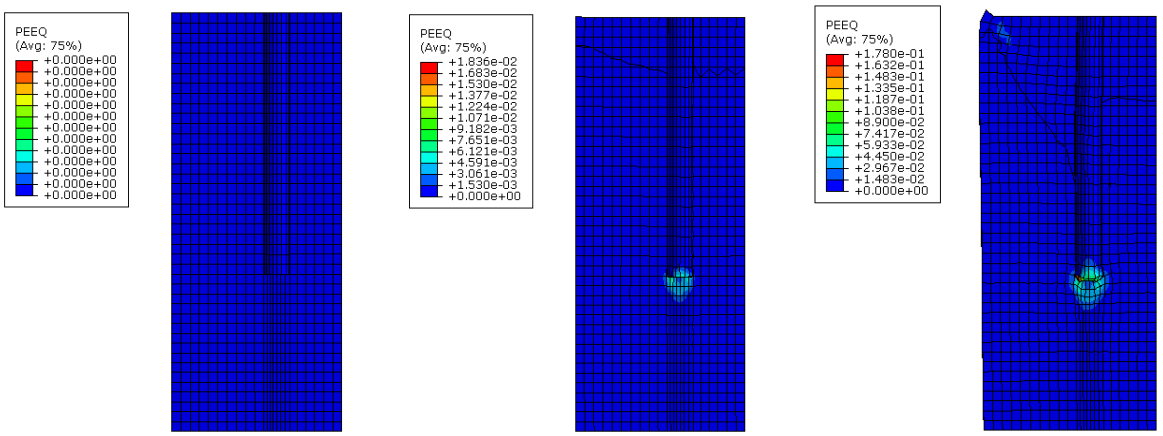

(a) PEEQ at increment 0 (u=0) **(b)** PEEQ at increment 5 (u=1) **(c)** PEEQ at increment 11 (u=4)

Figure 4.11: Comparison of Equivalent Plastic Strain (PEEQ) at different time steps for BM4D.

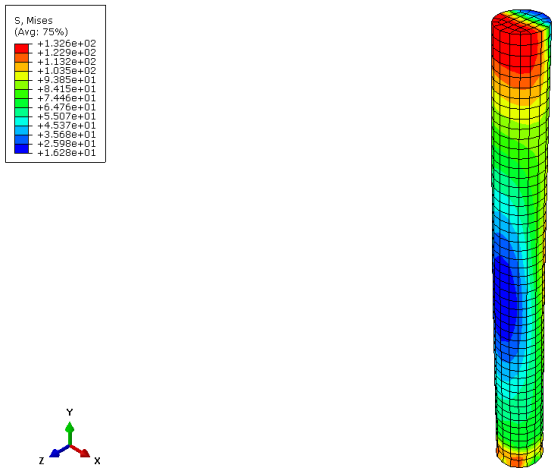

Figure 4.12: Global stress in the dowel at increment 11.

Overall, the stress and strain fields align well with the expected physical behaviour and the patterns observed in the reference model, supporting the accuracy of the numerical representation.

Failure modes

The reference model developed in the literature, which incorporates cohesive zone modelling (CZM) interactions between the timber and densified wood dowels, typically predicted a failure characterized by a combination of yielding and crushing of the timber substrate, together with damage initiation and propagation at the dowel–timber interface.

A similar behaviour was observed in the present model. The numerical results show plastic deformation and crushing of the timber in the region beneath the steel plate and around the dowel hole, while damage initiation occurred at the dowel–timber interface. This confirms that the cohesive behaviour implemented in the current model reproduces the same composite failure mechanism reported in the reference study.

figures of failure modes

To further interpret the observed failure response, comparisons were made with failure mechanisms reported for timber specimens reinforced with screws. The literature identifies three main failure modes (FM):

- FM1: Pushing-in of the screws into the timber, accompanied by compressive failure of the timber perpendicular to the grain at the loaded surface.
- FM2: Buckling of slender screws, combined with compressive failure of the timber perpendicular to the grain.
- FM3: Compressive failure perpendicular to the grain in a plane defined by the screw tips, typically observed for short screws.

The results from the current study are comparable to FM1 and FM3, where the local timber crushing dominates and load transfer occurs primarily through bearing stresses around the reinforcement. The similarity between these modes suggests that the densified wood dowels exhibit mechanical behaviour analogous to short screw reinforcement, likely due to a comparable length-to-diameter (l/d) ratio. This assumption will be further verified by comparing the geometrical parameters and load transfer mechanisms in both reinforcement types.

Contact behaviour

The contact interaction between the different model components was evaluated using the variables `CSTATUS` and `CPRESS`. Overall, the contact definitions behaved as intended and remained numerically stable throughout the analysis.

The `CSTATUS` results indicate full interaction between the steel and the timber surface, showing a continuous “sticking” contact condition across the entire interface. Similarly, full sticking contact was achieved between the dowel top and the steel surface, and between the dowel bottom and the timber surface, confirming that the prescribed cohesive and surface interactions were correctly established. Along the dowel sides, however, the contact was only partially active. Narrow bonded regions were observed in vertical strips along the dowel length, while the remaining side areas showed no contact activation.

(a) Contact area development at step 2.

(b) Close-up of the contact area development of figure 4.13a.

Figure 4.13: Contact area status at the timber–dowel interface.

The contact pressure (`CPRESS`) distribution supports these observations. At the timber–steel interface, higher pressures occurred near the edges of the steel block, which can be attributed to localized timber deformation and minor mesh-induced hourglassing. Extreme pressure peaks appeared at the dowel top–steel interface, but these values were disregarded as numerical artefacts. This conclusion is supported by the absence of corresponding plastic deformation or stress anomalies in the dowel and timber. The contact pressures at the dowel bottom–timber interface remained within the material limits and displayed magnitudes consistent with the expected load transfer mechanism. Along the dowel sides, the contact pressure was relatively uniform across the bonded strips, while the non-contact regions showed zero pressure, consistent with the observed partial contact initiation.

In summary, the contact interactions behaved as expected and showed no signs of numerical instability. The partial side contact of the dowel–timber interface appears to result from realistic deformation behavior rather than modeling errors, and the overall contact response can therefore be considered reliable.

Parametric sensitivity

K-Value Test

The k-values (k_{nn}, k_{ss}, k_{tt}) define the normal and shear stiffness parameters of the cohesive interaction between the dowel and the timber. Since no direct reference values were available in the literature, nor in the Abaqus manual, a sensitivity study was performed to evaluate the influence of these parameters on the global response. Four configurations were analysed:

$$(0, 0, 0),\ (120, 36, 36),\ (250, 75, 75),\ (1000, 300, 300)$$

A clear difference was observed between the model with $k = 0$ and those with non-zero stiffness values (Figure 4.14a). The $k = 0$ model showed a lower stiffness, reflected in a gentler slope of the force–displacement curve and a lower load-carrying capacity. In contrast, all non-zero configurations exhibited a steeper initial slope and higher peak force, indicating a stronger interaction between the dowel and the timber.

The $k = 0$ model was able to reach the full prescribed displacement of 10 mm without convergence issues. However, the simulations with non-zero k-values terminated earlier, as the increment size became too small due to local instability or damage localization. The higher the k-value, the earlier this effect occurred. Increasing the k-value beyond 1000 resulted in unstable models, which no longer converged at all. Besides this point, no significant difference was observed among the three non-zero configurations, suggesting that the model response is insensitive to increases in interface stiffness.

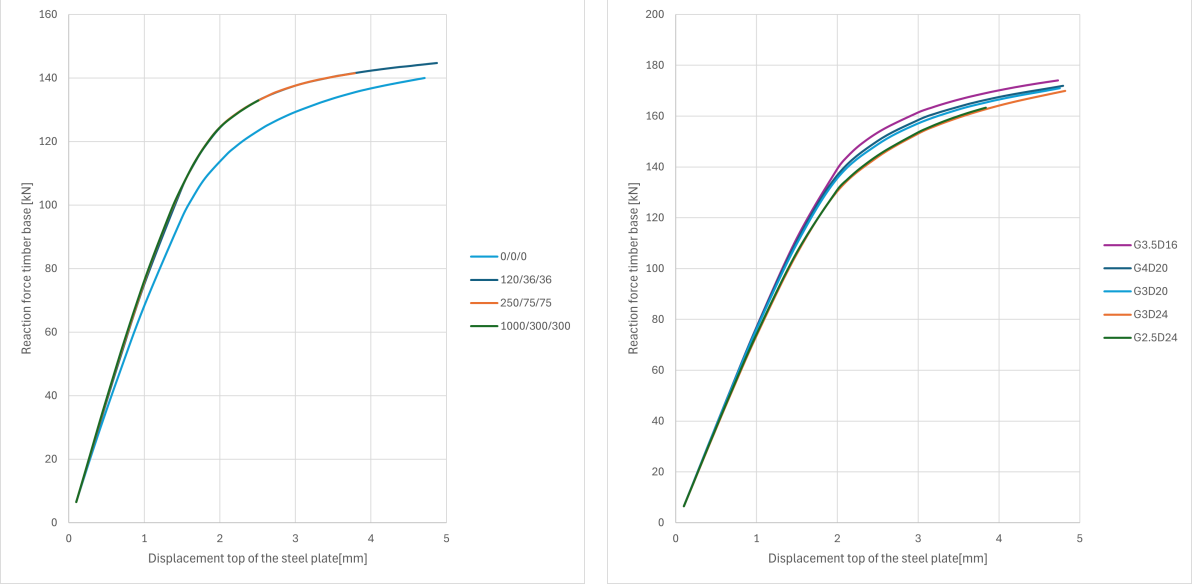

(a) Influence of contact stiffness K-values on the global force–displacement response.

(b) Mesh sensitivity of the global force–displacement response.

Figure 4.14: Sensitivity analysis of the base numerical model.

Mesh sensitivity

The initial mesh configuration was determined based on the coarsest element size that still allowed all implemented model features, such as interaction properties, plasticity, the Hill yield criterion, and cohesive behaviour, to function correctly. The complete model was first analysed using the smallest mesh size necessary to ensure convergence of all these components.

In general, a finer mesh leads to more accurate results but at the cost of significantly increased computational time. This effect is particularly pronounced in the region surrounding the dowel hole (and in the dowel itself). As shown in Figure 4.14b, refining the mesh locally around the hole results in a noticeable improvement in the predicted response. However, refining the global mesh size while maintaining the same local refinement around the dowel hole does not significantly influence the overall results.

Further mesh refinement beyond the configurations shown in Figure 4.14b leads to excessively long computation times, in some cases requiring several days to complete a single simulation. Therefore, an optimal mesh density was selected as a compromise between numerical accuracy and computational efficiency.

5

Results

This chapter presents the results obtained from the numerical and analytical investigations conducted in this study. The results are structured to progressively build insight from model development to application at design level.

First, the response of the validated base finite element model is presented, providing reference behaviour in terms of stiffness, load transfer, and failure mechanisms. Subsequently, results from derived numerical models are introduced to illustrate the influence of key parameters such as reinforcement layout and dowel interaction. These results form the basis for quantifying the effective contribution of individual reinforcement elements at component level.

In parallel, the analytical model used to assess reinforcement capacity is presented, and its predictions are compared with numerical outcomes. This comparison highlights differences arising from the assumed load-transfer mechanisms and provides context for the limitations and applicability of simplified design approaches. Where available, results are also compared with reference data from literature to ensure consistency with established experimental observations.

Finally, the chapter concludes with the presentation of the results from the third part of the case study, in which the developed numerical and analytical insights are applied to a representative connection detail. An example calculation is provided to demonstrate how the obtained resistance contributions translate into utilisation levels at structural scale.

Interpretation of the results and their implications for design and modelling assumptions are addressed in the subsequent discussion chapter.

5.1. Base models

5.1.1. Force - displacement curves

Force–displacement curves were extracted for the four reference configurations containing 0, 2, 4, and 6 dowels. The vertical reaction force (RF2) was calculated by summing the reaction components at the bottom surface elements of the timber block. Because quarter symmetry was applied in all models, the obtained reaction force was multiplied by a factor of four to represent the full specimen response.

The corresponding displacement was computed as the average vertical displacement (U2) of the top surface nodes of the steel loading plate, providing a representative measure of the global deformation under compressive loading.

Figure 5.1 shows the resulting curves, which allow a direct comparison of the global stiffness and load-bearing capacity between the configurations. As expected, the inclusion of dowels increases both the initial stiffness and the peak load, with the magnitude of improvement correlating with the number of dowels. The 0-dowel configuration exhibits the lowest capacity and softest response, while the 6-dowel configuration shows the highest resistance. These results confirm that the reinforcement mechanism observed in the numerical models aligns with the intended contribution of the dowels under compression perpendicular to the grain.

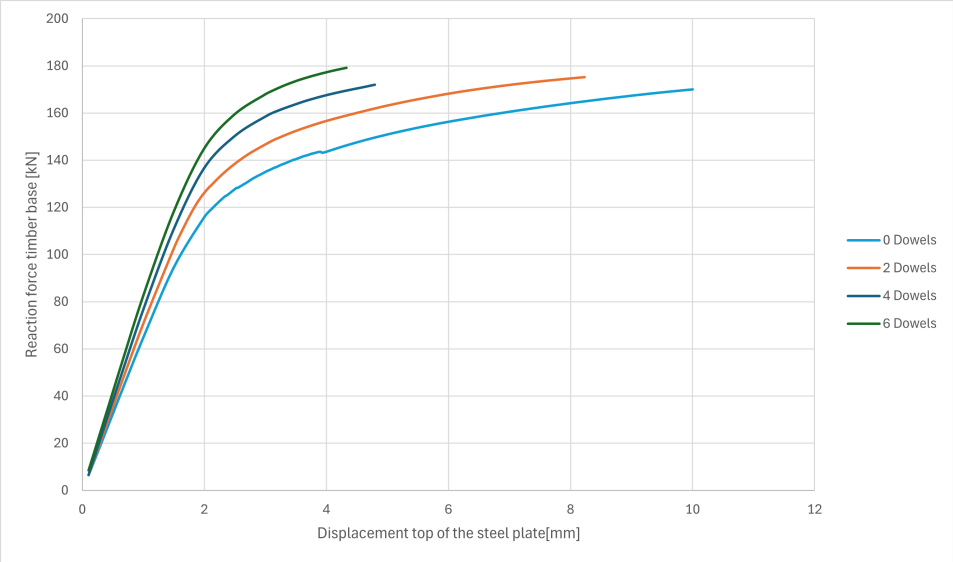

Figure 5.1: Force-displacement curves of the base models from the **developed** FEM model.

The maximum compressive capacity perpendicular to the grain used in this study is determined in accordance with NEN 408 clause 17.3.1. Due to the pronounced nonlinear load–deformation behaviour in compression perpendicular to the grain, the maximum compressive load $F_{c,90,\max}$ is not taken as the peak load, but is defined using an offset method based on the load–deformation curve (figure 5.2). The modulus of elasticity $E_{c,90}$ is first determined from the linear portion of the response between 10 % and 40 % of an estimated maximum load. A straight line parallel to this elastic reference line is then constructed with an initial deformation offset of $0.01\,h_0$, where h_0 is the original specimen height. The intersection of this offset line with the measured load–deformation curve defines $F_{c,90,\max}$. An iterative procedure is applied until convergence within the tolerance specified in NEN 408 is achieved.

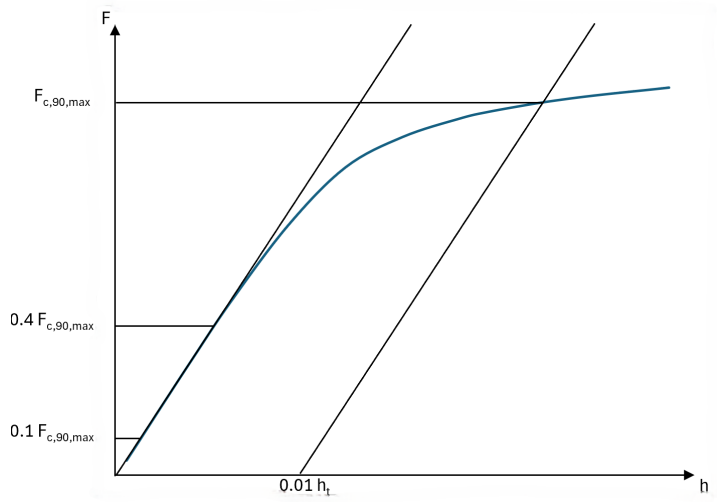

Figure 5.2: Load-deformation diagram according to EC 408.

Table 5.1 summarizes the numerical results obtained from the developed dowel-reinforced beam model for different configurations. The maximum compression perpendicular-to-grain force, $F_{c,90,\max}$, and the corresponding system stress, $f_{c,90,\mathrm{sys}}$, are reported for each case, highlighting the effect of increasing dowel reinforcement on the load-carrying capacity.

Table 5.1: Numerical results of the developed dowel-reinforced beam model: maximum compression perpendicular-to-grain force ($F_{c,90,\max}$) and system stress ($f_{c,90,\mathrm{sys}}$) for different dowel configurations.

Configuration	$F_{c,90,\max}$ (kN)	$f_{c,90,\mathrm{sys}}$ (MPa)
BM0D	143	9.94
BM2D	155	10.8
BM4D	165	11.5
BM6D	176	12.2

5.1.2. Force distribution

To evaluate how the applied load is transferred through the timber and influenced by the presence of wooden dowels, the stress distribution was analysed for all four base models (BMs). Stresses were extracted from the timber only (excluding the dowels) along a predefined path in the global x-direction. This path was located at mid-width of the dowel arrangement ($Y = 25$ mm) and evaluated at several heights in the specimen, namely $z = 30$, 57, 63, and 90 mm measured from the bottom surface. All results discussed in this subsection correspond to a downward displacement of the top steel plate of $U = 1$ mm.

Figure 5.3 illustrates the force distribution concept and the locations of the stress evaluation paths. The figure indicates the direction of the applied displacement, and the different z-levels at which the stresses were retrieved. For each level, the von Mises stress S and the normal stress S_{22} (perpendicular to the grain and aligned with the loading direction) were evaluated along the length of the specimen in the x-direction.

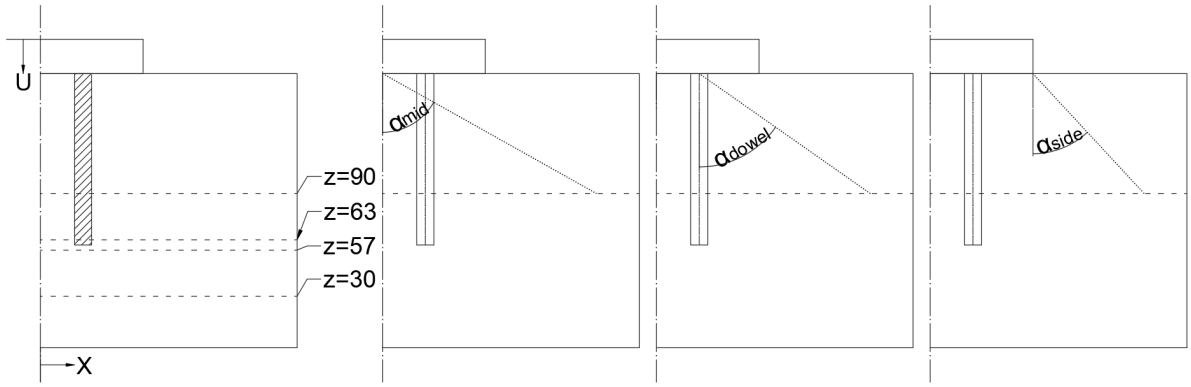

Figure 5.3: In the left figure, the different levels and directions. In the right figure the different calculated angles.

Stress distribution at $z = 30$ mm

The stress distribution at $z = 30$ mm is shown in Figure 5.4a. At this depth, the distribution of the compressive stress component S_{22} exhibits similar magnitudes across the specimen. Localised variations are observed in the vicinity of the dowel locations.

For the base models, higher stress levels are observed at this depth for models with a larger number of dowels, particularly near the centre of the specimen ($x = 0$). Towards the specimen edge ($x = 150$ mm), the stress levels of all base models decrease and converge. The overall shape and spatial spreading of the stress distributions are similar for all base models.

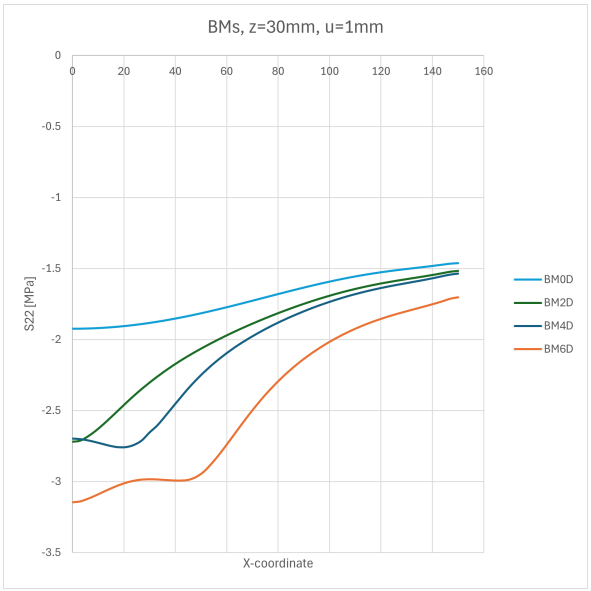

(a) Equivalent compressive stress distribution at $z = 30$ mm for the base models.

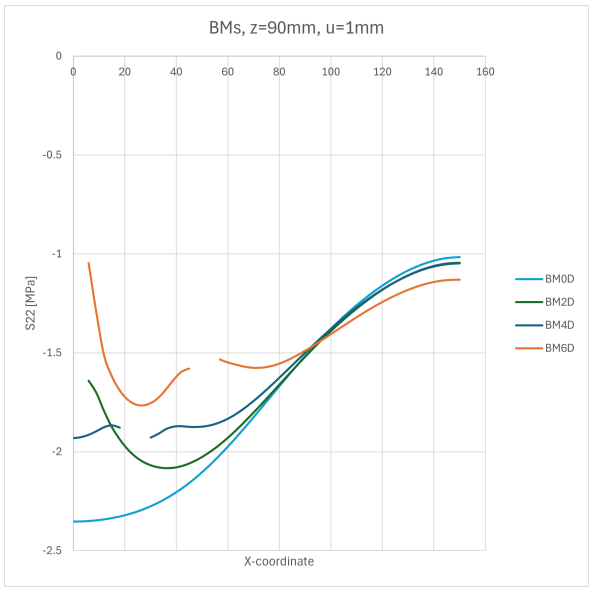

(b) Equivalent compressive stress distribution at $z = 90$ mm for the base models.

Figure 5.4: Equivalent compressive stress (S22) distributions obtained from the numerical models at two different vertical levels.

Stress distribution at $z = 90$ mm

The stress distributions at $z = 90$ mm are presented in Figure 5.4b. At this level, discontinuities are visible in the stress curves at the dowel locations. These discontinuities are more pronounced than at $z = 30$ mm, particularly in the regions around the dowels.

Higher stress levels are observed near the centre of the specimen ($x = 0$) for all base models. In this region, models with fewer dowels exhibit higher compressive stress values in the timber. Towards the specimen edge ($x = 150$ mm), the stress levels decrease and become nearly identical for all base

models. Despite local differences near the centre, the overall stress spreading behaviour remains similar across all base models.

Intermediate levels at $z = 57$ and 63 mm

At the intermediate levels $z = 57$ and 63 mm, pronounced local stress peaks are observed. At $z = 57$ mm, these peaks occur directly underneath the dowels. At $z = 63$ mm, high stress concentrations appear at the edges of the dowel holes, with stress values of opposite sign compared to the surrounding stress field.

Apart from these localised effects, the overall stress distributions at $z = 57$ and 63 mm are very similar. The presence of strong local peaks makes a direct comparison of stress magnitudes between the base models at these levels less consistent.

Force distribution in transverse direction

In addition to the stress spreading in the longitudinal direction, the distribution of compressive stress in the transverse direction, perpendicular to the analysed spreading path, was evaluated for BM0D and BM4D. The stresses were extracted at representative depths of $z = 30$ mm and $z = 90$ mm using the same procedure as described previously.

For BM0D, the transverse stress distribution is nearly uniform over the width of the timber block at both evaluated depths. No pronounced stress concentrations or gradients are observed at either $z = 30$ mm or $z = 90$ mm.

For BM4D, the transverse stress distribution is also largely uniform. At $z = 90$ mm, a local reduction in stress is observed in the vicinity of the dowel holes, while locally increased stresses occur directly beneath the dowels. At $z = 30$ mm, no notable deviations from a uniform stress distribution are observed across the specimen width.

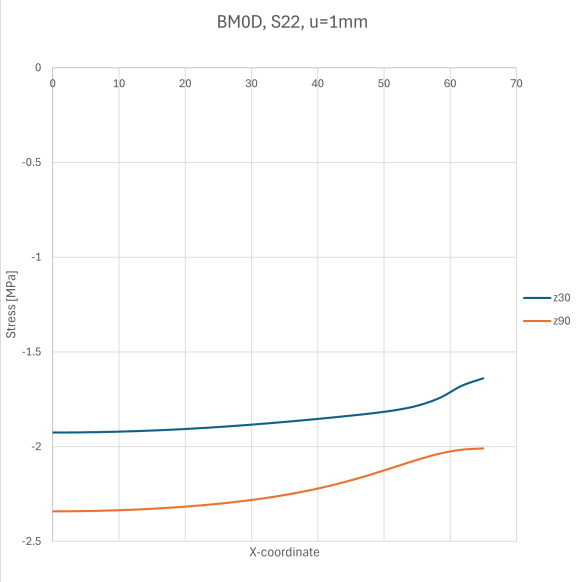

(a) Equivalent compressive stress distribution at $z = 30$ mm and $z = 90$ mm for the BM0D.

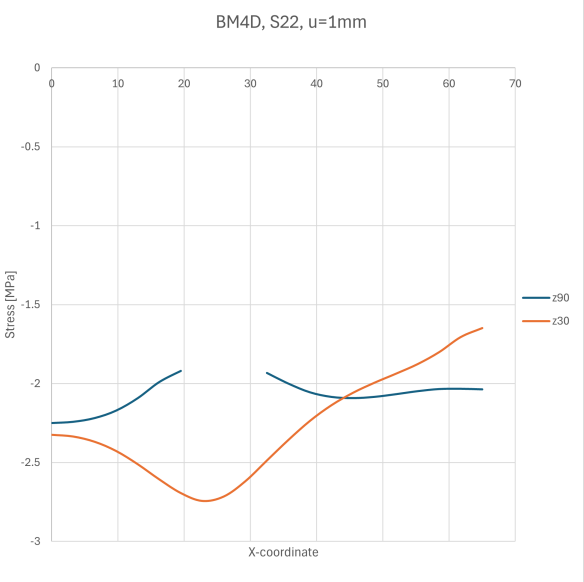

(b) Equivalent compressive stress distribution at $z = 30$ mm and $z = 90$ mm for the BM0D.

Figure 5.5: Equivalent compressive stress (S22) distributions obtained from the numerical models at two different vertical levels in transverse direction.

Force distribution along the dowel length

To investigate the force transfer mechanism between the dowel and the surrounding timber, the compressive stress component S_{22} was evaluated along the dowel length at multiple circumferential positions. The stress was extracted along paths running parallel to the dowel axis, located at a distance of 5 mm from the dowel–timber interface. This offset was chosen to avoid local numerical disturbances at the contact interface, while still capturing the stress state representative of the timber immediately

surrounding the dowel. The locations of the measurement paths, denoted as points A to E around the dowel circumference, are illustrated in figure‘5.6.

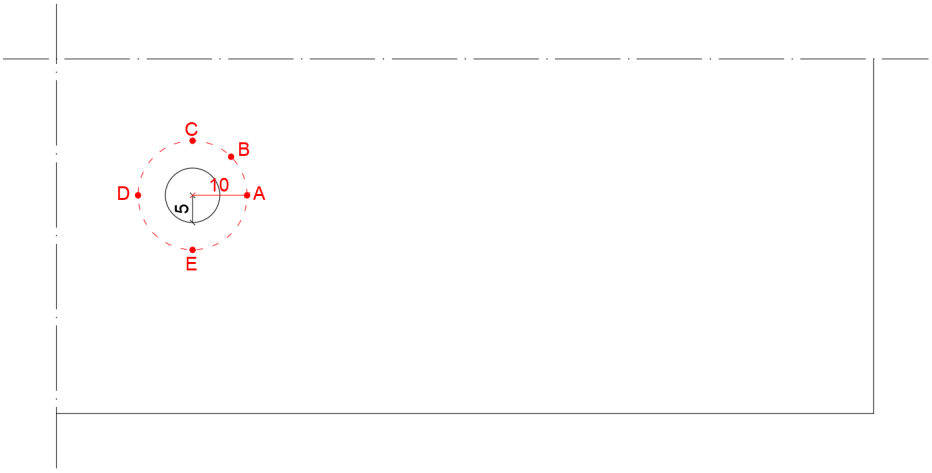

Figure 5.6: Schematic representation of a quarter of model BM4D showing the dowel and the measurement locations A–E distributed circumferentially around the dowel. The stress is evaluated along paths parallel to the dowel axis, positioned $5\ \mathrm{mm}$ away from the dowel–timber interface.

The stress distributions along the dowel length exhibit a consistent overall trend for all measured circumferential positions. Over the majority of the dowel length, the compressive stress S_{22} increases with depth, with values rising from approximately -1.0 to $-3.0\ \mathrm{MPa}$ near the top to about -2.5 to $-3.0\ \mathrm{MPa}$ at the deepest measurement locations. This indicates a progressive transfer of force from the dowel into the surrounding timber as the distance from the loaded surface increases.

In the upper region of the dowel, deviations from this monotonic increase are observed. In this zone, stress values vary more strongly between measurement points, with differences of up to approximately $1.5\ \mathrm{MPa}$ between circumferential locations. These deviations are attributed to local deformation and contact effects near the loaded surface. Below this region, the stress profiles converge and follow a similar shape, with circumferential variations reducing to typically less than $0.5\ \mathrm{MPa}$.

Although some variation remains between the different circumferential locations, the dominant trend is governed by depth along the dowel, with deeper positions consistently exhibiting higher compressive stresses. This confirms that the force transfer mechanism along the dowel length is similar for all measured positions, despite local non-uniformities around the dowel perimeter.

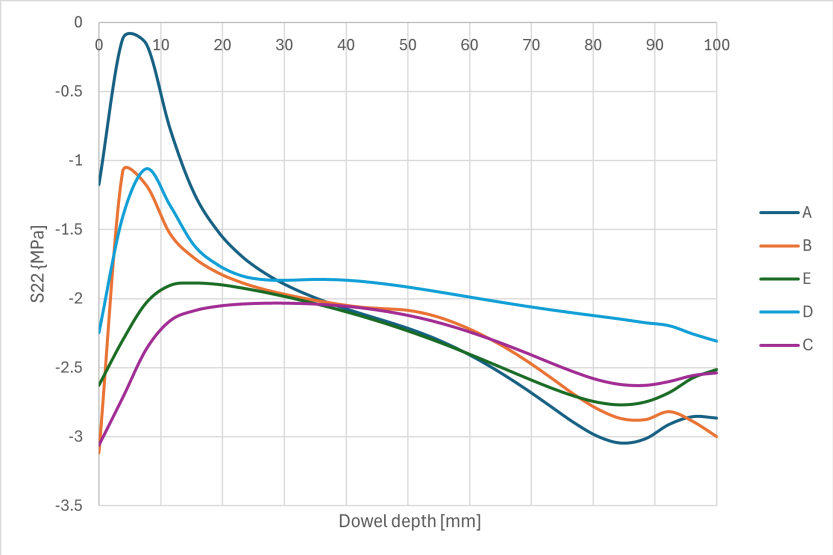

Figure 5.7: Compressive stress S_{22} measured along the dowel length at locations A–E for model BM4D, corresponding to the measurement paths illustrated in Figure 5.6.

5.1.3. Equivalent stress block and stress spreading angle

At a vertical level of $z = 90$ mm, a characteristic stress spreading width was determined by replacing the non-uniform compressive stress distribution with an equivalent rectangular stress block. The block was defined such that it results in the same resultant force as the numerical stress distribution,

$$\int \sigma(x)\,\mathrm{d}x = \sigma_{\mathrm{eq}}\, b_{\mathrm{eq}}, \tag{5.1}$$

and is centred at the same location. The block height was taken equal to the maximum compressive stress at the considered level, $\sigma_{\mathrm{eq}} = \sigma_{\max}$, resulting in a unique equivalent block width b_{eq}.

Three stress spreading angles are reported. The angle from the mid, α_{mid}, is defined with respect to the centreline of the specimen. The angle from the side, α_{side}, is defined with respect to the edge of the base plate. In addition, the angle from the dowel, α_{dowel}, is defined with respect to the centreline of the outermost dowel. The definitions of all three angles are illustrated in Figure 5.3.

The corresponding stress spreading angles for the base models are summarised in Table 5.3.

Table 5.2: Stress spreading angles determined from equivalent stress blocks for base models

	BM0D	BM2D	BM4D	BM6D
α_{mid} [°]	60.0	58.2	58.9	58.1
α_{dowel} [°]	–	59.3	55.2	47.9
α_{side} [°]	36.6	37.2	38.6	36.8

The stress spreading angles determined from the middle and the side of the equivalent stress block remain relatively uniform across all base models. This can be attributed to the identical dimensions of the steel bearing plate and the constant width of the timber member, which govern the overall stress dispersion. In contrast, the stress spreading angle associated with the outermost dowel decreases as the number of dowels increases. This is a direct consequence of the outward shift of the reference line for this angle as additional dowels are introduced, rather than a change in the underlying stress distribution mechanism.

Table 5.3 presents the stress spreading angles determined from the equivalent stress blocks for the base models with modified bearing plate dimensions for the configurations with two and four dowels.

In these models, the edge of the steel bearing plate is positioned at a constant distance of 15 mm from the centreline of the outermost dowel, resulting in different bearing plate dimensions for the two configurations.

Table 5.3: Stress spreading angles determined from equivalent stress blocks for modified base models

	BM2D	BM4D
α_{mid} [°]	52.6	54.7
α_{dowel} [°]	52.6	50.1
α_{side} [°]	49.4	44.5

Compared to the original base models, the modified bearing plate geometry leads to noticeable changes in the stress spreading angles. In particular, the angles defined with respect to the specimen centreline and the plate edge show a stronger dependency on the dowel configuration, reflecting the influence of the changed load introduction width. The stress spreading angle defined with respect to the outermost dowel remains of similar magnitude for both configurations.

5.2. Derived models

The following subsection presents the results obtained from the derived models, with a focus on the stress distribution and the obtained quantities introduced in the previous sections.

5.2.1. Dowel Side Test

To quantify the lateral bearing capacity of the dowel–timber interaction, a parametric study was conducted in which either the dowel diameter or the embedded dowel length was varied. Two sets of simulations were performed:

1. Diameter variation: $d = 10, 12, 14\,\text{mm}$ with a constant length of $l = 100\,\text{mm}$.
2. Length variation: $l = 50, 75, 100, 125, 150\,\text{mm}$ with a constant diameter of $d = 10\,\text{mm}$.

The resulting force–displacement curves are presented in Figures 5.8a and 5.8b, corresponding to the diameter and length variations, respectively.

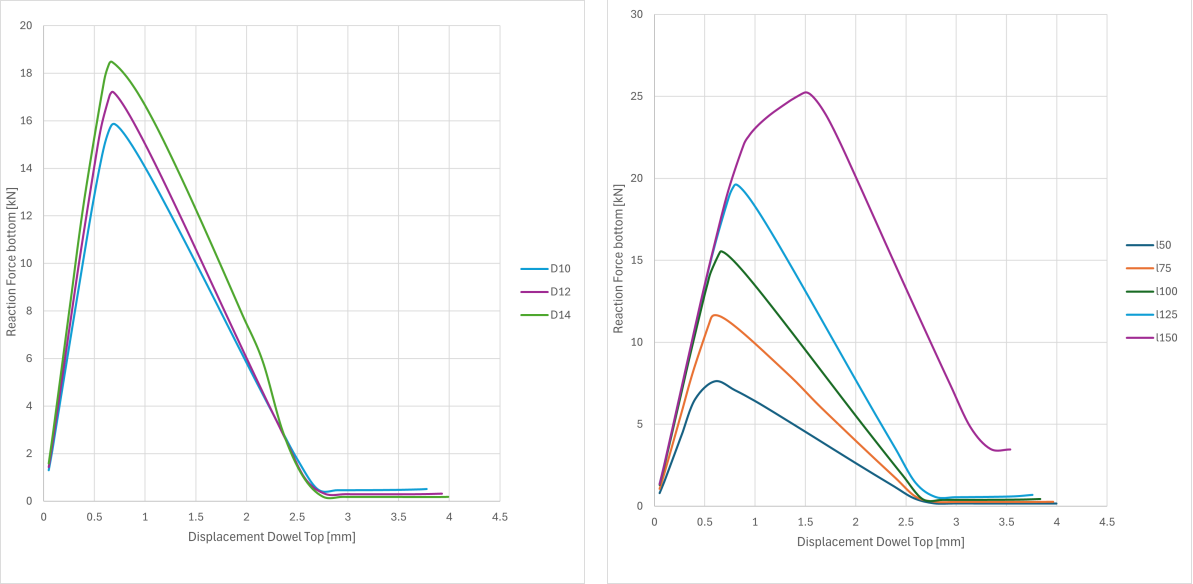

(a) Force–displacement curves for different dowel diameters.

(b) Force–displacement curves for different dowel lengths.

Figure 5.8: Force–displacement curves of the dowel side tests.

Both parameter studies show an approximately linear relationship between displacement and reac-

tion force up to the peak load. For the diameter variation, an increase in dowel diameter results in a proportional increase in stiffness and peak force.

For the length variation, the force–displacement response shows a linear increase in capacity up to the peak load for all configurations. For dowels with slenderness ratios below approximately

$$\frac{l}{d} \approx 15, \tag{5.2}$$

the post-peak response is characterised by a linear decrease in reaction force with increasing displacement.

Figure 5.9 illustrates the vertical displacement field U_3 for the DST configuration with and without a dowel at an identical global displacement level. The comparison highlights the influence of the dowel on the local deformation pattern of the surrounding timber.

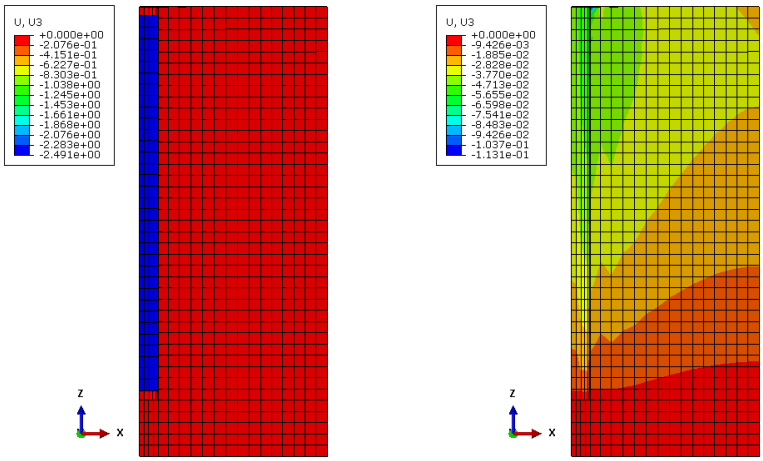

(a) DST with dowel **(b)** DST without dowel

Figure 5.9: Vertical displacement field U_3 of the Dowel Side Test (DST) at a global displacement of $u = 2.6$ mm.

Figure 5.9 shows the vertical displacement field U_3 for the Dowel Side Test (DST) at a global displacement of $u = 2.6$ mm, comparing the configuration with a dowel to the configuration without a dowel. Both results are extracted at the same analysis time step.

In addition, parametric studies were conducted to evaluate the influence of dowel geometry on the compressive capacity of the DST configuration. Table 5.4 summarises the effect of dowel diameter, while Table 5.5 presents the corresponding results for varying dowel embedment length. In both cases, the reported values correspond to the maximum compressive force perpendicular to the grain, $F_{c,90,max}$, obtained from the numerical simulations.

Table 5.4: Maximum compressive force perpendicular to grain as a function of dowel diameter (l=100 mm).

Dowel diameter [mm]	10	12	14
$F_{c,90,max}$ [kN]	15.9	17.1	18.3

Table 5.5: Maximum compressive force perpendicular to grain as a function of dowel length (d=10 mm).

Dowel length [mm]	50	75	100	125	150
$F_{c,90,max}$ [kN]	7.6	11.6	15.5	19.6	25.2

The linear force–displacement response observed in the Dowel Side Test reflects the lateral bearing behaviour of the dowel against the surrounding timber. With the dowel tip removed, load transfer is

governed solely by side-bearing stresses, and the stiffness scales with the effective contact area along the dowel shaft. For slenderness ratios below l/d ≈ 15, post-peak unloading indicates progressive localised damage, whereas higher slenderness ratios exhibit a secondary load increase, suggesting additional portions of the dowel engage in load transfer.

5.2.2. Dowel Tip Test

To isolate the bearing behaviour at the end of the dowel, a series of simulations was performed in which the dowel tip was modelled for four different diameters: $d = 8, 10, 12,$ and $14\,\mathrm{mm}$. In all cases, only the final portion of the dowel was included, ensuring that load transfer occurred exclusively through the dowel tip rather than through lateral surface contact.

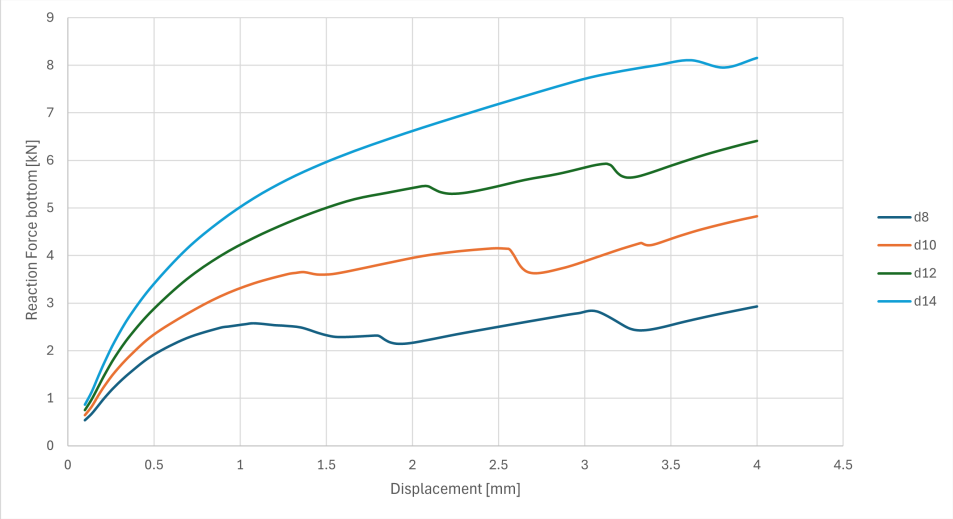

Figure 5.10: Force–displacement curves of the dowel tip test for varying diameters.

All configurations exhibit a short initial linear increase in reaction force, corresponding to the elastic response of the timber directly beneath the dowel tip. This linear region is limited in extent and shows a relatively low stiffness for all dowel diameters.

Following the initial linear phase, the force–displacement curves display a gradual reduction in slope and the appearance of small oscillations in the reaction force. No pronounced peak load is observed, and the reaction force remains relatively low compared to the forces obtained in the dowel side tests.

Figure 5.11 shows the vertical displacement field U_3 of the Dowel Side Test (DST) at a global displacement of $u = 2.6\,\mathrm{mm}$ with and without a dowel. The comparison highlights the influence of the dowel on the deformation pattern and load transfer mechanism within the model.

Table 5.6 presents the maximum compressive force perpendicular to the grain, $F_{\mathrm{c},90,\mathrm{max}}$, obtained from the DTT for different dowel diameters. These results provide insight into the effect of dowel diameter on the load-bearing capacity under perpendicular-to-grain compression.

Table 5.6: Maximum compressive force perpendicular to grain as a function of dowel diameter

Dowel diameter [mm]	8	10	12	14
$F_{\mathrm{c},90,\mathrm{max}}$ [kN]	2.9	4.8	6.4	8.2

5.2.3. Dowel Side + Tip Test

The Dowel Side and Tip Test (DSTT) represents the complete dowel configuration, in which both lateral dowel–timber interaction and compressive bearing at the dowel tip are activated simultaneously. The applied displacement is transferred through a steel loading component placed on top of the dowel,

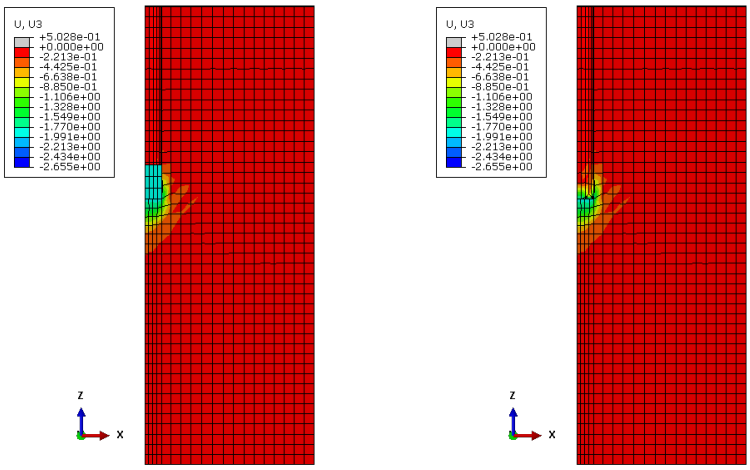

(a) DTT with dowel **(b)** DTT without dowel

Figure 5.11: Vertical displacement field U_3 of the Dowel Side Test (DST) at a global displacement of $u = 2.6$ mm.

resulting in a combined load transfer mechanism consisting of embedding stresses along the dowel shaft and compressive stresses beneath the dowel tip.

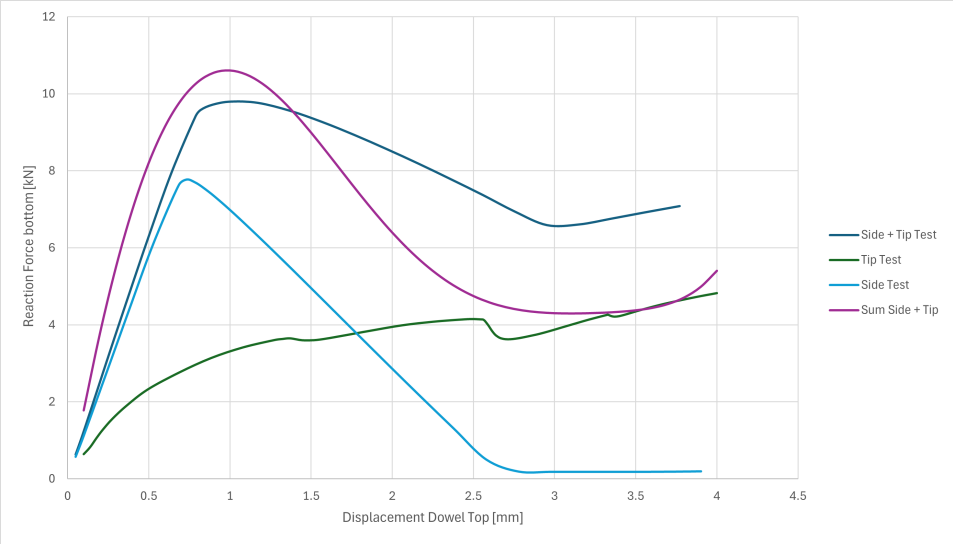

Figure 5.12: Force–displacement curves of the DTT, DST, and DSTT models for $d = 10$ mm, $l = 100$ mm.

Figure 5.12 compares the force–displacement responses of the individual DTT and DST models with the combined DSTT model for a dowel diameter of $d = 10$ mm and an embedded length of $l = 100$ mm.

The DSTT response exhibits a higher initial stiffness and a larger peak load compared to the individual DTT or DST responses. Manually superposing exponential fits of the DTT and DST curves produces an approximate combined response that matches the overall peak load of the DSTT model but slightly overestimates the initial stiffness. Beyond the peak load, the manually combined curve tends to converge toward the DTT response, whereas the DSTT curve maintains a smoother post-peak decline.

Figure 5.13 presents the vertical displacement field U_3 obtained from the Dowel Side Tip Test (DSTT) at a global displacement of $u = 2.6$ mm. Results are shown with and without a dowel to illustrate the deformation behavior in and around the dowel and local displacement distribution.

The combined dowel side and tip test demonstrates that lateral and tip mechanisms interact and cannot be fully represented by a simple superposition of the individual contributions. During early loading, both

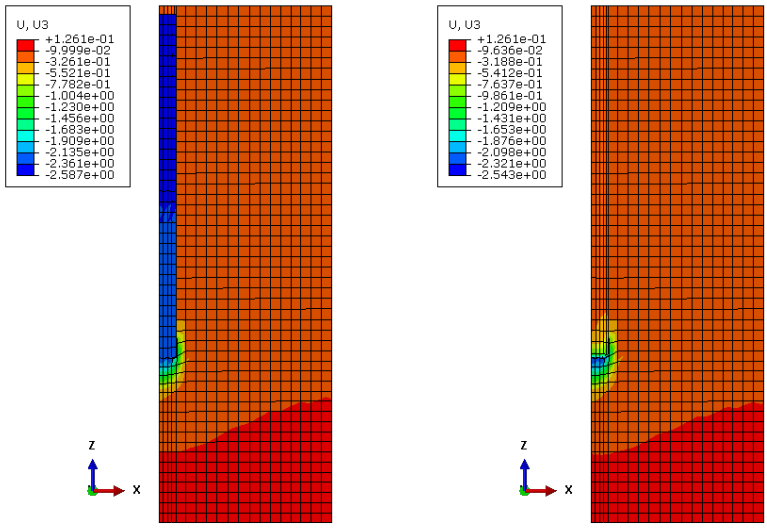

(a) DSTT with dowel **(b)** DSTT without dowel

Figure 5.13: Vertical displacement field U_3 of the Dowel Side Tip Test (DSTT) at a global displacement of $u = 2.6$ mm.

mechanisms contribute, producing a slightly lower combined stiffness than the manually summed curve due to stress redistribution along the dowel and within the timber. After peak load, the side-bearing contribution diminishes while tip-bearing stresses continue to act, resulting in a smoother post-peak decline.

5.3. Dowel material tests

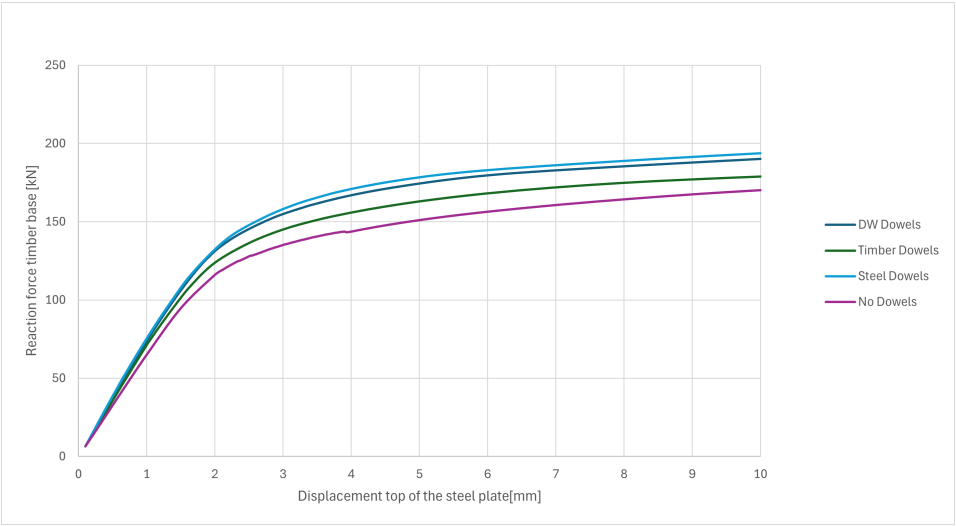

Figure 5.14: Force–displacement curves of different material tests.

A series of material substitution simulations were performed using the baseline model with four dowels, replacing the densified wood dowels with alternative materials: (i) Douglas Fir glulam (timber), (ii) structural steel, and (iii) no dowels (0D) as a lower-bound reference. The resulting force–displacement responses are presented in Figure 5.14.

All configurations exhibit a qualitatively similar behaviour, characterized by an initial elastic phase followed by a transition into crushing-dominated deformation. The primary differences are observed in the load-bearing capacity. Table 5.7 summarises the peak compressive forces perpendicular to the

grain, $F_{c,90}$, for each configuration. .

Although small variations in initial stiffness are apparent between the models, the post-yield slopes remain comparable, indicating consistent deformation behaviour across the different dowel materials.

Table 5.7: Dowel material tests results.

	No Dowels	Timber	DW	Steel
$F_{c,90}\,[\mathrm{kN}]$	144	156	167	171
$F_{c,90} \cdot \frac{F_{\mathrm{NumRef}}}{F_{\mathrm{NumDev}}}[\mathrm{kN}]$	125	139	149	152

5.4. Analytical model

This section presents the results of the analytical model based on Eurocode 5 (EN1995-1-1:2025). The analytical model is used to estimate the load-bearing capacity and stress distribution of timber elements subjected to compression perpendicular to the grain, both with and without dowel reinforcement. The results serve as a reference for comparison with numerical simulations and to assess the predictive value of EC5-based design rules.

5.4.1. Definition of the analytical model

A full explanation of the analytical model is given in Sections 2.8 and 4.1.4. For the purpose of comparison with the numerical (FEM) results and the reference experimental study, several adaptations to the standard Eurocode 5 formulation were applied.

Table 5.8: Geometrical and material parameters used in the analytical EC5-based model

Parameter	**Symbol**	**Value**	**Source / Remark**
Timber product	–		Case study and reference paper
Dowel product	–		Case study and reference paper
Mean compressive strength perpendicular to grain of the timber	$f_{c,90,timber}$	5 MPa	Case study and reference paper
Mean compressive strength parallel to grain of the dowel	$f_{c,0,dowel}$	130 MPa	Case study and reference paper
Bearing width	$b_{c,90}$	120 mm	Case study and reference paper
Bearing length	$l_{c,90}$	120 mm	Case study and reference paper
Timber height, width and length	h_t, b_t, l_t	160, 130, 300 mm	Case study and reference paper
Dowel length	l_{d}	100 mm	Parametric variable
Dowel diameter	d_d	10 mm	Parametric variable
Dowel spacing	a	50 mm	Parametric variable

For comparison between the developed numerical results and the analytical expressions, an effective material factor $k_{\mathrm{mat,eff}}$ is defined. This factor is derived from the maximum compressive force perpendicular to the grain obtained from the numerical models (subsection 5.5.1) and represents the additional load-carrying capacity mobilised due to post-elastic deformation beyond the characteristic compressive strength $f_{c,90,k}$. The parameter $k_{\mathrm{mat,eff}}$ is used as an interpretation measure and does not represent a prescribed design value.

Accordingly, the effective material factor is calculated as:

$$k_{\mathrm{mat,eff}} = \frac{F_{c,90,\max}}{A_{\mathrm{bearing}}\, f_{c,90,timber}} \tag{5.3}$$

Table 5.9: Effective material factors ($\mathrm{k_{mat,eff}}$) calculated for comparison between **developed** numerical results and analytical results.

	BM0D	BM2D	BM4D	BM6D
$\mathrm{k_{mat,eff}}$	1.98	2.15	2.30	2.44

5.4.2. Analytical results

This subsection presents the results obtained from the analytical model for the base configurations. The analytical predictions of the compression perpendicular-to-the-grain resistance, $F_{c,90}$, are reported for different modelling assumptions.

Table 5.10 presents the analytical results for each beam configuration using the previously determined effective material factors $k_{\mathrm{mat,eff}}$. Only the contribution from the dowel tip is considered, and a constant inclination angle of $\alpha = 45°$ is applied for this calculation series. The bold values indicate the chosen results for each configuration.

Table 5.10: Analytical results with the determined $\mathrm{k_{mat,eff}}$ factors, contribution of only the dowel tip and $\alpha = 45°$.

	BM0D	BM2D	BM4D	BM6D
$F_{c,90} = \min$	**142.6**	158.7	173.5	**187.5**
[kN]	–	**130.0**	**162.5**	195.0

The values highlighted in **bold** indicate the selected results for each configuration. It is noted that, with this approach, the calculated force for BM2D is lower than for BM0D. This behaviour results from the minimum condition governing the analytical expression and reflects the sensitivity of the formulation to the assumed stress distribution. The angle of $45°$ is chosen consistently for this calculation series (based on EN1995-1-1 figure 8.5); in the previous stress distribution analysis, other inclination angles were also determined. A subsequent calculation series using these specific angles will be presented in the next table.

Table 5.11: Analytical results with the determined $\mathrm{k_{mat,eff}}$ factors, contribution of only the dowel tip and the determined value for α.

	BM0D	BM2D	BM4D	BM6D
$F_{c,90} = \min$	**142.6**	**158.7**	**173.5**	**187.5**
[kN]	–	218.9	219.6	208.8

Using the inclination angles determined from the stress distribution analysis (Table 5.11) leads to a consistent increase in the calculated compressive capacity with increasing reinforcement. In this case, the governing capacities are controlled by the same expression for all configurations, resulting in a monotonic trend.

Table 5.13 presents a second set of analytical results in which the effective material factors $k_{\mathrm{mat,eff}}$ are adjusted using the ratios obtained from Table 5.16. These ratios represent the relation between the reference experimental results and the developed numerical results. The applied correction accounts for the slightly lower values of $F_{c,90,\max}$ observed in the experiments compared to the numerical simulations. As in the previous table, only the contribution of the dowel tip is considered, while the inclination angle α is taken from the stress distribution analysis.

In addition, two alternative correction approaches are evaluated. In the first approach, the upper ratio from Table 5.16, based on the comparison between the experimental reference model and the developed numerical model, is applied to the effective material factors.

Table 5.12: Analytical results with the determined $\mathrm{k_{mat,eff}}$ factors multiplied with the **top ratio** from table 5.16, contribution of only the dowel tip and the determined value for α.

	BM0D	BM2D	BM4D	BM6D
$F_{c,90} = \min$	**123.8**	**147.9**	**149.0**	**173.1**
[kN]	–	218.9	219.6	208.8

In the second approach, the lower ratio, derived from the comparison between the numerical reference model and the developed numerical model, is used.

Table 5.13: Analytical results with the determined $\mathrm{k}_{\mathrm{mat,eff}}$ factors multiplied with the **bottom ratio** from table 5.16, contribution of only the dowel tip and the determined value for α.

	BM0D	BM2D	BM4D	BM6D
$F_{c,90} = \min$	**123.8**	**143.3**	**155.3**	**171.7**
[kN]	–	218.9	219.6	208.8

Interpretation of the Analytical Results

The analytical results obtained using the effective material factors $k_{\mathrm{mat,eff}}$ show an overall increase in compressive capacity perpendicular to the grain with an increasing number of dowels. When only the dowel tip contribution is considered and a fixed inclination angle of $\alpha = 45°$ is applied, the calculated capacities exhibit non-monotonic behaviour, most notably the lower governing value for BM2D compared to BM0D. This behaviour is a direct consequence of the governing minimum condition in the analytical expression and the assumed stress distribution.

When inclination angles determined from the stress distribution analysis are used, the analytical results show a more consistent increase in compressive capacity with increasing reinforcement. In this case, the governing values are controlled by the same term of the analytical formulation for all configurations, resulting in a monotonic trend.

Applying the experimentally derived ratios to the effective material factors leads to a systematic reduction of the analytical capacities for all configurations. This correction compensates for the higher maximum compressive forces obtained in the developed numerical models compared to the experimental reference results, while preserving the relative differences between the configurations.

Overall, the analytical results highlight the sensitivity of the calculated compressive capacity perpendicular to the grain to both the assumed stress distribution angle and the calibration of the effective material factor, particularly for configurations with a limited number of dowels.

5.5. Comparison

This section presents a systematic comparison of the results obtained from the different approaches considered in this study. The reference experimental results, the reference numerical model, the developed numerical model, and the analytical predictions are evaluated side by side to assess their consistency and relative accuracy.

The comparison focuses on the maximum compressive force perpendicular to the grain, $F_{c,90,\max}$, and the corresponding system compressive strength, $f_{c,90,\mathrm{sys}}$, for the various dowel configurations. By examining the agreement and deviations between experimental observations, numerical simulations, and analytical formulations, the influence of modelling assumptions and calibration choices on the predicted load-carrying capacity is identified.

Table 5.14: Overview of results for experimental, numerical reference, numerical developed and analytical models.

Configuration	Exp. reference [kN]	Num. reference [kN]	Num. developed [kN]	Analytical [kN]
BM0D	124	123	143	124
BM2D	143	138	155	143
BM4D	141	147	165	155
BM6D	161	159	176	172

5.5.1. Comparison between developed model and reference model

The reference model

Figure 5.15 shows the force–displacement responses of the base model configurations obtained from the reference numerical model developed by O'Ceallaigh et al. (2021). The curves illustrate the global

compressive behaviour perpendicular to the grain for specimens with an increasing number of dowels, up to the maximum applied load.

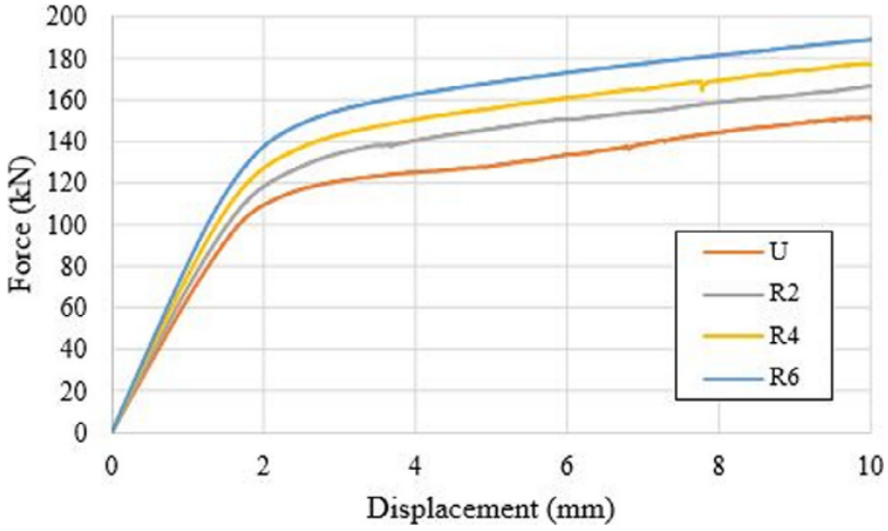

Figure 5.15: Force–displacement curves of **reference** models. Adapted from O'Ceallaigh et al. (2021) [39].

Table 5.15 summarises the corresponding maximum compressive force perpendicular to the grain, $F_{c,90,\max}$, and the associated system compressive strength, $f_{c,90,\mathrm{sys}}$, as obtained from the reference experimental tests and the reference numerical model. These results form the basis for validating the numerical modelling approach used in the present study.

Table 5.15: Numerical and experimental results from the **reference** model.

Configuration	Experimental ref. model		Numerical ref. model	
	$F_{c,90,\max}$ (kN)	$f_{c,90,\mathrm{sys}}$ (MPa)	$F_{c,90,\max}$ (kN)	$f_{c,90,\mathrm{sys}}$ (MPa)
BM0D	124	8.58	123	8.56
BM2D	143	9.94	138	9.57
BM4D	141	9.80	147	10.2
BM6D	161	11.2	159	11.1

Numerical reference vs numerical developed

The developed (figure 5.1) and reference (figure 5.15) load–displacement curves exhibit a very similar overall shape. The initial elastic response, the gradual transition to nonlinear behaviour, and the post-elastic stiffness degradation are consistent between the models. This indicates that the numerical model captures the dominant mechanical mechanisms governing compression perpendicular to the grain, including progressive timber crushing and load redistribution through the reinforcement. After applying a horizontal displacement shift, the elastic portions of the curves align closely. The displacement shift was applied to account for initial seating effects observed at low load levels.

Despite the alignment in the elastic range, a vertical offset in force remains between the two curves over the full displacement range. Achieving full overlap would require an additional force shift. In the present comparison, no force correction was applied. Instead, the difference in force level between the numerical and reference curves is retained and quantified explicitly.

In the reference study, the numerical force–displacement curves (figure 5.15) were aligned with the experimental response by shifting the numerical displacement such that it coincided with the mean experimental displacement at 10% of the maximum experimental load. This procedure cannot be reproduced in the present study, as the full experimental force–displacement histories required for this

alignment are not available. Moreover, the reported alignment appears to involve more than a pure displacement shift, since both force and displacement levels coincide after correction.

To enable a consistent and reproducible comparison, the agreement between numerical and experimental results is therefore evaluated using force ratios. Specifically, the ratios

$$\frac{F_{\mathrm{ExpRef}}}{F_{\mathrm{NumDev}}} \quad \text{and} \quad \frac{F_{\mathrm{NumRef}}}{F_{\mathrm{NumDev}}}$$

are considered, where F_{Num} denotes the peak load obtained from the numerical simulations.

Table 5.16 summarises the ratios of the maximum compressive force perpendicular to the grain obtained from the reference experimental and reference numerical results relative to the developed numerical model.

Table 5.16: Ratios of respectively experimental reference and numerical reference results against developed numerical results.

	BM0D	BM2D	BM4D	BM6D
$\frac{F_{\mathrm{ExpRef}}}{F_{\mathrm{NumDev}}}$	0.87	0.93	0.85	0.92
$\frac{F_{\mathrm{NumRef}}}{F_{\mathrm{NumDev}}}$	0.87	0.90	0.89	0.91

5.5.2. Comparison between developed model and analytical model

The analytical results show a strong dependence on the assumed stress spreading angle and the calibration of the effective material factor $k_{\mathrm{mat,eff}}$. When a fixed spreading angle of $\alpha = 45^\circ$ is applied (Table 5.10), the analytical capacities are consistently higher than those of the developed numerical model. The overestimation increases with the number of dowels and ranges from approximately $+2\%$ for BM0D and BM2D to about $+7\%$ for BM6D.

Using spreading angles derived from the numerical stress distributions (Table 5.11) leads to a substantial increase in the analytical capacities for the reinforced configurations. For BM2D, BM4D and BM6D, predicted capacities of approximately 210–$220\ \mathrm{kN}$ are obtained, exceeding the developed numerical results by roughly 35–45%. This indicates that, without calibration, the analytical formulation significantly overestimates the load-carrying capacity when only the dowel tip contribution is considered.

Applying the calibration based on the ratios from Table 5.16 markedly improves the agreement. Using the top ratio (Table 5.12), the analytical capacities differ from the developed numerical results by -5% for BM2D, -10% for BM4D and -2% for BM6D. When the bottom ratio is applied (Table 5.13), the deviations reduce further to within approximately 2–8% for all reinforced configurations.

Overall, the calibrated analytical models reproduce both the magnitude and the trend of the developed numerical results well. In contrast, uncalibrated analytical approaches systematically overpredict the compressive capacity perpendicular to the grain, particularly as the number of dowels increases.

5.6. Case study: part III

The case study focuses on the Woonzorgvoorziening Aveleijn in Wierden and investigates a two-story timber structure with a column–beam–column connection located at the midspan of a simply supported beam on the first floor. The beam is subjected to compression perpendicular to the grain and is reinforced using either wooden dowels or steel screws. The objective of the case study is to evaluate the applicability of the analytical model and to assess the added value of finite element modeling for practical design.

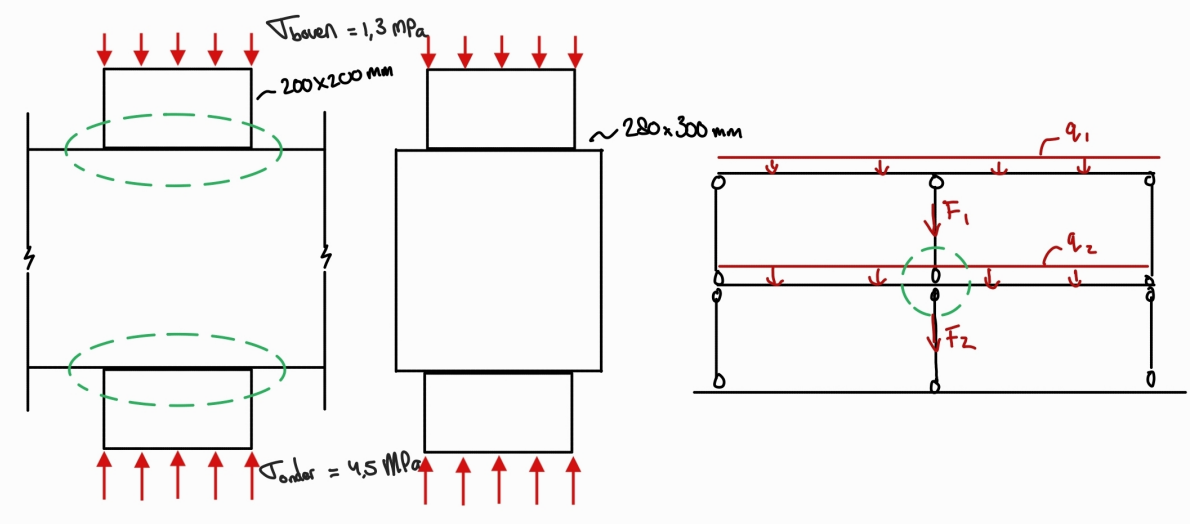

Figure 5.16: Basic configuration and geometric layout of the investigated timber joint in the case study.

5.6.1. Reinforcement layout and assumptions

For the wooden dowel configuration (see figure 5.17a), dowels with a length of 100 mm and a diameter of 10 mm were used. These dimensions were selected to match the materials applied in the numerical and experimental investigations presented earlier in this thesis. The reinforcement consists of a 5×5 dowel layout, resulting in a total of 25 dowels. The spacing between dowels was chosen as $5d$, in accordance with common detailing rules and to limit interaction effects between adjacent dowels.

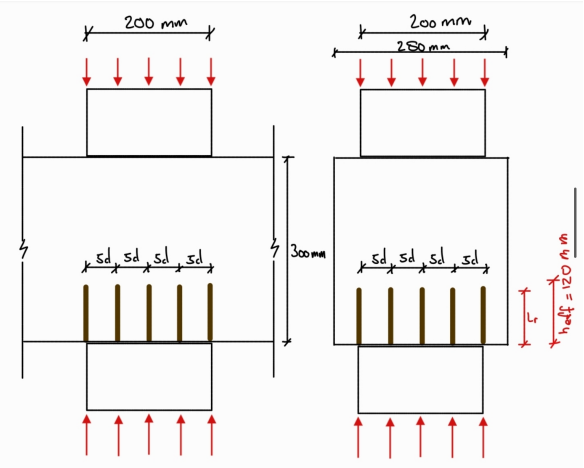

(a) Wooden dowel reinforcement layout used in the case study.

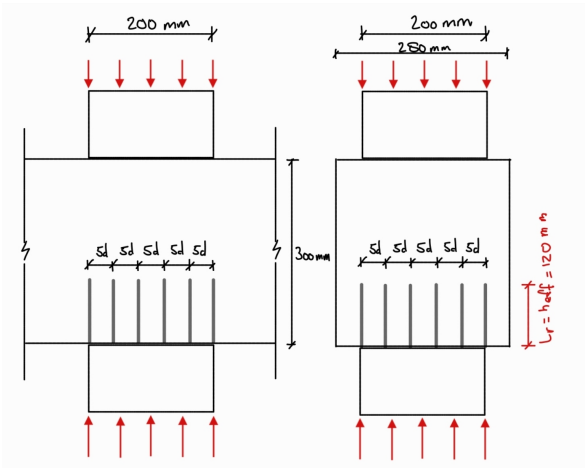

(b) Steel screw reinforcement layout used in the case study.

Figure 5.17: Reinforcement layouts investigated in the case study for timber loaded perpendicular to the grain.

For the steel reinforcement (see figure 5.17b), Rothoblaas VGZ screws with a length of 120 mm and a diameter of 8 mm were adopted (length of 120 mm was chosen to match the calculated effective

height). A 6×6 screw layout was used, corresponding to 36 screws, again based on a spacing of $5d$. The screw configuration was selected to provide a direct comparison with the dowel-reinforced system while reflecting typical practice for self-tapping screw reinforcement.

5.6.2. Results of reinforcement assessment

The assessment of the investigated reinforcement configurations shows that both wooden dowels and steel screws increase the load-bearing capacity of the joint compared to the unreinforced reference. However, for the examined layouts, neither reinforcement strategy fully satisfies the design requirements.

For wooden dowel reinforcement, the derived contribution per dowel obtained from the finite element results leads to utilisation levels exceeding unity. When the dowel capacity is based on the tip resistance derived from the numerical model, with an effective contribution of approximately 5.0 kN per dowel and accounting for the relevant safety factors, a unity check of 1.15 is obtained. In contrast, when the analytical model is applied using a tip capacity of 0.8 kN per dowel, the resulting unity check increases to 1.65. This pronounced difference highlights the sensitivity of the calculated resistance to the assumed load-transfer mechanism. When side interaction and withdrawal-related effects are implicitly included through the finite element model, the effective contribution per dowel increases, resulting in a lower unity check. These mechanisms are not captured in the analytical model, which considers tip bearing only, and therefore leads to more conservative estimates of the dowel contribution.

Steel screw reinforcement results in lower utilisation levels compared to the wooden dowel configuration for comparable reinforcement density. Based on an effective contribution of approximately 10.3 kN per screw (8.6 kN for screws of length 100 mm), the resulting unity check equals 1.15. The higher contribution per fastener reflects the ability of screws to engage a larger volume of timber along their embedded length, resulting in a more distributed load transfer mechanism. The influence of tip effects on the global response is less pronounced than for wooden dowels. The results further indicate that the performance of the screw-reinforced system is not yet optimal and may be improved by adjustments to screw length, diameter, or layout.

Overall, the results show that analytical design approaches provide conservative lower-bound estimates of resistance, while finite element modelling captures interaction effects and load sharing between reinforcement elements. These effects significantly influence the effective contribution of individual dowels and screws and are therefore essential for a realistic assessment of reinforced timber joints loaded perpendicular to the grain.

6

Discussion

Interpretation framework and modelling philosophy

The comparison between the analytical Eurocode-based models and the numerical simulations highlights a fundamental difference in modelling philosophy rather than an inconsistency in material representation. In the present study, this distinction is explicitly addressed through the introduction of k_{mat} factors, which enable a consistent comparison between Eurocode-based characteristic values and the mean material properties used in the finite element model.

The numerical model is primarily intended as a mechanistic investigation tool. Material parameters for timber and densified wood dowels are calibrated to reproduce observed stiffness, deformation behaviour, and stress redistribution, rather than to predict characteristic design resistance. As a result, conclusions drawn from the FEM simulations should be interpreted in terms of governing mechanisms, load-transfer paths, and relative trends, rather than absolute load-carrying capacity.

This interpretation is particularly relevant for Douglas fir glulam and densified wooden dowels, whose behaviour is represented through calibrated orthotropic material models rather than standardised strength classes. Although correction factors allow consistent comparison with analytical models, the numerical results remain dependent on modelling assumptions and idealisations.

A similar consideration applies to the treatment of shear. In the numerical model, shear-related yielding arises implicitly from normal stress-based interaction criteria and does not correspond directly to the characteristic shear strength $f_{\mathrm{v,k}}$ defined in Eurocode 5. The resulting equivalent shear response therefore reflects combined stress interaction rather than pure shear failure. This distinction is not critical for the present study, as failure is governed by compression perpendicular to the grain rather than shear.

The cohesive zone model (CZM) used at the dowel–timber interface is likewise introduced to support interpretation of load transfer and damage evolution. Its parameters are selected to capture relative interaction behaviour rather than to provide direct predictions of design-level resistance. Consequently, the numerical model should be regarded as a tool for understanding mechanisms rather than as a predictive design model.

Global load–displacement behaviour

The remaining force offset between the numerical and experimental results illustrates the sensitivity of predicted load-carrying capacity to material input parameters and modelling idealisations, such as the use of mean material properties and simplified contact conditions. These effects primarily influence the absolute calibration of the response.

Despite this offset, the numerical model reproduces the characteristic stiffness evolution, nonlinearity, and post-peak behaviour observed experimentally. The governing deformation mechanisms and stress redistribution patterns are therefore captured adequately. The model is considered suitable for

comparative analyses and parametric studies, where relative differences between configurations are of primary interest rather than exact resistance values.

Influence of modelling constraints

The finite element models used to determine stress distributions are based on a timber substrate with limited width. This geometric constraint may influence the development and spreading of compressive stresses perpendicular to the grain, potentially leading to a more localised stress field than would occur in wider or semi-infinite timber members.

While this limitation may affect the absolute stress magnitudes and orientations, the obtained distributions remain suitable for comparative use within the analytical framework. They allow consistent evaluation of differences between the investigated beam models and reinforcement configurations. However, the direct applicability of the derived stress angles for use in a general Eurocode-based analytical model remains uncertain. Additional numerical or experimental studies with varying substrate widths would be required to quantify this influence and verify the robustness of the proposed approach.

Partial dowel–timber side interaction

Validation of the numerical models shows that, although full sticking contact is achieved at the dowel end surfaces, the interaction along the dowel sides is only partially activated. Bonded contact develops in limited vertical strips, while large portions of the dowel side surface remain inactive throughout loading.

As a result, shear transfer along the dowel sides is not fully mobilised. This leads to a reduced effective contribution of the dowel relative to analytical models that implicitly assume uniform side interaction along the embedded length. To account for this effect, selected numerical results are scaled based on the effective contact area of the dowel sides.

After scaling, the numerical responses exhibit consistent trends in stiffness and load capacity, supporting their use for further comparative and parametric analyses. Nevertheless, the partial activation of side interaction represents a fundamental limitation when transferring isolated dowel capacities to the system level.

Individual dowel contribution and governing mechanisms

Building on the observed limitations in dowel–timber side interaction, the effective contribution of individual dowels at system level is examined. Although isolated dowel models indicate a higher potential capacity, this capacity is not fully mobilised in the developed base models.

The primary reason for this discrepancy is the non-uniform stress transfer along the dowel length. The distribution of compressive stress S22 parallel to the dowel axis shows a clear increase towards the dowel tip, while stresses along the upper part of the dowel remain significantly lower. This behaviour is caused by differential deformation between the dowel and the surrounding timber, which prevents uniform mobilisation of shear stresses along the dowel–timber interface.

Consequently, only a limited portion of the dowel length contributes effectively to load transfer. This behaviour is consistently observed in the global base models where stress concentrations and deformation localise near the dowel tip. The dowel side surface therefore contributes only partially, while the dowel tip governs the failure mechanism at system level.

Due to this non-uniform stress distribution and the uncertainty associated with quantifying the effective side contribution, only the dowel tip contribution is considered in the analytical model. The contribution of the dowel sides depends on interacting parameters such as material stiffness, contact conditions, and local timber deformation, which cannot be captured reliably within the current analytical framework.

Tip effects and comparison of reinforcement strategies

The dominance of the dowel tip in load transfer provides a key explanation for the observed differences between wooden dowel and steel screw reinforcement. Steel screws engage the surrounding timber through axial action and thread-induced withdrawal resistance, resulting in a distributed load introduction along the embedded length. In the Eurocode 5 design model, the resistance of screws acting perpendicular to the grain is therefore derived without any explicit contribution from a tip bearing

mechanism.

For wooden dowels, the load-transfer mechanism differs fundamentally. Although dowels possess a withdrawal capacity through friction and bearing along their embedded length, this capacity is not fully mobilised in the investigated joint configuration. As a result, the relative contribution of the dowel tip increases and accounts for approximately one fifth of the effective dowel resistance derived from the numerical model.

This increased reliance on tip bearing leads to pronounced local deformation and progressive crushing of the timber beneath the dowel tip, which governs the global response of the joint. The difference between screw- and dowel-reinforced systems therefore cannot be attributed to material properties alone, but is strongly influenced by the extent to which side interaction and withdrawal mechanisms are activated at system level.

This effect should be taken into account when comparing reinforcement strategies and when interpreting analytical models for wooden dowel reinforcement, particularly when simplified assumptions regarding uniform side interaction are adopted.

Implications for the analytical model

The analytical model developed in this study intentionally adopts a conservative representation of dowel behaviour by considering only the dowel tip contribution. This approach provides a lower-bound estimate of resistance that is consistent with the limited mobilisation of side interaction observed in the numerical models.

While this simplification neglects potential contributions from dowel withdrawal and side bearing, it avoids overestimating the effective dowel capacity under compression perpendicular to the grain. The comparison with finite element results demonstrates that analytical predictions are highly sensitive to assumptions regarding load-transfer mechanisms.

The analytical model is therefore most suitable for comparative assessment of reinforcement configurations and for identifying governing trends, rather than for direct prediction of system resistance. Any extension towards design application would require explicit consideration of side interaction mobilisation and experimental validation.

Limitations and Scope

This study is limited to dowel-reinforced timber members subjected to compression perpendicular to the grain, with a focus on load-transfer mechanisms and stress redistribution at both dowel and system level. The results are applicable to similar loading conditions and joint configurations and should not be generalised to other stress states or connection types without caution.

The numerical models employ idealised geometries, boundary conditions, and material descriptions to isolate key mechanisms such as dowel bearing and tip compression. Effects related to timber heterogeneity, moisture variation, manufacturing imperfections, and long-term deformation are not considered.

Furthermore, only short-term monotonic loading is investigated. Cyclic loading, fatigue, time-dependent behaviour, and environmental influences fall outside the scope of this study and require dedicated investigation.

7

Conclusions and Recommendations

7.1. Conclusion

Research objectives and approach

This thesis investigated timber-based reinforcement strategies for timber joints subjected to compression perpendicular to the grain, with a specific focus on column–beam–column connections reinforced with wooden dowels. The central motivation was to reduce the reliance on steel components in timber construction by improving the understanding and applicability of fully timber-based solutions.

Due to the highly localised and nonlinear nature of compression-perpendicular-to-the-grain behaviour, a combined analytical and numerical approach was adopted. Simplified analytical models were used to assess design-level resistance, while finite element modelling was employed to investigate load-transfer mechanisms, stress redistribution, and interaction effects that cannot be captured by Eurocode-based design rules alone. A practical case study was included to evaluate the implications of the findings at structural system level and to compare wooden dowel reinforcement with conventional steel screw solutions.

Key findings

The results show that the structural response of dowel-reinforced timber members loaded perpendicular to the grain is governed by highly localised deformation and non-uniform stress transfer. Although individual wooden dowels exhibit a substantial potential capacity under isolated loading conditions, this capacity is not fully mobilised at system level in the investigated joint configuration.

A key finding is that shear transfer along the dowel sides is only partially activated. Differential deformation between the dowel and the surrounding timber leads to stress concentrations near the dowel tip, while large parts of the dowel length contribute only marginally to load transfer. As a consequence, the dowel tip plays a dominant role in the effective resistance of the joint, despite representing only a limited portion of the dowel's theoretical capacity.

The study further demonstrates that load redistribution and interaction between multiple dowels significantly influence the global response of the joint. These effects reduce the direct transferability of isolated dowel capacities to structural applications and highlight the importance of considering system-level behaviour when evaluating timber-based reinforcement strategies.

Assessment of analytical vs numerical models

The comparison between analytical and numerical approaches reveals a clear distinction in their scope and applicability. Analytical models based on Eurocode principles provide conservative lower-bound estimates of resistance and are suitable for preliminary design checks. However, they rely on simplified assumptions regarding load-transfer mechanisms and cannot capture interaction effects, progressive crushing, or partial mobilisation of dowel–timber contact.

Finite element modelling, by contrast, enables explicit investigation of stress redistribution, deformation

compatibility, and local failure mechanisms. The numerical model developed in this study is therefore most valuable as a mechanistic tool, allowing interpretation of governing behaviour and identification of critical parameters. Its results should be interpreted in terms of relative trends and mechanisms rather than absolute design resistance.

The findings indicate that FEM-derived results can inform analytical modelling by identifying which mechanisms are effectively mobilised and which assumptions lead to unconservative or overly conservative predictions. Nevertheless, direct use of FEM output for design purposes requires careful interpretation and experimental validation.

Case study conclusions

Application of the developed models to the case study structure demonstrates that both wooden dowels and steel screws increase the load-bearing capacity of the joint compared to the unreinforced configuration. For the investigated layouts, neither reinforcement strategy fully satisfies the design requirements without further optimisation.

For wooden dowels, utilisation levels exceed unity when conservative analytical assumptions are adopted. When the dowel contribution is derived from the numerical model, which implicitly includes partial side interaction, lower utilisation levels are obtained, although the joint remains governing. The results confirm that dowel performance at system level is controlled by timber deformation and stress concentration beneath the dowel tip.

Steel screw reinforcement results in lower utilisation levels for comparable reinforcement density. This improved performance is attributed to the distributed load transfer along the screw length through thread-induced withdrawal resistance, which reduces the influence of localised crushing effects. However, the screw-reinforced system also shows potential for further optimisation through adjustments in length, diameter, and layout.

Comparison of wooden dowels and steel screws

The observed differences between wooden dowel and steel screw reinforcement cannot be explained by material strength alone, but are primarily governed by the extent to which load-transfer mechanisms are mobilised. In Eurocode-based design, the resistance of screws acting perpendicular to the grain is derived without any explicit contribution from tip bearing, reflecting the dominance of axial and withdrawal mechanisms.

For wooden dowels, withdrawal and side interaction mechanisms exist but are not fully mobilised in the investigated configuration. As a result, the relative contribution of the dowel tip becomes more significant, accounting for approximately one fifth of the effective dowel resistance derived from the numerical model. This increased reliance on tip bearing leads to pronounced local deformation and progressive crushing of the timber beneath the dowel tip, which governs the global joint response.

This distinction is essential when comparing reinforcement strategies and when interpreting analytical models for wooden dowels. Simplified models that neglect side interaction provide conservative estimates but may not reflect the true distribution of load-transfer mechanisms at system level.

Implications for design

The results indicate that fully timber-based reinforcement using wooden dowels is structurally feasible but requires careful consideration of load-transfer mechanisms and deformation compatibility. Conservative analytical models may underestimate dowel contribution, while unconstrained use of isolated test results risks overestimating system-level capacity.

For engineering practice, analytical models remain appropriate for preliminary assessment and lower-bound verification. Finite element modelling becomes valuable when optimisation, interaction effects, or unconventional reinforcement layouts are considered. In such cases, FEM should be used to identify governing mechanisms rather than to replace design models directly.

7.2. Answers to the research questions

Research question 6: *To what extent does the developed numerical model have predictive value for the actual mechanical behaviour of timber under compression perpendicular to the grain?*

The predictive value of the developed numerical model for timber under compression perpendicular to the grain lies primarily in its ability to reproduce the mechanical response mechanisms rather than absolute design resistances. The model captures the global load–displacement behaviour, stress redistribution, and governing deformation modes observed in experimental tests and numerical reference models, indicating that the essential material behaviour is represented consistently. The need for a displacement and force shift to align the curves highlights that initial seating effects and simplified boundary conditions are not fully captured, but this does not undermine the validity of the post-elastic response and failure progression.

The use of an anisotropic Hill yield criterion allows yielding to emerge from a combined stress state, which is particularly relevant for compression perpendicular to the grain where normal and shear stresses interact. Since no independent shear yield stress is prescribed, the equivalent shear yield stress derived for comparison with Eurocode 5 should be interpreted as a consistency check rather than a direct prediction of shear capacity. This fundamental difference explains deviations between the numerical results and Eurocode-based analytical values, which rely on empirically calibrated characteristic strengths and simplified stress assumptions.

Overall, the numerical model demonstrates strong predictive capability in terms of stiffness, deformation capacity, and relative load-sharing mechanisms within reinforced timber systems. However, its predictive value for absolute resistance levels remains limited by the use of mean material properties, idealised contact conditions, and the absence of statistical variability inherent to Eurocode design values. The model is therefore best suited for parametric studies, mechanism-based assessment, and comparative evaluation of reinforcement strategies, rather than direct substitution of Eurocode 5 design equations.

Research question 7: *How do dowel-reinforced members compare to Eurocode 5 design provisions for reinforced timber members?*

Dowel-reinforced members exhibit load-bearing behaviour that is only partially captured by the current Eurocode 5 design provisions for reinforced timber members. Eurocode 5 models reinforcement effects through simplified analytical expressions based on characteristic material strengths and idealised stress distributions, which are primarily calibrated for screws, nails, and steel fasteners. The densified wood dowels and their interaction with the surrounding timber therefore fall outside the direct scope of the code.

The numerical results show that dowel reinforcement significantly enhances stiffness and load capacity under compression perpendicular to the grain compared to unreinforced members. However, when compared at equivalent load or deformation levels, the Eurocode 5 analytical model generally provides conservative resistance predictions. This conservatism arises from the use of characteristic strength values, simplified stress spreading assumptions, and the neglect of stress redistribution and confinement effects captured in the numerical model.

Furthermore, the numerical simulations demonstrate that the contribution of individual dowels depends strongly on their interaction with the surrounding timber and the global load transfer mechanism. In contrast, Eurocode 5 implicitly assumes that reinforcement capacity can be superimposed in a simplified manner, without accounting for system effects or stiffness incompatibilities between reinforcement and timber. As a result, the effective contribution of dowels in a structural system is lower than what would be inferred from isolated reinforcement behaviour, which is not explicitly addressed in the code.

Overall, the comparison indicates that Eurocode 5 provides a safe but simplified representation of dowel-reinforced members. The developed numerical model highlights additional mechanisms—such as stress redistribution, confinement, and system-level stiffness effects—that are not captured by current design provisions. These findings suggest that while Eurocode 5 remains suitable for design verification, numerical modelling offers valuable insight for optimisation and for the development of refined design rules for dowel-reinforced timber members.

Research question 8: *What is the influence of the dowel material type on the compressive resistance and load–displacement response of timber reinforced perpendicular to the grain?*

The dowel material type has a clear influence on the compressive resistance perpendicular to the grain, while its influence on the global load–displacement response remains limited. All investigated configurations exhibit a similar deformation behaviour, characterised by an initial elastic response followed by crushing-dominated deformation of the timber. This indicates that the governing deformation mechanism is largely independent of the dowel material.

In terms of compressive resistance, increasing dowel stiffness and strength results in higher peak loads. Compared to the unreinforced configuration, timber dowels increase the maximum compressive force by approximately 11%, densified wood dowels by about 19%, and steel dowels by roughly 22%. The higher capacities achieved with densified wood and steel dowels reflect their improved ability to transfer load and delay local crushing of the timber perpendicular to the grain.

Despite these differences in peak capacity, the post-yield response and overall shape of the force–displacement curves remain comparable for all materials. This suggests that, once timber crushing is initiated, the structural response is governed primarily by the timber matrix, with the dowel material affecting mainly the magnitude of the load at which this response occurs rather than the subsequent deformation evolution.

Main research question:*How can fully timber-based reinforcement strategies be applied to enable reliable performance of timber joints under various loading conditions, and what is their potential to reduce or replace steel components in structural timber connections?*

Fully timber-based reinforcement strategies, such as densified wood dowels, can be applied by embedding them in regions of high stress concentration to enhance load transfer and mitigate brittle failure mechanisms, particularly under compression perpendicular to the grain. The numerical and analytical results demonstrate that these reinforcements are most effective when their contribution is governed by deformation compatibility with the surrounding timber, ensuring gradual load redistribution rather than abrupt localised failure. By activating both lateral bearing and limited tip resistance mechanisms, timber-based dowels improve the reliability and ductility of timber joints under varying loading conditions.

Comparison with Eurocode 5-based analytical models shows that the effective contribution of timber-based reinforcement is primarily controlled by the compressive capacity of the timber substrate rather than by the intrinsic strength of the dowel material. This highlights the importance of system-level design approaches that account for stress spreading and interaction effects, rather than assuming full mobilisation of reinforcement capacity. Within these constraints, densified timber dowels exhibit mechanical properties that exceed those of conventional structural timber and can therefore replace steel fasteners in applications governed by serviceability limits, local bearing resistance, or moderate ultimate limit states.

Overall, fully timber-based reinforcement strategies offer significant potential to reduce or partially replace steel components in structural timber connections, particularly in compression-dominated joints and hybrid systems. While such reinforcements are unlikely to fully substitute steel in tension- or ductility-critical connections, they enable a substantial reduction in steel content and contribute to improved material compatibility, sustainability, and circularity of timber structures when appropriately designed.

7.3. Recommendations

The findings of this study provide insight into the load-transfer mechanisms and reinforcing effect of wooden dowels in timber loaded perpendicular to the grain. At the same time, several limitations related to modelling assumptions, specimen geometry, and material characterisation were identified. Addressing these aspects through targeted follow-up research would improve both the robustness of the numerical framework and the reliability of analytical design approaches derived from it.

First, dedicated experimental validation is recommended to clarify the discrepancy between the load-bearing capacity of individual dowels observed in derived tests and the reduced contribution mobilised at system level. Isolated dowel tests or tests with enhanced boundary conditions could help identify governing interaction mechanisms and determine how dowel capacity can be more effectively activated in reinforced systems.

Second, further numerical and experimental studies with varying timber substrate widths are required to quantify the influence of specimen geometry on stress distribution and load transfer. Such studies are necessary to verify the proposed evaluation method and to assess the applicability of the derived stress angles and correction factors within an analytical Eurocode-based design framework.

Third, layout optimisation studies are recommended to investigate the influence of dowel spacing, embedment length, edge distances, and tip geometry on force distribution and damage evolution. Parametric analyses could help reduce premature timber crushing and improve reinforcement efficiency at system level.

Finally, extended material characterisation is advised, particularly for densified wooden dowels. Dedicated material testing would enable calibration of FEM input parameters to Eurocode 5 strength classes defined in EN 338, improving consistency between numerical simulations and analytical design verification.

For practical application, the analytical model developed in this study may be used as a preliminary design tool to assess the potential effectiveness of wooden dowel reinforcement under compression perpendicular to the grain. It is suitable for comparing reinforcement layouts, identifying governing load-transfer mechanisms, and estimating conservative resistance contributions using characteristic material properties in line with Eurocode 5. Mean material properties should be limited to sensitivity studies and conceptual evaluation.

Given the simplified representation of load transfer and the limited validation range, the analytical model is not recommended as a standalone design method for critical connections. When wooden dowels provide a significant contribution to the load-bearing capacity, or when geometries and materials fall outside the investigated configurations, supplementary finite element analyses are advised. FEM can capture deformation compatibility, local crushing, and partial mobilisation of dowel side interaction that are not accounted for analytically. Until broader validation is available, a combined analytical–numerical approach is recommended for reliable design application.

References

[1] A. Aloisio et al. “Capacity models for timber under compression perpendicular to grain with screw reinforcement”. In: *European Journal of Wood and Wood Products* 81 (2023), pp. 633–654. doi: 10.1007/s00107-022-01918-z.

[2] I. Bejtka and H. J. Blaß. “Self-tapping screws as reinforcement for glued laminated timber”. In: *Proceedings of the International Council for Research and Innovation in Building and Construction*. 2004.

[3] H. J. Blass and I. Bejtka. “Reinforcements perpendicular to the grain using self-tapping screws”. In: *Conference Proceedings*. n.d.

[4] Hans J Blass and Ilka Bejtka. “Joints with inclined screws”. In: *CIB-W18 Proceedings, Paper 35-7-5*. 2002.

[5] Daniel Brandon, Joachim Schmid, and Alar Just. “Effective cross-section method for parametric fire design of timber members”. In: *Fire Safety Journal* 91 (2017), pp. 1–11.

[6] Daniel Brandon, Joachim Schmid, and Alar Just. “Eurocode 5 design in comparison with fire resistance tests of unprotected timber beams”. In: *Proceedings of the 9th International Conference on Structures in Fire*. 2016.

[7] Andrew H. Buchanan and Steven B. Levine. “Wood-based building materials and atmospheric carbon emissions”. In: *Environmental Science & Policy* 2.6 (1999), pp. 427–437. doi: 10.1016/S1462-9011(99)00038-6.

[8] Ario Ceccotti. “Timber structures—recent developments”. In: *Progress in Structural Engineering and Materials* 4.3 (2002), pp. 264–275.

[9] Ario Ceccotti et al. “Seismic behavior of multi-storey cross-laminated timber buildings”. In: *Journal of Structural Engineering* 139.12 (2013).

[10] CLT Toolbox. *Understanding timber failure modes in mass timber connections*. Retrieved April 2025, from https://clttoolbox.com/blog/understanding-timber-failure-modes-in-mass-timber-connections-with-clt-toolbox/. 2023.

[11] P. Dietsch and R. Brandner. “Mechanical reinforcement of timber structures – A review of existing techniques”. In: *Construction and Building Materials* 97 (2015), pp. 78–89.

[12] T. Ehrhart, R. Steiger, and A. Frangi. “A non-contact method for the determination of fibre direction of European beech wood (Fagus sylvatica L.)” In: *European Journal of Wood and Wood Products* 76.6 (2018), pp. 925–935. doi: 10.1007/s00107-017-1279-3.

[13] European Committee for Standardization. *EN 1995-1-1: Design of timber structures – Part 1-1: General – Common rules and rules for buildings*. Eurocode 5. 2024.

[14] European Committee for Standardization. *EN 1995-1-2: Design of timber structures – Part 1-2: Structural fire design*. Eurocode 5. 2023.

[15] Massimo Fragiacomo, Arjan Jorissen, and Roberto Tomasi. “Design of timber structures with ductile connections”. In: *Engineering Structures* 33.11 (2011), pp. 2978–2986.

[16] Steffen Franke, Bettina Franke, and Annette M. Harte. “Failure modes and reinforcement techniques for timber beams – State of the art”. In: *Construction and Building Materials* 97 (2015), pp. 2–13. doi: 10.1016/j.conbuildmat.2015.06.021.

[17] L. Han et al. “Adhesive- and metal-free assembly techniques for prefabricated multi-layer engineered wood products: A review on wooden connectors”. In: *Forests* 14.2 (2023), p. 311. doi: 10.3390/f14020311.

[18] Amin Hassanieh, Hamid R Valipour, and Keith Crews. “Experimental and numerical investigation of glued-in rods in Australian hardwoods”. In: *Construction and Building Materials* 102 (2016), pp. 1105–1114.

[19] HESS TIMBER. *Museum Fondation Louis Vuitton*. [Photograph]. n.d. url: https://www.hess-timber.com/en/references/detail/museum-fondation-louis-vuitton/.

[20] HEVO. *Circulair gemeentehuis Krimpenerwaard: meer dan een gebouw*. Accessed: 2025-07-01. 2023. url: https://www.hevo.nl/actueel/nieuws/circulair-gemeentehuis-krimpenerwaard.

[21] P. Hoffmeyer, B. Sørensen, and B. Madsen. “Timber in compression perpendicular to the grain: Experimental study and modeling”. In: *Wood Science and Technology* 34 (2000), pp. 423–438.

[22] Sabina Huč, Tomaž Hozjan, and Robert Pečenko. “Effective cross-section of a timber beam exposed to natural fires”. In: *European Journal of Wood and Wood Products* 83.1 (2025), pp. 71–88.

[23] Robert Jockwer, René Steiger, and Andrea Frangi. “Design model for inclined screws under varying load to grain angles”. In: *Proceedings of the 1st Meeting of the International Network on Timber Engineering Research (INTER 2014)*. Bath, United Kingdom, Sept. 2014, Paper 47-7–5, 11 pages. url: https://www.dora.lib4ri.ch/empa/islandora/object/empa:11703.

[24] Arjan Jorissen. “Double shear timber connections with dowel-type fasteners”. PhD thesis. TU Delft, 1998.

[25] Arjan Jorissen and Massimo Fragiacomo. “General notes on ductility in timber structures”. In: *Engineering Structures* 33.11 (2011), pp. 2987–2997.

[26] Hermann Kaufmann and Simon Winter. *Detailing for Timber Structures: Principles, Process, and Practice*. Birkhäuser, 2015.

[27] A. Kitamori, T. Ohtani, and A. J. M. Leijten. “Evaluation on structural performance of compressed wood as shear dowel”. In: *Journal of Wood Science* 54.6 (2008), pp. 465–472.

[28] Klimaatplein. *De route naar het duurzame gemeentehuis Krimpenerwaard*. Accessed: 2025-07-01. 2023. url: https://klimaatplein.nl/de-route-naar-het-duurzame-gemeentehuis-krimpenerwaard.

[29] David E. Kretschmann. “Mechanical properties of wood”. In: *Wood handbook: Wood as an engineering material*. Gen. Tech. Rep. FPL-GTR-190. U.S. Department of Agriculture, Forest Service, Forest Products Laboratory, 2010. Chap. 5.

[30] Gemeente Krimpenerwaard. *Definitief ontwerp nieuw gemeentehuis*. Accessed: 2025-07-01. 2023. url: https://www.krimpenerwaard.nl/definitief-ontwerp-nieuw-gemeentehuis.

[31] David Lange, Andrea Frangi, and Erich Hugi. “Fire resistance of glulam beams exposed to parametric fires”. In: *Engineering Structures* 100 (2015), pp. 237–248.

[32] A. J. M. Leijten. “The bearing strength capacity perpendicular to grain of Norway spruce: Evaluation of three structural timber design models”. In: *Construction and Building Materials* 105 (2016), pp. 528–535. doi: 10.1016/j.conbuildmat.2015.12.170.

[33] S. Mehra et al. “Experimental investigation of the moment-rotation behaviour of beam-column connections produced using compressed wood connectors”. In: *Construction and Building Materials* 331 (2022), p. 127327. doi: 10.1016/j.conbuildmat.2022.127327.

[34] S. Mehra et al. “Structural characterisation of laterally loaded glued and compressed wood dowel laminated timber portal frames produced using compressed wood connectors”. In: *Construction and Building Materials* 457 (2024), p. 139107. doi: 10.1016/j.conbuildmat.2024.139107.

[35] MicMac.mx. *Types of connections in structural timber*. Retrieved April 2025, from https://micmac.mx/en/blog/madera-estructural/types-of-connections-in-structural-timber. 2023.

[36] J. Miller, R. Schmidt, and W. Bulleit. “A new yield model for wood dowel connections”. In: *Journal of Structural Engineering* 136.7 (2010). doi: 10.1061/(ASCE)ST.1943-541X.0000224.

[37] MTC Solutions. *Designing with internal knife plates*. Retrieved from https://mtcsolutions.com/resources/tech-blogs/designing-with-internal-knife-plates/. 2020.

[38] C. O'Ceallaigh et al. "Modified wood as compression reinforcement of timber perpendicular to the grain". In: *World Conference on Timber Engineering (WCTE 2021)*. 2021. url: https://www.researchgate.net/publication/353795039_Modified_Wood_as_Compression_Reinforcement_of_Timber_Perpendicular_to_the_Grain.

[39] C. O'Ceallaigh et al. "Numerical investigation of reinforcement of timber elements in compression perpendicular to the grain using densified wood dowels". In: *Construction and Building Materials* 288 (2021), p. 122990. doi: 10.1016/j.conbuildmat.2021.122990.

[40] Duurzaam Ondernemen. *Bouw meest circulaire gemeentehuis van Nederland gestart*. Accessed: 2025-07-01. 2023. url: https://www.duurzaam-ondernemen.nl/bouw-meest-circulaire-gemeentehuis-van-nederland-gestart.

[41] B.N. Paul et al. "Production processes, material properties and applications of densified wood: an overview". In: *Journal of the Indian Academy of Wood Science* 21 (2024), pp. 235–254. doi: 10.1007/s13196-024-00348-z. url: https://doi.org/10.1007/s13196-024-00348-z.

[42] M. B. U. Pedersen. *Dowel type timber connections: Strength modelling*. Tech. rep. Technical University of Denmark, 2001. url: https://orbit.dtu.dk/en/publications/d1a6e43b-31fc-46a9-ab47-0e20b69c45f2.

[43] J. Porteous and A. Kermani. *Structural Timber Design to Eurocode 5*. Wiley-Blackwell, 2013.

[44] Alexander Ringhofer, Gerhard Schickhofer, and Andrea Frangi. "Modelling of dowel-type fasteners in timber structures: A review". In: *European Journal of Wood and Wood Products* 75.6 (2017), pp. 847–865.

[45] Rothoblaas. *Brackets and plates*. [Figure]. n.d. url: https://www.rothoblaas.com/products/fastening/brackets-and-plates.

[46] V. H. Sæby. "Assessing the performance of wooden dowels in pure wood connections". Master's thesis. Norwegian University of Life Sciences, 2024.

[47] A. Sandoli, C. Ceraldi, and A. Prota. "Feasibility of timber pegged joints for seismic design of structures". In: *European Journal of Wood and Wood Products* (2023).

[48] Gerhard Schickhofer, Martin Trautz, and Thomas Zimmermann. "Large span structures made of glulam – Design, detailing and practical solutions". In: *Graz University of Technology Publications* (2015).

[49] Joachim Schmid, Alar Just, and Daniel Brandon. "Structural fire resistance of timber beams: Analysis of zero-strength layer thickness". In: *Fire Safety Journal* 71 (2015), pp. 71–80.

[50] Jan C. M. Schoenmakers. "Elementary and advanced modelling of the splitting strength of timber connections". PhD thesis. Eindhoven University of Technology, 2013. url: https://research.tue.nl.

[51] J. Shen, X. Zhu, and J. Chen. "Experimental and numerical study on shear properties of timber-to-timber joint using a dowel reinforced with a self-tapping screw". In: *BioResources* 18.3 (2023), pp. 6118–6131. doi: 10.15376/biores.18.3.6118-6131.

[52] Skidmore, Owings Merrill and Lorenzo Sanjuan. *The High Line – Moynihan Connector*. Thornton Tomasetti. [Photograph]. n.d. url: https://www.thorntontomasetti.com/project/high-line-moynihan-connector.

[53] Ian Smith, Eric N. Landis, and Minghao Gong. *Fracture and fatigue in wood*. John Wiley & Sons, 2003.

[54] Adeayo Sotayo et al. "Review of state of the art of dowel laminated timber members and densified wood materials as sustainable engineered wood products for construction and building applications". In: *Developments in the Built Environment* 1 (2020), p. 100004. doi: 10.1016/j.dibe.2019.100004. url: https://doi.org/10.1016/j.dibe.2019.100004.

[55] Stadszaken. *Meest duurzame en circulaire gemeentehuis komt in de Krimpenerwaard*. Accessed: 2025-07-01. 2023. url: https://stadszaken.nl/artikel/6287/meest-duurzame-en-circulaire-gemeentehuis-komt-in-de-krimpenerwaard.

[56] Smart WorkPlace. *Bouw nieuw gemeentehuis van start in Krimpenerwaard*. Accessed: 2025-07-01. 2023. url: https://www.smartwp.nl/nieuws/20241129-bouw-nieuw-gemeentehuis-van-start-in-krimpenerwaard.

[57] Bo-Han Xu et al. “An optional connection material in timber structures: densified poplar”. In: *Journal of Materials Science* 56 (Sept. 2021), pp. 14114–14125. doi: 10.1007/s10853-021-06194-5. url: https://doi.org/10.1007/s10853-021-06194-5.

[58] Bo-Han Xu et al. “Pull-Out Performance of Densified Wood Dowels Embedded into Glued Laminated Timber”. In: *Journal of Materials in Civil Engineering* 35.9 (2023), p. 06023004. doi: 10.1061/JMCEE7.MTENG-15299. url: https://doi.org/10.1061/JMCEE7.MTENG-15299.

[59] Bo-Han Xu et al. “Pull-Out Performance of Timber Joints with Glued-In Densified Wood Dowels”. In: *Journal of Materials in Civil Engineering* 35.8 (2023), p. 06023010. doi: 10.1061/JMCEE7.MTENG-15610. url: https://doi.org/10.1061/JMCEE7.MTENG-15610.

[60] F. Zhang, L. Zhao, S. Wang, et al. “Study on the transverse compression performance of wood reinforced with wood dowels and FEM simulation”. In: *European Journal of Wood and Wood Products* 83 (2025), p. 78. doi: 10.1007/s00107-025-02229-9.

A

Steel Calculation Ground Floor

Detail										
01a	Object	Name	Length [mm]	Width [mm]	Height [mm]	Diameter [mm]	Amount	Volume [mm^3]	Weight [kg]	Interesting?
	Plate		340	340	15		1	1734000	13,6	
	Rod	M16	240			16	4	193019	1,5	
	Achor	M16	400			16	4	321699	2,5	
	Total								17,7	

Detail										
01b	Object	Name	Length [mm]	Width [mm]	Height [mm]	Diameter [mm]	Amount	Volume [mm^3]	Weight [kg]	Interesting?
	Plate		340	340	25		1	2890000	22,7	
	Rod	M20	400			20	6	753982	5,9	
	Achor	M20	700			20	4	879646	6,9	
	Total								35,5	

Detail										
02	Object	Name	Length [mm]	Width [mm]	Height [mm]	Diameter [mm]	Amount	Volume [mm^3]	Weight [kg]	Interesting?
	Plate		320	340	20		1	2176000	17,1	
	Achor		700			24	6	1900035	14,9	
	Bolt		300			16	3	180956	1,4	
	Total								33,4	

Detail										
03a	Object	Name	Length [mm]	Width [mm]	Height [mm]	Diameter [mm]	Amount	Volume [mm^3]	Weight [kg]	Interesting?
	Plate		320	340	25		1	2720000	21,4	
	Rod	M20	400			20	6	753982	5,9	
	Achor	M24	700			24	4	1266690	9,9	
	Total								37,2	

Detail										
03b	Object	Name	Length [mm]	Width [mm]	Height [mm]	Diameter [mm]	Amount	Volume [mm^3]	Weight [kg]	Interesting?
	Plate		400	400	25		1	4000000	31,4	
	Rod	M20	400			20	6	753982	5,9	
	Achor	M24	700			24	4	1266690	9,9	
	Total								47,3	

Detail										
03c	Object	Name	Length [mm]	Width [mm]	Height [mm]	Diameter [mm]	Amount	Volume [mm^3]	Weight [kg]	Interesting?
	Plate		340	400	25		1	3400000	26,7	
	Rod	M20	400			20	4	502655	3,9	
	Achor	M24	700			24	4	1266690	9,9	
	L		3000	200	10		1	6000000	47,1	
	L	NINO15080	132	146	2,5		33	1589940	12,5	
	Bolt	M12	195			12	66	1455563	11,4	
	Nail		50			4	660	414690	3,3	
	Total								114,8	

Detail										
04	Object	Name	Length [mm]	Width [mm]	Height [mm]	Diameter [mm]	Amount	Volume [mm^3]	Weight [kg]	Interesting?
	L	NINO15080	132	146	2,5		?	#VALUE!	#VALUE!	
	Bolt	M12	195			12	?	#VALUE!	#VALUE!	
	Nail		50			4	?	#VALUE!	#VALUE!	
	Total								#VALUE!	

Detail										
04b	Object	Name	Length [mm]	Width [mm]	Height [mm]	Diameter [mm]	Amount	Volume [mm^3]	Weight [kg]	Interesting?
	L		100	120	6		1	72000	0,6	
	Bolt	M12	50			12	2	11310	0,1	
	Nail		60			5	11	12959	0,1	
	Total								0,8	

Detail										
05	Object	Name	Length [mm]	Width [mm]	Height [mm]	Diameter [mm]	Amount	Volume [mm^3]	Weight [kg]	Interesting?
	Tube		200	100	120	10	1	720000	5,7	
	Plate 1		220	380	15		1	1254000	9,8	
	1		220	340	15		1	1122000	8,8	
	Rod	M16	240			16	4	193019	1,5	
	Achor	M16	400			16	4	321699	2,5	
	Total								28,3	

Detail										
06	Object	Name	Length [mm]	Width [mm]	Height [mm]	Diameter [mm]	Amount	Volume [mm^3]	Weight [kg]	Interesting?
	Plate		600	600	15		1	5400000	42,4	
	Rod	M16	240			16	6	289529	2,3	
	Achor	M16	400			16	6	482549	3,8	
	Total								48,5	

Detail										
07	Object		Name	Length [mm]	Width [mm]	Height [mm]	Diameter [mm]	Amount	Volume [mm^3]	Weight [kg]	Interesting?
	Plate	1		340	400	15		1	2040000	16,0	
	Rod		M16	240			16	6	289529	2,3	
	Achor		M16	400			16	4	321699	2,5	
	Total									20,8	

Detail										
08	Object		Name	Length [mm]	Width [mm]	Height [mm]	Diameter [mm]	Amount	Volume [mm^3]	Weight [kg]	Interesting?
	Plate			750	460	15		1	5175000	40,6	
	Rod		M16	240			16	6	289529	2,3	
	Achor		M16	400			16	6	482549	3,8	
	Total									46,7	

Detail										
09a	Object		Name	Length [mm]	Width [mm]	Height [mm]	Diameter [mm]	Amount	Volume [mm^3]	Weight [kg]	Interesting?
	Plate			400	400	15		1	2400000	18,8	
	Rod		M16	240			16	6	289529	2,3	
	Achor		M16	500			16	4	402124	3,2	
	Total									24,3	

Detail										
09b	Object		Name	Length [mm]	Width [mm]	Height [mm]	Diameter [mm]	Amount	Volume [mm^3]	Weight [kg]	Interesting?
	Plate			400	400	25		1	4000000	31,4	
	Rod		M20	400			20	6	753982	5,9	
	Achor		M20	700			20	4	879646	6,9	
	Total									44,2	

Detail										
10	Object		Name	Length [mm]	Width [mm]	Height [mm]	Diameter [mm]	Amount	Volume [mm^3]	Weight [kg]	Interesting?
	Plate			750	360	15		1	4050000	31,8	
	Rod		M16	240			16	6	289529	2,3	
	Achor		M16	400			16	4	321699	2,5	
	Total									36,6	

Detail										
11	Object		Name	Length [mm]	Width [mm]	Height [mm]	Diameter [mm]	Amount	Volume [mm^3]	Weight [kg]	Interesting?
	Plate			170	1150	15		1	2912200	22,9	
	Rod		M16	240			16	5	241274	1,9	
	Achor		M16	400			16	4	321699	2,5	
	Total									27,3	

Detail										
12	Object		Name	Length [mm]	Width [mm]	Height [mm]	Diameter [mm]	Amount	Volume [mm^3]	Weight [kg]	Interesting?
	Screw			200			8	1	10053	0,1	
	Total									0,1	

Detail										
13	Object		Name	Length [mm]	Width [mm]	Height [mm]	Diameter [mm]	Amount	Volume [mm^3]	Weight [kg]	Interesting?
	L		SST ABR7015					1	10926	0,1	
	Screw		CSA					16		0,3	
	Total									0,4	

Detail										
14a	Object		Name	Length [mm]	Width [mm]	Height [mm]	Diameter [mm]	Amount	Volume [mm^3]	Weight [kg]	Interesting?
	Screw			100			8	1	5027	0,0	
	Total									0,0	

Detail										
14b	Object		Name	Length [mm]	Width [mm]	Height [mm]	Diameter [mm]	Amount	Volume [mm^3]	Weight [kg]	Interesting?
	Screw			140			8	1	7037	0,1	
	Total									0,1	

Detail											
15	Object		Name	Length [mm]	Width [mm]	Height [mm]	Diameter [mm]	Amount	Volume [mm^3]	Weight [kg]	Interesting?
	L_front	L		120	180	6		1	129600	1,0	
		Bolt	FAZII M12	70			12	2	15834	0,1	
		Screw		60			5	11	12959	0,1	
	Trekstrip	Plate		2200	250	15		1	8250000	64,8	
		Plate		150	250	20		1	750000	5,9	
		Plate		150	150	15		1	168750	1,3	
		Screw	SSH					107	x	3,7	
	L_side	L		2980	175	10		1	5215000	40,9	
		Screw	SSH					58,6	x	2,1	
		Bolt	M12	70			12	16	126669	1,0	
	Achor		M30	1000			30	2	1413717	11,1	
	Total									132,0	Yes

Detail

16	Object		Name	Length [mm]	Width [mm]	Height [mm]	Diameter [mm]	Amount	Volume [mm^3]	Weight [kg]	Interesting?
	Trekstrip	Plate		2800	500	15		1	21000000	164,9	
		Plate		250	500	20		1	2500000	19,6	
		Plate		200	200	20		1	400000	3,1	
		Screw	SSH					274	x	9,6	
	L_side	L		6200	175	10		1	10850000	85,2	
		Screw	SSH					154	x	5,4	
		Bolt	M12	70			12	21	166253	1,3	
	Achor		M30	1000			30	4	2827433	22,2	
	Total									311,3	Yes

		Plate	Rod	Anchor	L	Screw	Bolt	Nail	Tube	Other	Appears n times	Total		
Detail:	**01a**	13,6	1,5	2,5							12	211,8		
	01b	22,7	5,9	6,9							1	35,5		
	02	17,1		14,9			1,4				8	267,3		
	03a	21,4	5,9	9,9							10	372,1		
	03b	31,4	5,9	9,9							14	661,7		
	03c	26,7	3,9	9,9	59,6		11,4	3,3			2	229,7		
	05	18,7	1,5	2,5					5,7		18	510,2		
	06	42,4	2,3	3,8							2	96,9		
	07	16,0	2,3	2,5							8	166,5		
	08	40,6	2,3	3,8							2	93,4		
	09a	18,8	2,3	3,2							39	946,5		
	09b	31,4	5,9	6,9							1	44,2		
	10	31,8	2,3	2,5							4	146,4		
	11	22,9	1,9	2,5							6	163,7		
	Anchor									56,3	8	450,4		
	Bracing									312,4	2	624,8		
	15	72,0		11,1	42,0	5,9	1,1				2	264,1		
	16	187,6		22,2	85,2	15,0	1,3				2	622,5		
	Total	3208,7	343,6	717,7	373,4	41,8	39,1	6,5	101,7	1075,2		**5907,7**	[kg]	1,9 [kg/m^2]
												3050	[m^2]	
												430,9	[kg]	0,1 [kg/m^2]

B

Steel Calculation First Floor

Detail

101	Object		Name	Length [mm]	Width [mm]	Height [mm]	Diameter [mm]	Amount	Volume [mm^3]	Weight [kg]	Interesting?
	Shoe	f1		340	290	25		1	2465000	19,4	
		l1		440	260	30		1	3432000	26,9	
		f2		400	290	25		1	2900000	22,8	
		Bolt_v	M16	250			16	8	402124	3,2	
		Bolt_h	M16	360			16	4	289529	2,3	
	Total									74,5	

Detail

102	Object		Name	Length [mm]	Width [mm]	Height [mm]	Diameter [mm]	Amount	Volume [mm^3]	Weight [kg]	Interesting?
	Shoe	f1		340	290	25		1	2465000	19,4	
		l1		440	260	30		1	3432000	26,9	
		f2		400	290	25		1	2900000	22,8	
		Bolt_v	M20	250			20	8	628319	4,9	
		Bolt_h	M20	360			20	4	452389	3,6	
	Total									77,5	

Detail

103	Object		Name	Length [mm]	Width [mm]	Height [mm]	Diameter [mm]	Amount	Volume [mm^3]	Weight [kg]	Interesting?
	Shoe	f1		370	370	25		1	3422500	26,9	
		l1		440	350	30		1	4620000	36,3	
		f2		370	370	25		1	3422500	26,9	
		Bolt_v	M16	250			16	8	402124	3,2	
		Bolt_h	M16	360			16	4	289529	2,3	
	Total									95,4	

Detail

104	Object		Name	Length [mm]	Width [mm]	Height [mm]	Diameter [mm]	Amount	Volume [mm^3]	Weight [kg]	Interesting?
	Plate	1		370	440	30		1	4884000	38,3	
		2		370	300	30		1	3330000	26,1	
		3		490	200	30		1	2940000	23,1	
	Bolt		M16	360			16	1	72382	0,6	
	Total									88,1	Yes

Detail

105	Object		Name	Length [mm]	Width [mm]	Height [mm]	Diameter [mm]	Amount	Volume [mm^3]	Weight [kg]	Interesting?
	Shoe	f1		370	290	25		1	2682500	21,1	
		l1		440	260	30		1	3432000	26,9	
		f2		370	290	25		1	2682500	21,1	
		Bolt_v	M16	250			16	8	402124	3,2	
		Bolt_h	M16	360			16	2	144765	1,1	
	T	f1		340	150	10		2	1020000	8,0	
		l1		340	160	10		2	1088000	8,5	
	Total									89,9	

Detail

106	Object		Name	Length [mm]	Width [mm]	Height [mm]	Diameter [mm]	Amount	Volume [mm^3]	Weight [kg]	Interesting?
	Opleghandje	Plate_1		220	280	30		1	1848000	14,5	
		Plate_2		960	280	25		1	6720000	52,8	
		Plate_3		960	180	15		1	2592000	20,3	
		Bolt_h	M20	300			20	6	565487	4,4	
	HEA+plate	HEA	HEA300	380						34,2	
		Plate_1		262	145	15		2	1139700	8,9	
		Bolt_v	M16	250			16	4	201062	1,6	
	L	L		3500	200	10		1	7000000	55,0	
		Screw	SSH Ø8-120					3		0,1	
		Screw	SSH Ø8-180					17,5		1,1	
	Total									192,9	

Detail

106a	Object		Name	Length [mm]	Width [mm]	Height [mm]	Diameter [mm]	Amount	Volume [mm^3]	Weight [kg]	Interesting?
	Opleghandje	Plate_1		220	280	30		1	1848000	14,5	
		Plate_2		960	280	25		1	6720000	52,8	
		Plate_3		960	180	15		1	2592000	20,3	
		Bolt_h	M20	300			20	6	565487	4,4	
	HEA+plate	HEA	HEA300	380						34,2	
		Plate_1		262	145	15		2	1139700	8,9	
		Bolt_v	M16	250			16	4	201062	1,6	
	L	L		3500	200	10		1	7000000	55,0	
		Screw	SSH Ø8-120					3		0,1	
		Screw	SSH Ø8-180					17,5		1,1	
	L	L		2200	200	10		2	8800000	69,1	
			SSH Ø8-80					55		1,7	
	Total									192,9	

Detail

108	Object		Name	Length [mm]	Width [mm]	Height [mm]	Diameter [mm]	Amount	Volume [mm^3]	Weight [kg]	Interesting?
	Shoe	f1		370	370	25		1	3422500	26,9	
		l1		440	350	30		1	4620000	36,3	
		f2		370	370	25		1	3422500	26,9	
		Bolt_v	M20	250			20	8	628319	4,9	
		Bolt_h	M16	430			16	12	1037480	8,1	
	T	f1		400	380	15		1	2280000	17,9	
		l1		230	380	15		2	2622000	20,6	

	Dowel	Ø20-120	120			20	12	452389	3,6	
Total									145,1	

Detail

109	Object		Name	Length [mm]	Width [mm]	Height [mm]	Diameter [mm]	Amount	Volume [mm^3]	Weight [kg]	Interesting?
	Shoe	f1		340	290	25		1	2465000	19,4	
		l1		440	260	30		1	3432000	26,9	
		f2		400	290	25		1	2900000	22,8	
		Bolt_v	M16	250			16	8	402124	3,2	
		Bolt_h	M16	360			16	2	144765	1,1	
	T	f1		340	150	10		1	510000	4,0	
		l1		340	160	10		1	544000	4,3	
		Dowel	Ø16-120	120			16	3	72382	0,6	
	Total									82,2	

Detail

110	Object		Name	Length [mm]	Width [mm]	Height [mm]	Diameter [mm]	Amount	Volume [mm^3]	Weight [kg]	Interesting?
	T	f1		180	110	10		1	198000	1,6	
		l1		180	140	10		1	252000	2,0	
		Dowel	Ø16-150	150			16	3	90478	0,7	
		Bolt	M16	120			16	6	144765	1,1	
	T	f1		320	400	10		1	1280000	10,0	
		l1		320	150	15		2	1440000	11,3	
		Bolt	M16	220			16	12	530803	4,2	
	Total									30,9	

Detail

111	Object		Name	Length [mm]	Width [mm]	Height [mm]	Diameter [mm]	Amount	Volume [mm^3]	Weight [kg]	Interesting?
	T	f1		180	120	10		2	432000	3,4	
		l1		180	150	10		2	540000	4,2	
		Dowel	Ø16-150	150			16	6	180956	1,4	
		Bolt	M16	320			16	4	257359	2,0	
	Total									11,1	

Detail

112	Object		Name	Length [mm]	Width [mm]	Height [mm]	Diameter [mm]	Amount	Volume [mm^3]	Weight [kg]	Interesting?
	T	f1		180	120	10		2	432000	3,4	
		l1		180	150	10		2	540000	4,2	
		Dowel	Ø16-150	150			16	3	90478	0,7	
		Bolt	M16	280			16	4	225189	1,8	
	Screw		Ø8-360					6		0,7	
	Screw		Ø10-500	500				2		0,2	
	Total									11,1	

Detail

113	Object		Name	Length [mm]	Width [mm]	Height [mm]	Diameter [mm]	Amount	Volume [mm^3]	Weight [kg]	Interesting?
	T	Plate_1		340	370	10		1	1258000	9,9	
		Plate_2		260	370	20		1	1924000	15,1	
		Plate_3		340	180	10		2	1224000	9,6	
		Bolt_1	M16	360			16	2	144765	1,1	
		Bolt_2	M20	260			20	12	980177	7,7	
	Plate	Plate_1		300	400	20		1	2400000	18,8	
		Bolt_1	M16	450			16	12	1085734	8,5	
	Screw		Ø10-500	500				2		0,2	
	Total									71,0	

Detail

114	Object		Name	Length [mm]	Width [mm]	Height [mm]	Diameter [mm]	Amount	Volume [mm^3]	Weight [kg]	Interesting?
	Shoe	f1		340	290	25		1	2465000	19,4	
		l1		440	260	30		1	3432000	26,9	
		f2		400	290	25		1	2900000	22,8	
		Bolt_v	M16	250			16	8	402124	3,2	
		Bolt_h	M20	360			20	2	226195	1,8	
	Total									74,0	

Detail

118	Object		Name	Length [mm]	Width [mm]	Height [mm]	Diameter [mm]	Amount	Volume [mm^3]	Weight [kg]	Interesting?
	Shoe	f1		370	370	25		1	3422500	26,9	
		l1		440	350	30		1	4620000	36,3	
		f2		370	370	25		1	3422500	26,9	
		Bolt_v	M16	250			16	8	402124	3,2	
		Bolt_h	M16	360			16	4	289529	2,3	
	T	f1		1020	150	10		1	1530000	12,0	
		l1		1020	180	10		1	1836000	14,4	
		Dowel	Ø20-130	120			16	6	144765	1,1	
		Screw	Ø8-220					12		1,0	
	L	Plate		400	130	5		1	260000	2,0	
		Bolt	M12	180			12	8	162860	1,3	
	Total									127,3	

Detail

121	Object		Name	Length [mm]	Width [mm]	Height [mm]	Diameter [mm]	Amount	Volume [mm^3]	Weight [kg]	Interesting?
	Shoe	f1		340	290	25		1	2465000	19,4	
		l1		440	260	30		1	3432000	26,9	
		f2		400	290	25		1	2900000	22,8	
		Bolt_v	M20	350			20	4	439823	3,5	

	Bolt_h	M16	360			16	4	289529	2,3	
Plate	Plate_1		550	520	15		1	4290000	33,7	
	Plate_2		450	200	15		1	1350000	10,6	
	L		400	140	24		2	2688000	21,1	
	Strip		520	100	10		1	520000	4,1	
	Bolt_1	M24	350			24	2	316673	2,5	
	Bolt_2	M16	350			16	2	140743	1,1	
	Bolt_3	M20	50			20	2	31416	0,2	
Total									148,1	

Detail

122	Object		Name	Length [mm]	Width [mm]	Height [mm]	Diameter [mm]	Amount	Volume [mm^3]	Weight [kg]	Interesting?
	Shoe	f1		370	370	25		1	3422500	26,9	
		l1		440	350	30		1	4620000	36,3	
		f2		370	370	25		1	3422500	26,9	
		Bolt_v	M20	350			20	4	439823	3,5	
		Bolt_h	M16	360			16	4	289529	2,3	
	Plate	Plate_1		550	520	15		1	4290000	33,7	
		Plate_2		450	200	15		1	1350000	10,6	
		L		400	140	24		2	2688000	21,1	
		Strip		520	100	10		1	520000	4,1	
		Bolt_1	M24	350			24	2	316673	2,5	
		Bolt_2	M16	350			16	2	140743	1,1	
		Bolt_3	M20	50			20	2	31416	0,2	
	Total									169,0	

Detail

123	Object		Name	Length [mm]	Width [mm]	Height [mm]	Diameter [mm]	Amount	Volume [mm^3]	Weight [kg]	Interesting?
	Shoe	f1		340	290	25		1	2465000	19,4	
		l1		440	260	30		1	3432000	26,9	
		f2		400	290	25		1	2900000	22,8	
		Bolt_v	M16	250			16	8	402124	3,2	
		Bolt_h	M16	430			16	2	172913	1,4	
	T	f1		280	220	15		1	924000	7,3	
		l1		280	180	15		1	756000	5,9	
		Bolt	M16	240			16	3	144765	1,1	
	Total									87,9	

Detail

124	Object		Name	Length [mm]	Width [mm]	Height [mm]	Diameter [mm]	Amount	Volume [mm^3]	Weight [kg]	Interesting?
	Shoe	f1		370	370	25		1	3422500	26,9	
		l1		440	350	30		1	4620000	36,3	
		f2		370	370	25		1	3422500	26,9	
		Bolt_v	M16	250			16	8	402124	3,2	
		Bolt_h	M16	430			16	8	691653	5,4	
	T	f1		400	380	10		1	1520000	11,9	
		l1		240	380	15		2	2736000	21,5	
		Dowel	Ø20-100	100			20	12	376991	3,0	
	Total									135,0	

Detail

125	Object		Name	Length [mm]	Width [mm]	Height [mm]	Diameter [mm]	Amount	Volume [mm^3]	Weight [kg]	Interesting?
	Shoe	f1		370	370	25		1	3422500	26,9	
		l1		440	350	30		1	4620000	36,3	
		f2		370	370	25		1	3422500	26,9	
		Bolt_v	M16	250			16	8	402124	3,2	
		Bolt_h	M16	430			16	8	691653	5,4	
	T	f1		400	380	10		1	1520000	11,9	
		l1		240	380	15		2	2736000	21,5	
		Dowel	Ø20-100	100			20	6	188496	1,5	
		Dowel	Ø20-160	160			20	6	301593	2,4	
	L	l1		2700	200	10		3	16200000	127,2	
		Screw	Ø8-80					162		4,9	
	Total									267,9	

Detail

126	Object		Name	Length [mm]	Width [mm]	Height [mm]	Diameter [mm]	Amount	Volume [mm^3]	Weight [kg]	Interesting?
	Shoe	f1		340	290	25		1	2465000	19,4	
		l1		440	260	30		1	3432000	26,9	
		f2		400	290	25		1	2900000	22,8	
		Bolt_v	M16	250			16	8	402124	3,2	
		Bolt_h	M16	430			16	8	691653	5,4	
	T	f1		400	380	10		1	1520000	11,9	
		l1		240	380	15		2	2736000	21,5	
		Dowel	Ø20-100	100			20	6	188496	1,5	
		Dowel	Ø20-160	160			20	6	301593	2,4	
	L	l1		2700	200	10		3	16200000	127,2	
		Screw	Ø8-80					162		4,9	
	Total									246,9	

Detail

127	Object		Name	Length [mm]	Width [mm]	Height [mm]	Diameter [mm]	Amount	Volume [mm^3]	Weight [kg]	Interesting?
	Shoe	f1		370	370	25		1	3422500	26,9	
		l1		440	350	30		1	4620000	36,3	
		f2		370	370	25		1	3422500	26,9	
		Bolt_v	M16	250			16	8	402124	3,2	

		Bolt_h	M16	360			16	4	289529	2,3	
	L	L						1	800000	6,3	
		Bolt	M12	180			12	8	162860	1,3	
	Total									103,0	

Detail

128	Object		Name	Length [mm]	Width [mm]	Height [mm]	Diameter [mm]	Amount	Volume [mm^3]	Weight [kg]	Interesting?
	Shoe	f1		370	370	25		1	3422500	26,9	
		l1		440	350	30		1	4620000	36,3	
		f2		370	370	25		1	3422500	26,9	
		Bolt_v	M16	250			16	8	402124	3,2	
		Bolt_h	M16	360			16	4	289529	2,3	
	Opleghandje	Plate_1		150	150	30		1	675000	5,3	
		Plate_2		1100	160	15		1	2640000	20,7	
		Plate_3		1100	200	20		1	4400000	34,5	
		Plate_4		220	180	30		1	1188000	9,3	
		Dowel	Ø20-130	130			20	6	245044	1,9	
		Screw	Ø8-220	220			8	6	66350	0,5	
	Total									167,8	

Detail

129	Object		Name	Length [mm]	Width [mm]	Height [mm]	Diameter [mm]	Amount	Volume [mm^3]	Weight [kg]	Interesting?
	Shoe	f1		400	300	20		1	2400000	18,8	
		l1		320	280	30		1	2688000	21,1	
		f2		400	300	25		1	3000000	23,6	
		Bolt_v	M16	250			16	8	402124	3,2	
		Bolt_h	M16	400			16	4	321699	2,5	
	T	f1		230	120	10		1	276000	2,2	
		l1		230	160	10		2	736000	5,8	
		Dowel	Ø20-100	100			20	12	376991	3,0	
	Total									80,1	

Detail

130	Object		Name	Length [mm]	Width [mm]	Height [mm]	Diameter [mm]	Amount	Volume [mm^3]	Weight [kg]	Interesting?
	T	f1		220	120	10		2	528000	4,1	
		l1		220	160	10		2	704000	5,5	
		Dowel	Ø16-120	120			16	6	144765	1,1	
		Screw	Ø8-140	140			8	12	84446	0,7	
	T	f1		220	120	10		2	528000	4,1	
		l1		220	250	10		2	1100000	8,6	
		Dowel	Ø16-120	120			16	16	386039	3,0	
		Screw	Ø8-140	140			8	12	84446	0,7	
	Opleghandje			120	80	20		2	384000	3,0	
	Total									31,0	

Detail

131	Object		Name	Length [mm]	Width [mm]	Height [mm]	Diameter [mm]	Amount	Volume [mm^3]	Weight [kg]	Interesting?
	Shoe	f1		370	370	25		1	3422500	26,9	
		l1		440	350	30		1	4620000	36,3	
		f2		370	370	25		1	3422500	26,9	
		Bolt_v	M16	250			16	8	402124	3,2	
		Bolt_h	M16	360			16	4	289529	2,3	
	Total									95,4	

Detail

140	Object		Name	Length [mm]	Width [mm]	Height [mm]	Diameter [mm]	Amount	Volume [mm^3]	Weight [kg]	Interesting?
	Shoe	f1		370	370	25		1	3422500	26,9	
		l1		440	350	30		1	4620000	36,3	
		f2		370	370	25		1	3422500	26,9	
		Bolt_v	M16	250			16	8	402124	3,2	
		Bolt_h	M16	430			16	8	691653	5,4	
	T	f1		400	380	10		1	1520000	11,9	
		l1		240	380	15		2	2736000	21,5	
		Dowel	Ø20-100	120			20	12	452389	3,6	
	Total									135,5	

	Appears n tir	Shoe		Opleghandje				T				L			Plate	Bolt	HEA	Screw	Other	Subtotal	
		Plate	Bolt	Plate	Dowel	Bolt	Screw	Plate	Dowel	Bolt	Screw	Plate	Bolt	Screw							
101	17	69,1	5,4																	1266,3	
102	2	69,1	8,5																	155,1	
103	26	90,0	5,4																	2481,2	
104	4														87,6	0,6				352,5	
105	6	69,1	4,3					16,5												539,4	
106	8			87,6			4,4					55,0		1,2	8,9	1,6	34,2			1543,1	
106a	8			87,6			4,4					124,0		2,8	8,9	1,6	34,2			2109,0	
108	2	90,0	13,1					38,5		3,6										290,2	
109	4	69,1	4,3					8,3		0,6										328,8	
110	6							24,9		0,7	5,3									185,4	
113	18							34,6			8,8				18,8	8,5		0,2		1278,4	
114	4	69,1	4,9																	296,0	
118	1	90,0	5,4					26,4		1,1	1,0	2,0	1,3							127,3	
121	10	69,1	5,7												69,5	3,8				1480,8	
122	10	90,0	5,7												69,5	3,8				1690,2	
123	2	69,1	4,5					13,2			1,1									175,8	
124	4	90,0	8,6					33,4		3,0										539,8	
125	1	90,0	8,6					33,4		3,8		127,2		4,9						267,9	
126	1	69,1	8,6					33,4		3,8		127,2		4,9						246,9	
127	2	90,0	5,4									6,3	1,3							206,0	
128	2	90,0	5,4	69,9	1,9		0,5													335,5	
129	2	63,5	5,7					7,9		3,0										160,2	
130	2			3,0				22,5		4,2	1,3									61,9	
131	2	90,0	5,4																	190,9	
140	2	90,0	8,6					33,4		3,6										271,1	
Anchor	8																		56,3	450,4	
Subtotal		7983,6	580,8	1547,5	3,8	71,0	1,0	1362,1	55,7	193,0	3,7	1700,8	3,8	41,6	2221,6	257,7	547,2	4,3	450,4	17029,8	[kg]
		8564,4		1623,4				1614,5				1746,3									
		2,6	0,2	0,5	0,0	0,0	0,0	0,4	0,0	0,1	0,0	0,6	0,0	0,0	0,7	0,1	0,2	0,0	0,1	5,6	[kg/m^2]
		2,8		0,5				0,5				0,6									[kg/m^2]

C

Example Calculation Alternative 1

			Required	Eurocode (NEN EN)	Equation	Extra's
Timber Properties						
	ρ_k	350 [kg/m^3]		338:2016 Table 1		
	f_c,0,k	24 [N/mm^2]		338:2016 Table 1		
	f_c,90,k	2,5 [N/mm^2]		338:2016 Table 1		
	f_w,k	0,64 [N/mm^2]		338:2016 Table 1		Value from Literature
	f_m,y,k	24,0 [N/mm^2]		338:2016 Table 1		
	f_v,k	4 [N/mm^2]		338:2016 Table 1		
	f_c,0,d	15,4 [N/mm^2]				
	f_c,90,d	1,6 [N/mm^2]				
	f_w,d	0,4 [N/mm^2]				
	f_m,y,d	16,2 [N/mm^2]				
	f_v,d	3,2 [N/mm^2]				
Dowel Properties					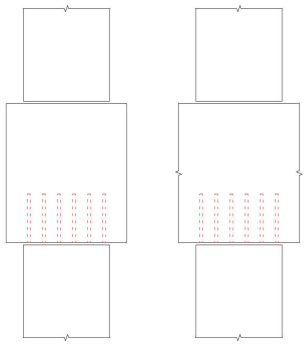	
	ρ_k	620 [kg/m^3]		338:2016 Table 3		D50
	d_d	7 [mm]				
	l_d	105 [mm]				
	f_c,0,k	30 [N/mm^2]				
	f_c,0,d	19,2 [N/mm^2]				
Screw Properties						Rothoblaas VGZ
	l_r	120 [mm]				
	d_r	9 [mm]				
	d_1	5,9 [mm]				
	f_y,k	1000 [N/mm^2]				
Factors						
	k_mat	1,40 [-]		1995-1-1:2023 Table 8.1		
	γ_M	1,25 [-]				
	k_mod_G	0,60 [-]				
	k_mod_Q	0,80 [-]		1995-1-1:2023 Table 4.4		
	k_var	1,00 [-]				
	k_h	1,06 [-]				
	k_c,90	1,14 [-]		1995-1-1:2023 Formula 8.6		
Column Geometry						
	w_c	200 [mm]				
	l_c	200 [mm]				
Beam Geometry						
	h_b	300 [mm]				
	w_b	280 [mm]				
	L	7200 [mm]				
	l	200 [mm]				
	l_1	3400 [mm]				
	l_ef	260 [mm]				
	h_ef	120 [mm]		1995-1-1:2023 Formula 8.8		
	A_ef	52000 [mm^2]				
	l_c,90	200 [mm]				
	b_c,90	200 [mm]				
Load Case 1						
	G_k,1	0,2 [N/mm]				
	G_k,2	7,2 [N/mm]				
	Q_k,1	3,6 [N/mm]				
	γ_G,1	1,35 [-]				
	γ_G,2	1,2 [-]				
	γ_Q	1,5 [-]				
	LC01	10,0 [N/mm]			$q_1 = \gamma_G * G_{k,1} + \gamma_Q * Q_{k,1}$	
	LC02	14,3 [N/mm]				
	F_1	64260 [N]				
	σ_1	1,24 [N/mm^2]				
Load Case 2						
	G_k,1	0,42 [N/mm]				
	G_k,2	15,2 [N/mm]				
	Q_k,1	11,0 [N/mm]				
	γ_G,1	1,35 [-]				
	γ_G,2	1,2 [-]				
	γ_Q	1,5 [-]				
	LC01	21,1 [N/mm]			$q_2 = \gamma_G * G_{k,2} + \gamma_Q * Q_{k,2}$	

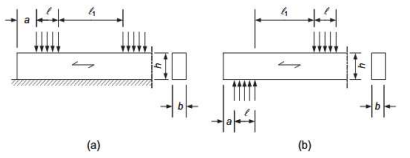

Figuur 6.2 — Element op (a) continue en (b) discrete steunpunten

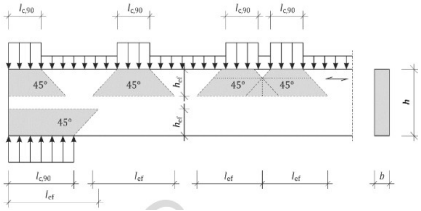

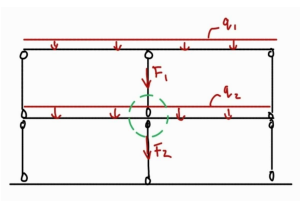

	LC02	35,2	[N/mm]	
	F_2	222858	[N]	
	σ_2	4,29	[N/mm^2]	

Screw Reinforcement				1995-1-1:2023 8.1.6.2
	a_1	45	[mm]	1995-1-1:2023 Table 11.24
	a_2	22,5	[mm]	1995-1-1:2023 Table 11.24
	a_3	90	[mm]	1995-1-1:2023 Table 11.24
	a_4	18	[mm]	1995-1-1:2023 Table 11.24
	n_0	3	[-]	
	n_1	8	[-]	
	n	24	[-]	
	l_ef,1	260	[mm]	1995-1-1:2023 Formula 8.13
	l_ef,2	330	[mm]	1995-1-1:2023 Formula 8.15
Withdrawal Capacity				1995-1-1:2023 11.2.2.3
	k_ρ	0,8	[-]	1995-1-1:2023 Table 11.2 (9)
	k_mat	1	[-]	1995-1-1:2023 Table 11.2 (8)
	k_w	1	[-]	1995-1-1:2023 Table 11.2 (7)
	k_screw	7,5	[-]	1995-1-1:2023 Table 11.2
	f_w,k	3,6	[N/mm^2]	1995-1-1:2023 Table 11.2 (6)
	F_w,k,r	12233,6	[N]	1995-1-1:2023 Formula 11.4
Compressive Resistance				1995-1-1:2023 11.2.2.5
	γ_M1	1,1	[-]	1995-1-1:2023 Table 4.4
	γ_R	1,3	[-]	1995-1-1:2023 Table 4.4
	(EI)_S	358833,7		1995-1-1:2023 Formula 11.13
	c_h	104,3		1995-1-1:2023 Formula 11.12
	N_ki,k	6117,7		1995-1-1:2023 Formula 11.11
	N_pl,k	27339,7		1995-1-1:2023 Formula 11.10
	λ_k	2,1		1995-1-1:2023 Formula 11.9
	k	3,2		1995-1-1:2023 Formula 11.8
	k_c	0,2		1995-1-1:2023 Formula 11.7
	F_c,k,r	5759,2	[N]	1995-1-1:2023 Formula 11.6
Capacity of the Reinforced Contact Area	F_c,90,Rk	231	[kN]	1995-1-1:2023 Formula 11.4

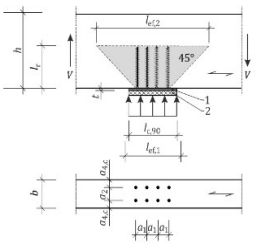

Dowel Reinforcement			
	n_d,0	6	[-]
	n_d,1	6	[-]
	n_d	36	[-]
	F_w,k,d	1477,8	[N]
	F_punt	96,2	[N]
	l_ef,1,d	200	[mm]
	l_ef,2,d	385	[mm]
	F_c,90,Rk,d	156,7	[kN]

$$F_{w,k} = \pi * d_d * l_d * f_{w,k}$$
$$F_{punt} = 0.25 * \pi * d_d * f_{c,90,k}$$

$$F_{c,90,Rk,d} = min\begin{cases} k_{mat} * b_{c,90} * l_{ef,1} * f_{c,90,k} + n_d * (\mathrm{F_{w,k,d}} + \mathrm{F_{punt}}) \\ b * l_{ef,2} * f_{c,90,k} \end{cases}$$

Bending Check				
	z	155,4	[mm]	
	I_y	629546201	[mm^4]	
	W_y	4051071,95	[mm^3]	
	σ_m,y,d	14,1	[N/mm^2]	
	u.c.	0,87	[-]	1995-1-1:2023 Formula 8.20

Shear Check				
	f_v,k,ref	2,75	[N/mm^2]	1995-1-1:2023 Formula 8.30
	k_h,v	1,07	[-]	1995-1-1:2023 Formula 5.10
	k_v	0,7	[-]	1995-1-1:2023 Formula 8.29
	V_Ed	63439,2	[N]	
	A_v	53060	[mm^2]	
	τ_d	1,2	[N/mm^2]	
	u.c.	0,51	[-]	1995-1-1:2023 Formula 8.27

Shear + Compression Check				
	f_c,90,d,eff	4,44	[N/mm^2]	
	σ_c,90,d	4,29	[N/mm^2]	
	u.c.	0,27	[-]	1995-1-1:2023 Formula 8.35

Effective Cross-Section

A_eff	79590	[mm^2]

Load Case: Fire

γ_G	1	[-]
γ_Q	1	[-]
ψ_2	0,3	[-]
LC01,1	7,4	[N/mm]
LC02,1	8,5	[N/mm]
LC01,2	15,6	[N/mm]
LC02,2	18,9	[N/mm]
F_1	38160	[N]
F_2	85140	[N]
σ_1	0,73	[N/mm^2]
σ_2	1,64	[N/mm^2]

Reduced Cross-Section

k_n	1,23	[-]		1995-1-2:2023 7.2.2 (2)
β_0	0,65	[mm/min]		1995-1-2:2023 Table 5.4
t	60	[min]		
d_0	14	[mm]		1995-1-2:2023 7.2.2 (8)
d_char	47,97	[mm]	49	1995-1-2:2023 Formula 5.1
d_ef	61,97	[mm]	49	1995-1-2:2023 Formula 7.3
A_red	36902,8	[mm^2]		

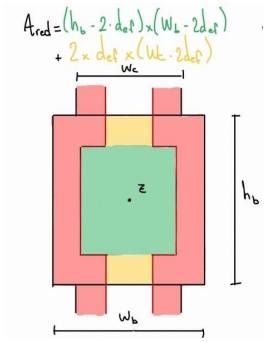

Bending Check Red.

z	150	[mm]		
I_y	204500536	[mm^4]	282449353,7	
W_y	1363336,91	[mm^3]	1882995,691	
σ_m,y,d	22,5	[N/mm^2]	16,3	
u.c.	1,38	[-]	1,00	1995-1-1:2023 Formula 8.20

Shear Check Red.

V_Ed	34056	[N]	
A_v	24601,9	[mm^2]	
τ_d	1,4	[N/mm^2]	
u.c.	0,59	[-]	1995-1-1:2023 Formula 8.27

Shear + Compression Check Red.

u.c.	0,19	[-]	1995-1-1:2023 Formula 8.35

D

Example Calculation Alternative 2

				Required	Eurocode	Equation	Extra's
Timber Properties							
	ρ_k	385	[kg/m^3]	>350	1995-1-1:2023 11.2.3.2 (13)		GL24h
	f_c,90,k	2,5	[N/mm^2]				
	f_c,0,k	24	[N/mm^2]				
	f_m,y,k	24	[N/mm^2]				
	f_v,k	3,5	[N/mm^2]				
	f_c,90,d	1,6	[N/mm^2]				
	f_c,0,d	15,4	[N/mm^2]				
	f_m,y,d	16,2	[N/mm^2]				
	f_v,d	2,2	[N/mm^2]				
Plate Properties							BauBuche S
	f_c,0,k	57,6	[N/mm^2]				
	f_c,90,k	14	[N/mm^2]				
	f_c,0,d	36,9	[N/mm^2]				
	f_c,90,d	9,0	[N/mm^2]				
	ρ_k	730	[kg/m^3]				
Dowel_1 Properties				D30 or higher	1995-1-1:2023 11.2.3.2 (13)		D50
	f_m,k	50	[N/mm^2]				
	ρ_d	620	[kg/m^3]				
	n	3	[-]				
	n_row	3	[-]				
Factors							
	γ_R	1,3	[-]		1995-1-1:2023 Table 4.3		
	γ_M	1,25	[-]		1995-1-1:2023 Table 4.4		
	k_mod	0,80	[-]				
	k_h,m,y	1,06	[-]				
Column Geometry							
	L	7200	[mm]				
	w_c	200	[mm]				
	w_c,new	90	[mm]				
	l_c	200	[mm]				
Beam Geometry							
	h_b	300	[mm]				
	w_b	280	[mm]				
	w_b,new	130	[mm]				
Plate Geometry							
	t_p	20	[mm]				
	w_p	190	[mm]				
	l_p,c	160	[mm]				
Dowel Geometry							
	d_d	20	[mm]	16<d<30	1995-1-1:2023 11.2.3.2 (13)		
	α	0	[°]	0 of 90			
Embedment Strength							
	f_h,1,k	21,0	[N/mm^2]		1995-1-1:2023 11.2.3.3 Table 11.7		
	f_h,2,k	39,8	[N/mm^2]		1995-1-1:2023 11.2.3.3 Table 11.7		
	β	1,9	[-]		1995-1-1:2023 11.2.3.2 Formula 11.16		
Yield Moment							
	M_y,k	29452,4	[Nmm]		1995-1-1:2023 11.2.3.4 Table 11.8		
Embedments Depths							
	t_h,1,req	34,8	[mm]	FM (f)	1995-1-1:2023 11.2.3.2 Table 11.5		
	t_h,2,req	8,2	[mm]	FM (f)	1995-1-1:2023 11.2.3.2 Table 11.5		
	t_h,1,req	10,1	[mm]	FM (d)	1995-1-1:2023 11.2.3.2 Table 11.6		
	t_h,2,req	21,1	[mm]	FM (d)	1995-1-1:2023 11.2.3.2 Table 11.6		
	t_h,1,req	40,0	[mm]	>2d	1995-1-1:2023 11.2.3.2 (13)		
	t_h,2,req	40,0	[mm]	>2d	1995-1-1:2023 11.2.3.2 (13)		
	t_h,1	90,0	[mm]				
	t_h,2	10,0	[mm]				
Failure Modes							
	F_D,k,a	37810,1	[N]	FM (a)	1995-1-1:2023 11.2.3.2 Formula 11.15		
	F_D,k,b	7965,8	[N]	FM (b)	1995-1-1:2023 11.2.3.2 Formula 11.15		
	F_D,k,d	14839,1	[N]	FM (d)	1995-1-1:2023 11.2.3.2 Formula 11.15		
	F_D,k,f	5692,4	[N]	FM (f)	1995-1-1:2023 11.2.3.2 Formula 11.15		1,15 = 1,0 for wooden dowels
	F_D,k	5,7	[kN]				
	F_v,k	11,4	[kN]				
Design Resistance							
	F_v,Rd	82,0	[kN]				
Load Case 1							
	G_k,1	0,2	[N/mm]				
	G_k,2	7,2	[N/mm]				

	Q_k,1	3,6	[N/mm]
	γ_G,1	1,35	[-]
	γ_G,2	1,2	[-]
	γ_Q	1,5	[-]
	LC01	10,0	[N/mm]
	LC02	14,3	[N/mm]
	F_1	64260	[N]

Load Case 2			
	G_k,1	0,42	[N/mm]
	G_k,2	15,2	[N/mm]
	Q_k,1	11,0	[N/mm]
	γ_G,1	1,35	[-]
	γ_G,2	1,2	[-]
	γ_Q	1,5	[-]
	LC01	21,1	[N/mm]
	LC02	35,2	[N/mm]
	F_2	158598	[N]
	σ_2	8,8	[N/mm^2]

Checks (A)			
	F_v,Ed < F_v,Rd	0,78	
	Plate compr.	0,46	
	Min. Spacing	180	[mm]

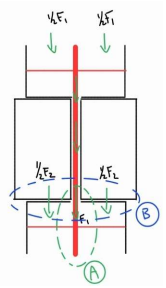

Effective area			
	h_ef	120	[mm]
	l_ef	440	[mm]
	k_c,90	1,5	[-]
	k_mat	1,4	
	A	18000	[mm^2]

Checks (B)				
	σ_c,90,d	4,4	[N/mm^2]	
	u.c. Beam	1,52	[-]	1995-1-1:2023 Formula 8.4
	σ_c,0,d	4,4	[N/mm^2]	
	u.c. Column	0,29	[-]	1995-1-1:2023 Formula 8.3

Dowel_2 Properties				D50
	ρ_k	730	[kg/m^3]	338:2016 Table 3
	d_d	7	[mm]	
	l_d	105	[mm]	
	f_c,0,k	30	[N/mm^2]	
	f_c,0,d	19,2	[N/mm^2]	

Dowel Reinforcement (B)			
	n_d,0	2	[-]
	n_d,1	6	[-]
	n_d	12	[-]
	f_w,k,d	1,4	[N/mm^2]
	F_w,k,d	3232,7	[N]
	F_punt	96,2	[N]
	l_ef,1,d	200	[mm]
	l_ef,2,d	385	[mm]
	F_c,90,Rk,d	84,9	[kN]
	u.c. new	0,93	[-]

$$F_{w,k} = \pi \cdot d_d \cdot l_d \cdot f_{c,90,k}$$
$$F_{punt} = 0.25 \cdot \pi \cdot d_d^2 \cdot f_{c,90,k}$$

$$F_{c,90,Rk,d} = min\begin{cases} k_{mat} \cdot b_{c,90} \cdot l_{ef,1} \cdot f_{c,90,k} + n \cdot F_c \\ b \cdot l_{ef,2} \cdot f_{c,90,k} \end{cases}$$

Bending Check				
	z	150,0	[mm]	
	I_y	585000000	[mm^4]	
	W_y	3900000	[mm^3]	
	σ_m,y,d	14,6	[N/mm^2]	
	u.c.	0,90	[-]	1995-1-1:2023 Formula 8.20

Shear Check				
	f_v,k,ref	2,75	[N/mm^2]	1995-1-1:2023 Formula 8.30
	k_h,v	1,07	[-]	1995-1-1:2023 Formula 5.10
	k_var	1,00	[-]	
	k_v	0,8	[-]	1995-1-1:2023 Formula 8.29
	V_Ed	63439	[N]	
	A_v	52000	[mm^2]	
	τ_d	1,2	[N/mm^2]	
	u.c.	0,65	[-]	1995-1-1:2023 Formula 8.27

Shear + Compression Check				
	f_c,90,d,eff	4,72	[N/mm^2]	
	σ_c,90,d	8,81	[N/mm^2]	
	u.c.	0,18	[-]	1995-1-1:2023 Formula 8.35

Column check			
	l_c,ef	140	

	A_c,ef	28000	
	σ_c	6,07	[N/mm^2]
	u.c.	0,40	[-]

Load Case: Fire

γ_G	1	[-]
γ_Q	1	[-]
ψ	0,3	[-]
LC01,1	7,4	[N/mm]
LC02,1	8,5	[N/mm]
LC01,2	15,6	[N/mm]
LC02,2	18,9	[N/mm]
F_1	38160	[N]
F_2	85140	[N]
σ_D	2,37	[N/mm^2]

Reduced geometry

d_ef	49	[mm]
w_b,fire	81	[mm]
A_b,fire	48600	[mm^2]
w_c,fire	41	[mm]
l_c,fire	102	[mm]
A_c,fire	8364	[mm^2]
w_p,fire	102	[mm]
t_h2,fire	41	[mm]
reduction of n	NO	
n_fire	3	[-]
reduction of n_0	NO	
n_0,fire	2	[-]

Bending Check Red.

z	150	[mm]	
I_y	364500000	[mm^4]	
W_y	2430000	[mm^3]	
σ_m,y,d	12,6	[N/mm^2]	
u.c.	0,78	[-]	1995-1-1:2023 Formula 8.20

Shear Check Red.

V_Ed	34056	[N]	
A_v	32400,0	[mm^2]	
τ_d	1,1	[N/mm^2]	
u.c.	0,56	[-]	1995-1-1:2023 Formula 8.27

Shear + Compression Check Red.

u.c.	0,33	[-]	1995-1-1:2023 Formula 8.35

Dowel Reinforcement Fire

n_d,0	2	[-]
n_d,1	6	[-]
n_d	12	[-]
f_w,k,d	1,4	[N/mm^2]
F_w,k,d	3233	[N]
F_punt	62	[N]
l_ef,1,d	260	[mm]
l_ef,2,d	385	[mm]
F_c,90,Rk,d	77963	[N]
u.c. new	0,55	[-]

Plate Fire

u.c. compr.	0,51	[-]

Failure Modes Fire

F_D,k,a	37810	[N]
F_D,k,b	32660	[N]
F_D,k,d	6760	[N]
F_D,k,f	5692	[N]
F_D,k	5692	[N]
F_v,k	11385	[N]
F_v,Rd	81971	[N]
u.c.	0,47	[-]

E

Example Calculation Alternative 3

			Required	Eurocode	Equation	Extra's
Timber Properties						
	ρ_k	385 [kg/m^3]				GL24h
	f_c,90,k	2,5 [N/mm^2]				
	f_c,0,k	24 [N/mm^2]				
	f_v,k	3,5 [N/mm^2]				
	f_m,y,k	24 [N/mm^2]				
	f_c,90,d	1,6 [N/mm^2]				
	f_c,0,d	15,4 [N/mm^2]				
	f_v,d	2,2 [N/mm^2]				
	f_m,y,d	16,2 [N/mm^2]				
	E,90,mean	300,0 [N/mm^2]				
Dowel_1 Properties					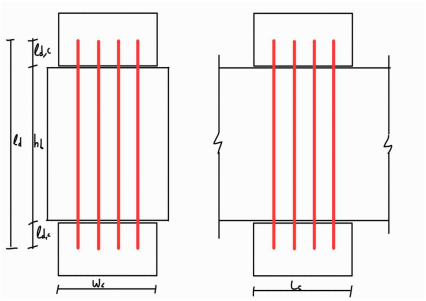	BauBuche S
	f_c,0,k	57,5 [N/mm^2]				
	f_c,0,d	36,8 [N/mm^2]				
	E	14900 [N/mm^2]				
	n_1,0	3 [-]				
	n_1,1	3 [-]				
	d	16 [mm]				
	spacing check	1,0 [-]				
Dowel_2 Properties					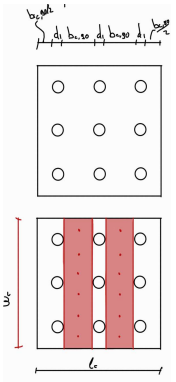	BauBuche S
	f_c,0,k	60 [N/mm^2]				
	f_c,0,d	38,4 [N/mm^2]				
	E	14900 [N/mm^2]				
	n_2,0	5 [-]				
	spacing check	1,0 [-]				
	n_2,1	1 [-]				
	spacing check	1,2 [-]				
	d	10 [mm]				
	l_d,2	150 [mm]				
Factors						
	γ_R	1,3 [-]		1995-1-1:2023 Table 4.3		
	γ_M	1,25 [-]		1995-1-1:2023 Table 4.4		
	k_mod	0,80 [-]				
	k_h	1,06 [-]				
Column Geometry						
	w_c	250 [mm]				
	l_c	250 [mm]				
	A_c	62500 [mm^2]				
	A_c,new	60690 [mm^2]				
Beam Geometry						
	h_b	300 [mm]				
	w_b	290 [mm]				
	L	7200 [mm]				
	A_b	87000 [mm^2]				
	A_b,new	69600 [mm^2]				
Load Case 1						
	G_k,1	0,2 [N/mm]				
	G_k,2	7,2 [N/mm]				
	Q_k,1	3,6 [N/mm]				
	γ_G,1	1,35 [-]				
	γ_G,2	1,2 [-]				
	γ_Q	1,5 [-]				
	LC01	10,0 [N/mm]				
	LC02	14,3 [N/mm]				
	F_d,1	64260 [N]				
	F_c,90,SLS,1	49500 [N]				
Load Case 2						
	G_k,1	0,42 [N/mm]				
	G_k,2	15,2 [N/mm]				
	Q_k,1	11,0 [N/mm]				
	γ_G,1	1,35 [-]				
	γ_G,2	1,2 [-]				
	γ_Q	1,5 [-]				
	LC01	21,1 [N/mm]				
	LC02	35,2 [N/mm]				
	F_d,2	158598 [N]				
	F_c,90,SLS,2	119790 [N]				

Dowel_1

uc	0,96	[-]	$uc = \frac{F_{Rd}}{F_{Ed}}$
l_d,c	4,44	[mm]	
	7,30	[mm]	
	65,71	[mm]	
k	1	[-]	
N_cr,1	1578	[N]	$N_{cr} = \frac{\pi EI}{(kl)^2}$
k_s	10	[-]	
N_cr,2	43787	[N]	$N_{cr,2} = 2 \cdot \sqrt{k_s \cdot EI}$
knik	4,52	[-]	$uc = \frac{F_{d,2}}{n_{1,0} \cdot n_{1,1} \cdot N_{cr}} \leq 1.0$

Compression Check

b_c,90	67,3	[mm]		
l_c,90	250	[mm]		
h_ef	120	[mm]		
l_ef	490	[mm]		
k_mat	1,4	[-]	1995-1-1:2023 Table 8.1	
k_c,90	1,4	[-]	1995-1-1:2023 Formula 8.6	$k_{c,90} = \sqrt{\frac{l_{ef}}{l_{c,90}}} \leq 4.0$
σ_c,90,d	2,6	[N/mm^2]		
uc	0,83	[-]		$uc = \frac{\sigma_{c,90,d}}{k_{mat} k_{c,90} f_{c,90,d}} \leq 1.0$
w_sls,z	1,1	[mm]	1995-1-1:2023 Formula 9.31	$w_{SLS,z} = \frac{h_{ef} \cdot F_{c,90,SLS}}{2 \cdot b_{c,90} \cdot E_{90,mean}} \cdot \left(\frac{1}{l_{c,90}} + \frac{1}{l_{ef}}\right)$

Dowel_2

Necessary	NO		
k_mat	1,75	[-]	
l_ef,1	310	[mm]	
l_ef,2	500	[mm]	
F_w,k	11781	[N]	$F_{w,k} = \pi \cdot d_d \cdot l_d \cdot f_{c,90,k}$
F_punt	196	[N]	$F_{punt} = 0.25 \cdot \pi \cdot d_d^2 \cdot f_{c,90,k}$
N_cr,1	1021	[N]	
N_cr,2	17104	[N]	
F_b	1021	[N]	
F_c,90,Rk,d	84167	[N]	$F_{c,90,Rk,d} = min\begin{cases} k_{mat} \cdot 2b_{c,90} \cdot l_{ef,1} \cdot f_{c,90,k} + n \cdot F_b \\ b_{c,90} \cdot l_{ef,2} \cdot f_{c,90,k} \end{cases}$

Bending Check

z	150,0	[mm]	
I_y	544500000	[mm^4]	
W_y	3630000	[mm^3]	
σ_m,y,d	15,7	[N/mm^2]	
u.c.	0,97	[-]	1995-1-1:2023 Formula 8.20

Shear Check

f_v,k,ref	2,75	[N/mm^2]	1995-1-1:2023 Formula 8.30
k_h,v	1,07	[-]	1995-1-1:2023 Formula 5.10
k_var	1,0	[-]	
k_v	0,8	[-]	1995-1-1:2023 Formula 8.29
V_Ed	63439	[N]	
A_v	46400	[mm^2]	
τ_d	1,4	[N/mm^2]	
u.c.	0,72	[-]	1995-1-1:2023 Formula 8.27

Shear + Compression Check

f_c,90,d,eff	4,03	[N/mm^2]	
σ_c,90,d	2,61	[N/mm^2]	
u.c.	0,56	[-]	1995-1-1:2023 Formula 8.35

Load Case: Fire

γ_G	1	[-]	
γ_Q	1	[-]	
ψ	0,3	[-]	
LC01,1	7,40	[N/mm]	
LC02,1	8,48	[N/mm]	
LC01,2	15,62	[N/mm]	
LC02,2	18,92	[N/mm]	
F_1	38160	[N]	
F_2	85140	[N]	

Dowel fire check

In Beam	NOT AFFECTED	[-]
In column	AFFECTED	[-]

Reduced geometry

d_ef	49	[mm]
w_b,fire	144	[mm]
A_b,fire	43200	[mm^2]
A_c,fire	20535	[mm^2]

Bending Check Red.

z	150	[mm]
I_y	324000000	[mm^4]
W_y	2160000	[mm^3]
σ_m,y,d	14,2	[N/mm^2]
u.c.	0,87	[-]

Shear Check Red.

V_Ed	34056	[N]
A_v	28800,0	[mm^2]
τ_d	1,2	[N/mm^2]
u.c.	0,63	[-]

Shear + Compression Check Red.

u.c.	0,28	[-]

Column Check Red.

u.c.	0,39	[-]

F

Timber Characteristic Values

wood class	Strength properties (N/mm^2)						Stiffness Properties (N/mm^2)				(kg/m^3)	
	Bending	Tension ||	Tension Perp	Compression ||	Compression Perp	Shear	Mean MoE||	5% MoE ||	Mean MoE perp	Mean shear modulus	Density	Density
	f_m,k	**f_t,0,k**	**f_t,90,k**	**f_c,0,k**	**f_c,90,k**	**f_v,k**	**E_0,mean**	**E_0,05**	**E_90,mean**	**G_mean**	**ρ_k**	**ρ_mean**
C24	24	14	0,4	21	2,5	4	11000	7400	370	690	350	420
D24	24	14	0,6	21	7,8	4	10000	8500	670	620	485	580
D50	50	30	0,6	30	6,2	4,5	14000	11800	930	880	620	740
D70	70	42	0,6	36	12	5	20000	16800	1330	1250	800	960
GL24c	24	17	0,5	21,5	2,5	3,5	11000	9100	300	650	365	400
GL24h	24	19,2	0,5	24	2,5	3,5	11500	9600	300	650	385	420
LVL (X grade)	36	26	6	26	9	4,5	10500	8800		600	480	510
LVL S	50	31	0,9	40	3,6	2,6	14000	12000		570	480	540
BauBuche S	80	60	1,5	57,5	14	8	16800	14900	470	760	730	800
DW	270			105	75		40					1300

G

Case Study part III: Hand Calculations

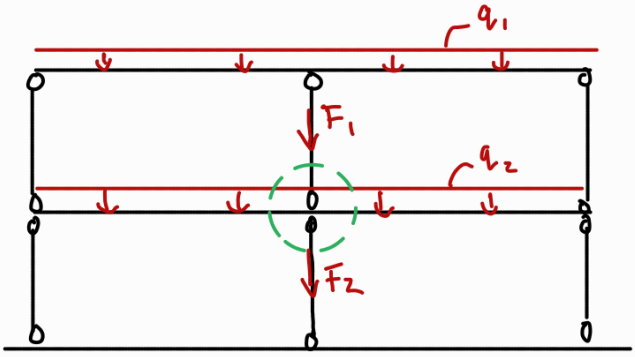

Example calculation Aveleijn Wierden.

GL24C → $f_{c,0,g,k} = 21{,}5\ N/mm^2$ Column 200 x 200
$f_{c,90,g,k} = 2{,}5\ N/mm^2$ Beam 280 x 300

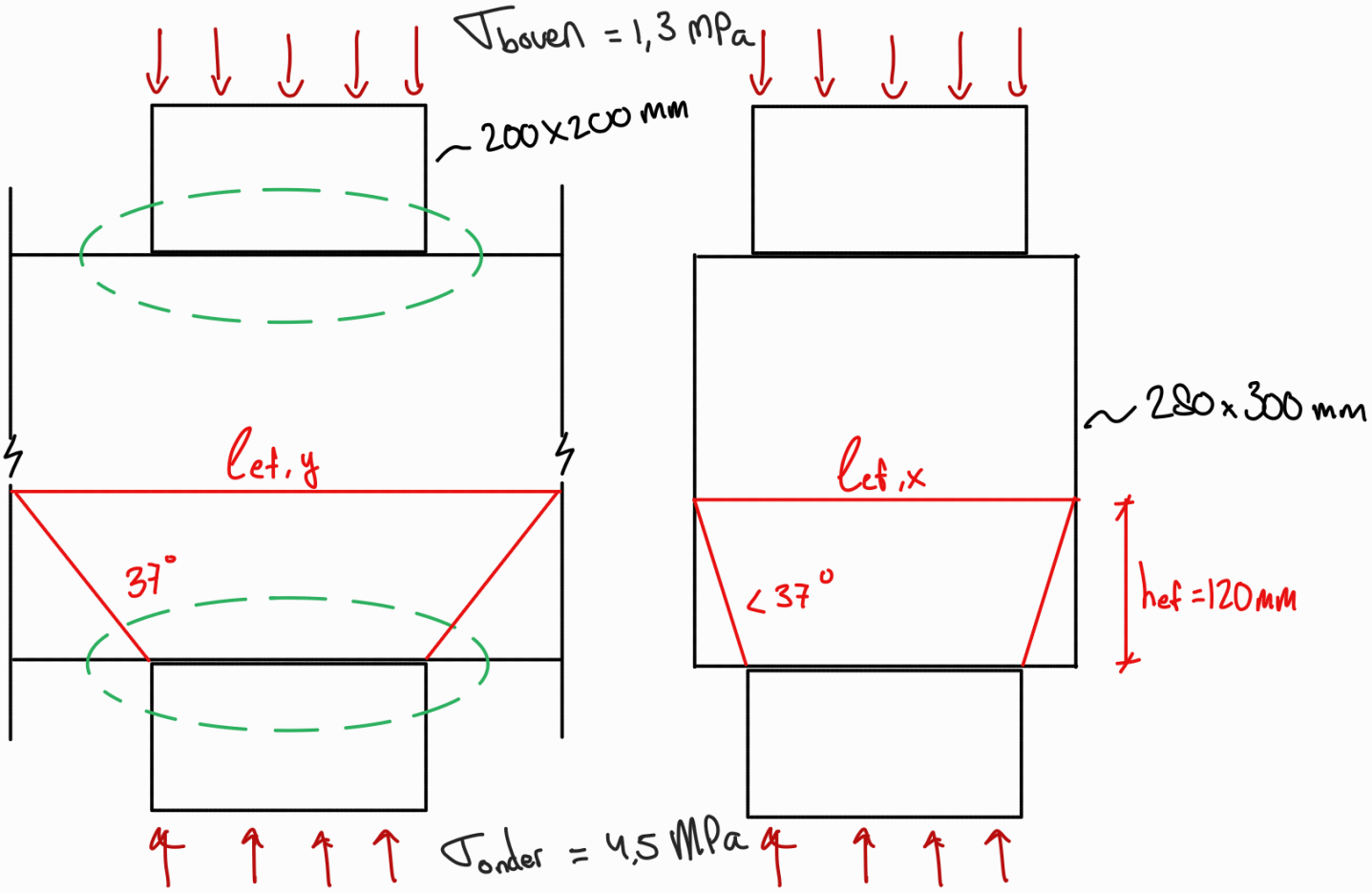

$$\sigma_{c,90,d} \leq K_{c,90} \cdot f_{c,90,d}$$

$$f_{c,90,d} = \frac{K_{mod}}{\gamma_M} \cdot f_{c,90,g,k} = \frac{0{,}7}{1{,}25} \cdot 2{,}5 = 1{,}4\ MPa$$

$\sigma_{boven} = 1{,}3 < 1{,}4$ MPa ✓

$\sigma_{onder} = 4{,}5 > 1.4$ MPa ✗

$$h_{ef} = \min(0{,}4 \cdot h; 140) = 120\ mm$$

DW dowel d10L100

according to FEM: +5 kN per dowel → $\frac{0,7}{1,25} \times 5 = 2,8$ kN
5x5 dowels fit with a = 50 mm (5d)
→ 5·5·2,8 = 70 kN extra
$K_{mat} = 1,75$ (according to EC5 8.1.6.2 (6))

$$F_{c,90,Rk} = \begin{cases} K_{mat} \cdot b_{c,90} \cdot l_{ef,1} \cdot f_{c,90,k} + 70\,kN \\ b \cdot l_{ef,2} \cdot f_{c,90,k} \end{cases} = \begin{cases} 245\,kN \\ 280\,kN \end{cases}$$

$f_{c,90,Rk} = 245 \cdot 10^3 / 200^2 = 6,13$ MPa → $f_{c,90,d} = \frac{0,7}{1,25} \cdot 6,13 = 3,43$ MPa

U.C. = 1,31 ✗

Analytical method

$K_{c,90,dowel} = \sqrt{\frac{50}{10}} \cdot \sqrt{\frac{50}{10}} = 5$ → should be ≤ 4
$F_{t.p,k} = 0.25 \cdot \pi \cdot 10^2 \cdot K_{c,90\,dowel} \cdot f_{c,90,k} = 0,79$ kN per dowel

$$F_{c,90,Rk} = \min \begin{cases} K_{mat} \cdot b_{c,90} \cdot l_{ef,1} \cdot f_{c,90,k} + n \cdot F_{t.p,k} \\ b \cdot l_{ef,2} \cdot f_{c,90,k} \end{cases} = \begin{cases} 195\,kN \\ 280\,kN \end{cases}$$

$f_{c,90,Rk} = 195 \cdot 10^3 / 200^2 = 4,87$ MPa → $f_{c,90,d} = \frac{0,7}{1,25} \cdot 4,87 = 2,72$ MPa

U.C. = 1,65 ✗

Steel Reinforcement: spacing → table 11.24

Rothoblaas VGZ 120 mm Ø8 $f_{y,k} = 1000$ N/mm²
$f_{ax,k} = 11,7$ N/mm²

$\min(F_{w,k}; F_{c,k})$??

$F_{w,k} = \pi \cdot d \cdot l_w \cdot f_{w,k} \rightarrow f_{w,k} = k_{screw} \cdot k_w \cdot k_{mat}\, d^{-0.33} \left(\frac{\rho_k}{350}\right)^{k_p}$

$= 7.5 \cdot 1.0 \cdot 0.83 \cdot 8^{-0.33} (1.0)^{1.10} = 3{,}4\ N/mm^2$

$F_{w,k} = 10{,}3\ kN$

$F_{c,k} = \frac{\gamma_R}{\gamma_{M1}} \cdot k_c \cdot N_{pl,k} = \frac{1.0}{1.3} \cdot 0.79 \cdot 50.3 = 31\ kN$

$F_{c,k} = 31{,}0\ kN$

$5d = 40\ mm \rightarrow 200/40 = 5 \rightarrow 6 \times 6$ screws

$F_{c,90,Rk} = \min \begin{cases} k_{mat} \cdot b_{c,90} \cdot l_{ef,1} \cdot f_{c,90,k} + n \cdot \min(F_{w,k}; F_{a,k}) \\ b \cdot l_{ef,2} \cdot f_{c,90,k} \end{cases} = \begin{cases} 545\ kN \\ 280\ kN \end{cases}$

$f_{c,90,Rk} = 280 \cdot 10^3 / 200^2 = 7{,}0\ MPa \rightarrow f_{c,90,d} = \frac{0{,}7}{1{,}25} \cdot = 3{,}92\ MPa$

$u.c. = 1.15$ ✗

Remarks: optimization in d; l; n, etc.

H

BM4D Abaqus Script

```
# -*- coding: mbcs -*-
from part import *
from material import *
from section import *
from assembly import *
from step import *
from interaction import *
from load import *
from mesh import *
from optimization import *
from job import *
from sketch import *
from visualization import *
from connectorBehavior import *

#Create part: Timber
mdb.models['Model-1'].ConstrainedSketch(name='__profile__', sheetSize=200.0)
mdb.models['Model-1'].sketches['__profile__'].rectangle(point1=(0.0, 0.0),
    point2=(150.0, 160.0))
mdb.models['Model-1'].Part(dimensionality=THREE_D, name='Timber', type=
    DEFORMABLE_BODY)
mdb.models['Model-1'].parts['Timber'].BaseSolidExtrude(depth=65.0, sketch=
    mdb.models['Model-1'].sketches['__profile__'])
del mdb.models['Model-1'].sketches['__profile__']

# Create part: Steel
mdb.models['Model-1'].ConstrainedSketch(name='__profile__', sheetSize=200.0)
mdb.models['Model-1'].sketches['__profile__'].rectangle(point1=(0.0, 0.0),
    point2=(60.0, 50.0))
mdb.models['Model-1'].Part(dimensionality=THREE_D, name='Steel', type=
    DEFORMABLE_BODY)
mdb.models['Model-1'].parts['Steel'].BaseSolidExtrude(depth=60.0, sketch=
    mdb.models['Model-1'].sketches['__profile__'])
del mdb.models['Model-1'].sketches['__profile__']

# Create part: Dowel
mdb.models['Model-1'].ConstrainedSketch(name='__profile__', sheetSize=200.0)
mdb.models['Model-1'].sketches['__profile__'].CircleByCenterPerimeter(center=(
    0.0, 0.0), point1=(5.0, 0.0))
mdb.models['Model-1'].Part(dimensionality=THREE_D, name='Dowel', type=
    DEFORMABLE_BODY)
mdb.models['Model-1'].parts['Dowel'].BaseSolidExtrude(depth=100.0, sketch=
    mdb.models['Model-1'].sketches['__profile__'])
del mdb.models['Model-1'].sketches['__profile__']

#Create Material: TIMBER
mdb.models['Model-1'].Material(name='TIMBER')
mdb.models['Model-1'].materials['TIMBER'].Elastic(table=((11600.0, 350.0,
    350.0, 0.48, 0.3, 0.56, 385.0, 338.0, 38.5), ), type=ENGINEERING_CONSTANTS)
mdb.models['Model-1'].materials['TIMBER'].Plastic(scaleStress=None, table=((
    37.5, 0.0), (38.5, 0.1)))
mdb.models['Model-1'].materials['TIMBER'].plastic.Potential(table=((1.0, 0.133,
    0.133, 0.231, 0.231, 0.231), ))

#Create Material: DENSIFIED WOOD
mdb.models['Model-1'].Material(name='DENSIFIED WOOD')
mdb.models['Model-1'].materials['DENSIFIED WOOD'].Elastic(table=((28000.0,
    2240.0, 1400.0, 0.48, 0.3, 0.35, 2000.0, 1880.0, 200.0), ), type=
    ENGINEERING_CONSTANTS)
mdb.models['Model-1'].materials['DENSIFIED WOOD'].Plastic(scaleStress=None,
    table=((130.0, 0.0), (132.5, 0.1)))
mdb.models['Model-1'].materials['DENSIFIED WOOD'].plastic.Potential(table=((
    1.0, 0.615, 0.615, 1.066, 1.066, 1.066), ))

#Create Material: STEEL
mdb.models['Model-1'].Material(name='STEEL')
mdb.models['Model-1'].materials['STEEL'].Elastic(table=((210000.0, 0.3), ))
```

```
mdb.models['Model-1'].materials['STEEL'].Plastic(scaleStress=None, table=((
    355.0, 0.0), ))


#Create Sections
mdb.models['Model-1'].HomogeneousSolidSection(material='TIMBER', name=
    'Timber_Sec', thickness=None)
mdb.models['Model-1'].HomogeneousSolidSection(material='DENSIFIED WOOD', name=
    'Dowel_Sec', thickness=None)
mdb.models['Model-1'].HomogeneousSolidSection(material='STEEL', name=
    'Steel_Sec', thickness=None)

#Assign Sections
mdb.models['Model-1'].parts['Timber'].Set(cells=
    mdb.models['Model-1'].parts['Timber'].cells.getSequenceFromMask(('[#1 ]',
    ), ), name='Set-TimberSec')
mdb.models['Model-1'].parts['Timber'].SectionAssignment(offset=0.0,
    offsetField='', offsetType=MIDDLE_SURFACE, region=
    mdb.models['Model-1'].parts['Timber'].sets['Set-TimberSec'], sectionName=
    'Timber_Sec', thicknessAssignment=FROM_SECTION)
mdb.models['Model-1'].parts['Dowel'].Set(cells=
    mdb.models['Model-1'].parts['Dowel'].cells.getSequenceFromMask(('[#1 ]', ),
    ), name='Set-DowelSec')
mdb.models['Model-1'].parts['Dowel'].SectionAssignment(offset=0.0, offsetField=
    '', offsetType=MIDDLE_SURFACE, region=
    mdb.models['Model-1'].parts['Dowel'].sets['Set-DowelSec'], sectionName=
    'Dowel_Sec', thicknessAssignment=FROM_SECTION)
mdb.models['Model-1'].parts['Steel'].Set(cells=
    mdb.models['Model-1'].parts['Steel'].cells.getSequenceFromMask(('[#1 ]', ),
    ), name='Set-SteelSec')
mdb.models['Model-1'].parts['Steel'].SectionAssignment(offset=0.0, offsetField=
    '', offsetType=MIDDLE_SURFACE, region=
    mdb.models['Model-1'].parts['Steel'].sets['Set-SteelSec'], sectionName=
    'Steel_Sec', thicknessAssignment=FROM_SECTION)

# Create Cut
mdb.models['Model-1'].ConstrainedSketch(gridSpacing=11.43, name='__profile__',
    sheetSize=457.49, transform=
    mdb.models['Model-1'].parts['Timber'].MakeSketchTransform(
    sketchPlane=mdb.models['Model-1'].parts['Timber'].faces[1],
    sketchPlaneSide=SIDE1,
    sketchUpEdge=mdb.models['Model-1'].parts['Timber'].edges[1],
    sketchOrientation=RIGHT, origin=(0.0, 160.0, 0.0)))
mdb.models['Model-1'].parts['Timber'].projectReferencesOntoSketch(filter=
    COPLANAR_EDGES, sketch=mdb.models['Model-1'].sketches['__profile__'])
mdb.models['Model-1'].sketches['__profile__'].CircleByCenterPerimeter(center=(
    -25.0, 25.0), point1=(-20.0, 25.0))
mdb.models['Model-1'].parts['Timber'].CutExtrude(depth=100.0,
    flipExtrudeDirection=OFF, sketch=
    mdb.models['Model-1'].sketches['__profile__'], sketchOrientation=RIGHT,
    sketchPlane=mdb.models['Model-1'].parts['Timber'].faces[1],
    sketchPlaneSide=SIDE1, sketchUpEdge=
    mdb.models['Model-1'].parts['Timber'].edges[1])
del mdb.models['Model-1'].sketches['__profile__']

# Create Top Partitions
mdb.models['Model-1'].ConstrainedSketch(gridSpacing=8.17, name='__profile__',
    sheetSize=326.95, transform=
    mdb.models['Model-1'].parts['Timber'].MakeSketchTransform(
    sketchPlane=mdb.models['Model-1'].parts['Timber'].faces[3],
    sketchPlaneSide=SIDE1,
    sketchUpEdge=mdb.models['Model-1'].parts['Timber'].edges[3],
    sketchOrientation=RIGHT, origin=(0.0, 160.0, 0.0)))
mdb.models['Model-1'].parts['Timber'].projectReferencesOntoSketch(filter=
    COPLANAR_EDGES, sketch=mdb.models['Model-1'].sketches['__profile__'])
mdb.models['Model-1'].sketches['__profile__'].Line(point1=(-150.0, 25.0),
    point2=(0.0, 25.0))
```

```
mdb.models['Model-1'].sketches['__profile__'].HorizontalConstraint(
    addUndoState=False, entity=
    mdb.models['Model-1'].sketches['__profile__'].geometry[7])
mdb.models['Model-1'].sketches['__profile__'].Line(point1=(-25.0, 0.0), point2=
    (-25.0, 65.0))
mdb.models['Model-1'].sketches['__profile__'].VerticalConstraint(addUndoState=
    False, entity=mdb.models['Model-1'].sketches['__profile__'].geometry[8])
mdb.models['Model-1'].sketches['__profile__'].autoTrimCurve(curve1=
    mdb.models['Model-1'].sketches['__profile__'].geometry[8], point1=(
    -24.5758972167969, 23.3163261413574))
mdb.models['Model-1'].sketches['__profile__'].autoTrimCurve(curve1=
    mdb.models['Model-1'].sketches['__profile__'].geometry[7], point1=(
    -26.2834854125977, 25.1530609130859))
mdb.models['Model-1'].sketches['__profile__'].autoTrimCurve(curve1=
    mdb.models['Model-1'].sketches['__profile__'].geometry[10], point1=(
    -25.1785583496094, 27.7040824890137))
mdb.models['Model-1'].sketches['__profile__'].autoTrimCurve(curve1=
    mdb.models['Model-1'].sketches['__profile__'].geometry[12], point1=(
    -23.5714263916016, 25.6632652282715))
mdb.models['Model-1'].parts['Timber'].PartitionFaceBySketch(faces=
    mdb.models['Model-1'].parts['Timber'].faces.getSequenceFromMask(('[#8 ]',
    ), ), sketch=mdb.models['Model-1'].sketches['__profile__'], sketchUpEdge=
    mdb.models['Model-1'].parts['Timber'].edges[3])
del mdb.models['Model-1'].sketches['__profile__']

# Create Side Partions
mdb.models['Model-1'].ConstrainedSketch(gridSpacing=11.43, name='__profile__',
    sheetSize=457.49, transform=
    mdb.models['Model-1'].parts['Timber'].MakeSketchTransform(
    sketchPlane=mdb.models['Model-1'].parts['Timber'].faces[9],
    sketchPlaneSide=SIDE1,
    sketchUpEdge=mdb.models['Model-1'].parts['Timber'].edges[20],
    sketchOrientation=RIGHT, origin=(150.0, 0.0, 65.0)))
mdb.models['Model-1'].parts['Timber'].projectReferencesOntoSketch(filter=
    COPLANAR_EDGES, sketch=mdb.models['Model-1'].sketches['__profile__'])
mdb.models['Model-1'].sketches['__profile__'].Line(point1=(150.0, -60.0),
    point2=(0.0, -60.0))
mdb.models['Model-1'].sketches['__profile__'].HorizontalConstraint(
    addUndoState=False, entity=
    mdb.models['Model-1'].sketches['__profile__'].geometry[7])
mdb.models['Model-1'].parts['Timber'].PartitionFaceBySketch(faces=
    mdb.models['Model-1'].parts['Timber'].faces.getSequenceFromMask(('[#200 ]',
    ), ), sketch=mdb.models['Model-1'].sketches['__profile__'], sketchUpEdge=
    mdb.models['Model-1'].parts['Timber'].edges[20])
del mdb.models['Model-1'].sketches['__profile__']

# Create Partitions
mdb.models['Model-1'].parts['Timber'].PartitionCellByExtrudeEdge(cells=
    mdb.models['Model-1'].parts['Timber'].cells.getSequenceFromMask(('[#1 ]',
    ), ), edges=(mdb.models['Model-1'].parts['Timber'].edges[4],
    mdb.models['Model-1'].parts['Timber'].edges[7],
    mdb.models['Model-1'].parts['Timber'].edges[10],
    mdb.models['Model-1'].parts['Timber'].edges[13]), line=
    mdb.models['Model-1'].parts['Timber'].edges[24], sense=FORWARD)
mdb.models['Model-1'].parts['Timber'].PartitionCellByExtrudeEdge(cells=
    mdb.models['Model-1'].parts['Timber'].cells.getSequenceFromMask(('[#1 ]',
    ), ), edges=(mdb.models['Model-1'].parts['Timber'].edges[35],
    mdb.models['Model-1'].parts['Timber'].edges[38],
    mdb.models['Model-1'].parts['Timber'].edges[39],
    mdb.models['Model-1'].parts['Timber'].edges[43]), line=
    mdb.models['Model-1'].parts['Timber'].edges[25], sense=FORWARD)
mdb.models['Model-1'].parts['Timber'].PartitionCellByExtrudeEdge(cells=
    mdb.models['Model-1'].parts['Timber'].cells.getSequenceFromMask(('[#1f ]',
    ), ), edges=(mdb.models['Model-1'].parts['Timber'].edges[43],
    mdb.models['Model-1'].parts['Timber'].edges[50]), line=
    mdb.models['Model-1'].parts['Timber'].edges[13], sense=REVERSE)

```

```
# Assembly
mdb.models['Model-1'].rootAssembly.DatumCsysByDefault(CARTESIAN)
mdb.models['Model-1'].rootAssembly.Instance(dependent=ON, name='Timber-1',
    part=mdb.models['Model-1'].parts['Timber'])
mdb.models['Model-1'].rootAssembly.Instance(dependent=ON, name='Dowel-1', part=
    mdb.models['Model-1'].parts['Dowel'])
mdb.models['Model-1'].rootAssembly.Instance(dependent=ON, name='Steel-1', part=
    mdb.models['Model-1'].parts['Steel'])
mdb.models['Model-1'].rootAssembly.rotate(angle=270.0, axisDirection=(150.0,
    0.0, 0.0), axisPoint=(0.0, 0.0, 0.0), instanceList=('Dowel-1', ))
mdb.models['Model-1'].rootAssembly.translate(instanceList=('Dowel-1', ),
    vector=(25.0, 60.0, 25.0))
mdb.models['Model-1'].rootAssembly.translate(instanceList=('Steel-1', ),
    vector=(0.0, 160.0, 0.0))

#Create Step-1
mdb.models['Model-1'].StaticStep(adaptiveDampingRatio=0.05,
    continueDampingFactors=False, initialInc=0.01, maxNumInc=1000, minInc=1e-06
    , name='Step-1', nlgeom=ON, previous='Initial', stabilizationMagnitude=
    0.0001, stabilizationMethod=DISSIPATED_ENERGY_FRACTION)

#Create Step-2
mdb.models['Model-1'].StaticStep(adaptiveDampingRatio=0.05,
    continueDampingFactors=False, initialInc=0.01, maxInc=0.05, maxNumInc=1000,
    minInc=1e-06, name='Step-2', previous='Step-1', stabilizationMagnitude=
    0.0001, stabilizationMethod=DISSIPATED_ENERGY_FRACTION)

#Create Interaction: IntProp-Normal_Contact
mdb.models['Model-1'].ContactProperty('IntProp-Normal_Contact')
mdb.models['Model-1'].interactionProperties['IntProp-Normal_Contact'].NormalBehavior(
    allowSeparation=ON, constraintEnforcementMethod=DEFAULT,
    pressureOverclosure=HARD)
mdb.models['Model-1'].interactionProperties['IntProp-Normal_Contact'].TangentialBehavior(
    dependencies=0, directionality=ISOTROPIC, elasticSlipStiffness=None,
    formulation=PENALTY, fraction=0.005, maximumElasticSlip=FRACTION,
    pressureDependency=OFF, shearStressLimit=None, slipRateDependency=OFF,
    table=((0.5, ), ), temperatureDependency=OFF)

#Create Interaction: IntProp-CZM
mdb.models['Model-1'].ContactProperty('IntProp-CZM')
mdb.models['Model-1'].interactionProperties['IntProp-CZM'].NormalBehavior(
    allowSeparation=ON, constraintEnforcementMethod=DEFAULT,
    pressureOverclosure=HARD)
mdb.models['Model-1'].interactionProperties['IntProp-CZM'].TangentialBehavior(
    dependencies=0, directionality=ISOTROPIC, elasticSlipStiffness=None,
    formulation=PENALTY, fraction=0.005, maximumElasticSlip=FRACTION,
    pressureDependency=OFF, shearStressLimit=None, slipRateDependency=OFF,
    table=((0.5, ), ), temperatureDependency=OFF)
mdb.models['Model-1'].interactionProperties['IntProp-CZM'].Damage(evolTable=((
    2.5, ), ), initTable=((5.0, 5.0, 5.0), ), useEvolution=ON)
mdb.models['Model-1'].interactionProperties['IntProp-CZM'].CohesiveBehavior(
    defaultPenalties=OFF, table=((120.0, 36.0, 36.0), ))

#Create Interaction: Steel-Timber
mdb.models['Model-1'].rootAssembly.Surface(name='m_Surf-Steel_Timber',
    side1Faces=
    mdb.models['Model-1'].rootAssembly.instances['Steel-1'].faces.getSequenceFromMask(
    ('[#8 ]', ), ))
mdb.models['Model-1'].rootAssembly.Surface(name='s_Surf-Steel_Timber',
    side1Faces=
    mdb.models['Model-1'].rootAssembly.instances['Timber-1'].faces.getSequenceFromMask(
    mask=('[#0 #238 ]', ), )+\
    mdb.models['Model-1'].rootAssembly.instances['Dowel-1'].faces.getSequenceFromMask(
    mask=('[#2 ]', ), ))
mdb.models['Model-1'].SurfaceToSurfaceContactStd(adjustMethod=NONE,
    clearanceRegion=None, createStepName='Step-1', datumAxis=None,
    initialClearance=OMIT, interactionProperty='IntProp-Normal_Contact', main=
```

```
        mdb.models['Model-1'].rootAssembly.surfaces['m_Surf-Steel_Timber'], name=
        'Steel_Timber_Int', secondary=
        mdb.models['Model-1'].rootAssembly.surfaces['s_Surf-Steel_Timber'],
        sliding=FINITE, thickness=ON)

    #Create Interaction: Dowel_Timber
    mdb.models['Model-1'].rootAssembly.Surface(name='m_Surf-Dowel_Timber',
        side1Faces=
        mdb.models['Model-1'].rootAssembly.instances['Dowel-1'].faces.getSequenceFromMask(
        ('[#5 ]', ), ))
    mdb.models['Model-1'].rootAssembly.Surface(name='s_Surf-Dowel_Timber',
        side1Faces=
        mdb.models['Model-1'].rootAssembly.instances['Timber-1'].faces.getSequenceFromMask(
        ('[#80000000 #c3 ]', ), ))
    mdb.models['Model-1'].SurfaceToSurfaceContactStd(adjustMethod=NONE,
        clearanceRegion=None, createStepName='Step-1', datumAxis=None,
        initialClearance=OMIT, interactionProperty='IntProp-CZM', main=
        mdb.models['Model-1'].rootAssembly.surfaces['m_Surf-Dowel_Timber'], name=
        'Dowel_Timber_Int', secondary=
        mdb.models['Model-1'].rootAssembly.surfaces['s_Surf-Dowel_Timber'],
        sliding=SMALL, thickness=ON)

    #Create BC: BC-1_XSYM
    mdb.models['Model-1'].rootAssembly.Set(faces=
        mdb.models['Model-1'].rootAssembly.instances['Timber-1'].faces.getSequenceFromMask(
        mask=('[#10000030 #100 ]', ), )+\
        mdb.models['Model-1'].rootAssembly.instances['Steel-1'].faces.getSequenceFromMask(
        mask=('[#1 ]', ), ), name='Set-XSYM')
    mdb.models['Model-1'].XsymmBC(createStepName='Initial', localCsys=None, name=
        'BC-1_XSYM', region=mdb.models['Model-1'].rootAssembly.sets['Set-XSYM'])

    #Create BC: BC-2_ZSYM
    mdb.models['Model-1'].rootAssembly.Set(faces=
        mdb.models['Model-1'].rootAssembly.instances['Steel-1'].faces.getSequenceFromMask(
        mask=('[#20 ]', ), )+\
        mdb.models['Model-1'].rootAssembly.instances['Timber-1'].faces.getSequenceFromMask(
        mask=('[#4000240 #2000 ]', ), ), name='Set-ZSYM')
    mdb.models['Model-1'].ZsymmBC(createStepName='Initial', localCsys=None, name=
        'BC-2_ZSYM', region=mdb.models['Model-1'].rootAssembly.sets['Set-ZSYM'])

    #Create BC: BC-3_TIMBER_BOTTOM
    mdb.models['Model-1'].rootAssembly.Set(faces=
        mdb.models['Model-1'].rootAssembly.instances['Timber-1'].faces.getSequenceFromMask(
        ('[#3c0000 #800 ]', ), ), name='Set-TimberBottom')
    mdb.models['Model-1'].EncastreBC(createStepName='Initial', localCsys=None,
        name='BC-3_TIMBER_BOTTOM', region=
        mdb.models['Model-1'].rootAssembly.sets['Set-TimberBottom'])

    #Create BC: BC-4_DOWEL
    mdb.models['Model-1'].rootAssembly.Set(faces=
        mdb.models['Model-1'].rootAssembly.instances['Dowel-1'].faces.getSequenceFromMask(
        ('[#2 ]', ), ), name='Set-DowelTop')
    mdb.models['Model-1'].DisplacementBC(amplitude=UNSET, createStepName='Initial',
        distributionType=UNIFORM, fieldName='', localCsys=None, name='BC-4_DOWEL',
        region=mdb.models['Model-1'].rootAssembly.sets['Set-DowelTop'], u1=SET, u2=
        SET, u3=SET, ur1=SET, ur2=SET, ur3=SET)
    mdb.models['Model-1'].boundaryConditions['BC-4_DOWEL'].deactivate('Step-1')

    #Create BC: BC-5_STEEL_TOP
    mdb.models['Model-1'].rootAssembly.Set(faces=
        mdb.models['Model-1'].rootAssembly.instances['Steel-1'].faces.getSequenceFromMask(
        ('[#2 ]', ), ), name='Set-SteelTop')
    mdb.models['Model-1'].DisplacementBC(amplitude=UNSET, createStepName='Initial',
        distributionType=UNIFORM, fieldName='', localCsys=None, name=
        'BC-5_STEEL_TOP', region=
        mdb.models['Model-1'].rootAssembly.sets['Set-SteelTop'], u1=SET, u2=UNSET,
        u3=SET, ur1=SET, ur2=SET, ur3=SET)
```

```
336
337   #Create BC: BC-6_CONTACT_STEEL
338   mdb.models['Model-1'].DisplacementBC(amplitude=UNSET, createStepName='Step-1',
339       distributionType=UNIFORM, fieldName='', fixed=OFF, localCsys=None, name=
340       'BC-6_CONTACT_STEEL', region=
341       mdb.models['Model-1'].rootAssembly.sets['Set-SteelTop'], u1=0.0, u2=-0.1,
342       u3=0.0, ur1=0.0, ur2=0.0, ur3=0.0)
343   mdb.models['Model-1'].boundaryConditions['BC-6_CONTACT_STEEL'].deactivate(
344       'Step-2')
345
346   #Create BC: BC-7_CONTACT_DOWEL
347   mdb.models['Model-1'].DisplacementBC(amplitude=UNSET, createStepName='Step-1',
348       distributionType=UNIFORM, fieldName='', fixed=OFF, localCsys=None, name=
349       'BC-7_CONTACT_DOWEL', region=
350       mdb.models['Model-1'].rootAssembly.sets['Set-DowelTop'], u1=0.0, u2=-0.05,
351       u3=0.0, ur1=0.0, ur2=0.0, ur3=0.0)
352   mdb.models['Model-1'].boundaryConditions['BC-7_CONTACT_DOWEL'].deactivate(
353       'Step-2')
354
355   #Create BC: BC-8_DISPLACEMENT
356   mdb.models['Model-1'].DisplacementBC(amplitude=UNSET, createStepName='Step-2',
357       distributionType=UNIFORM, fieldName='', fixed=OFF, localCsys=None, name=
358       'BC-8_DISPLACEMENT', region=
359       mdb.models['Model-1'].rootAssembly.sets['Set-SteelTop'], u1=0.0, u2=-10.0,
360       u3=0.0, ur1=0.0, ur2=0.0, ur3=0.0)
361
362   #Mesh Part: Timber
363   mdb.models['Model-1'].parts['Timber'].setMeshControls(algorithm=MEDIAL_AXIS,
364       regions=mdb.models['Model-1'].parts['Timber'].cells.getSequenceFromMask((
365       '[#1ff ]', ), ), technique=SWEEP)
366   mdb.models['Model-1'].parts['Timber'].seedEdgeByNumber(constraint=FINER, edges=
367       mdb.models['Model-1'].parts['Timber'].edges.getSequenceFromMask((
368       '[#0:2 #1e ]', ), ), number=4)
369   mdb.models['Model-1'].parts['Timber'].seedPart(deviationFactor=0.1,
370       minSizeFactor=0.1, size=3.0)
371   mdb.models['Model-1'].parts['Timber'].generateMesh()
372
373   #Mesh Part: Dowel
374   mdb.models['Model-1'].parts['Dowel'].setMeshControls(algorithm=MEDIAL_AXIS,
375       regions=mdb.models['Model-1'].parts['Dowel'].cells.getSequenceFromMask((
376       '[#1 ]', ), ))
377   mdb.models['Model-1'].parts['Dowel'].seedEdgeByNumber(constraint=FINER, edges=
378       mdb.models['Model-1'].parts['Dowel'].edges.getSequenceFromMask(('[#3 ]', ),
379       ), number=16)
380   mdb.models['Model-1'].parts['Dowel'].generateMesh()
381
382   #Mesh Part: Steel
383   mdb.models['Model-1'].parts['Steel'].seedPart(deviationFactor=0.1,
384       minSizeFactor=0.1, size=4.0)
385   mdb.models['Model-1'].parts['Steel'].generateMesh()
386
387   #Material Orientation: Timber
388   mdb.models['Model-1'].parts['Timber'].DatumCsysByThreePoints(coordSysType=
389       CARTESIAN, line1=(1.0, 0.0, 0.0), name='Datum csys-Timber', origin=(0.0,
390       0.0, 0.0), point2=(1.0, 1.0, 0.0))
391   mdb.models['Model-1'].parts['Timber'].MaterialOrientation(
392       additionalRotationField='', additionalRotationType=ROTATION_NONE, angle=0.0
393       , axis=AXIS_3, fieldName='', localCsys=
394       mdb.models['Model-1'].parts['Timber'].datums[12], orientationType=SYSTEM,
395       region=Region(
396       cells=mdb.models['Model-1'].parts['Timber'].cells.getSequenceFromMask(
397       mask=('[#1ff ]', ), )), stackDirection=STACK_3)
398
399   #Material Orientation: Dowel
400   mdb.models['Model-1'].parts['Dowel'].DatumCsysByThreePoints(coordSysType=
401       CARTESIAN, name='Datum csys-Dowel', origin=
402       mdb.models['Model-1'].parts['Dowel'].InterestingPoint(
```

```
        mdb.models['Model-1'].parts['Dowel'].edges[1], CENTER), point1=
        mdb.models['Model-1'].parts['Dowel'].InterestingPoint(
        mdb.models['Model-1'].parts['Dowel'].edges[0], CENTER), point2=
        mdb.models['Model-1'].parts['Dowel'].InterestingPoint(
        mdb.models['Model-1'].parts['Dowel'].edges[0], MIDDLE))
    mdb.models['Model-1'].parts['Dowel'].MaterialOrientation(
        additionalRotationField='', additionalRotationType=ROTATION_NONE, angle=0.0
        , axis=AXIS_3, fieldName='', localCsys=
        mdb.models['Model-1'].parts['Dowel'].datums[5], orientationType=SYSTEM,
        region=Region(
        cells=mdb.models['Model-1'].parts['Dowel'].cells.getSequenceFromMask(mask=(
        '[#1 ]', ), )), stackDirection=STACK_3)

    # Modify Output Parameters
    mdb.models['Model-1'].rootAssembly.regenerate()
    mdb.models['Model-1'].fieldOutputRequests['F-Output-1'].setValuesInStep(
        stepName='Step-2', variables=('S', 'PE', 'PEEQ', 'PEMAG', 'LE', 'U', 'RF',
        'CF', 'CSTRESS', 'CDISP', 'CSMAXSCRT'))
    mdb.models['Model-1'].HistoryOutputRequest(createStepName='Step-2', name=
        'H-Output-2', rebar=EXCLUDE, region=
        mdb.models['Model-1'].rootAssembly.sets['Set-SteelTop'], sectionPoints=
        DEFAULT, variables=('U2', 'RF2'))
    mdb.models['Model-1'].HistoryOutputRequest(createStepName='Step-2', name=
        'H-Output-3', rebar=EXCLUDE, region=
        mdb.models['Model-1'].rootAssembly.sets['Set-TimberBottom'], sectionPoints=
        DEFAULT, variables=('RF2', ))
```